

## ABSTRACT

Title of Document: THERMODYNAMICS AND STRUCTURE OF  
POLY(ETHYLENE OXIDE) IN ETHANOL  
AND WATER MIXTURE

Sang Hak Shin, Doctor of Philosophy, 2011

Directed By: Professor Robert M. Briber, Materials Science  
and Engineering  
Dr. Boualem Hammouda, National Institute of  
Standards and Technology

Poly(ethylene oxide) (PEO) is one of the most researched synthetic polymers due to the complex behavior which arises from the interplay of the hydrophilic and hydrophobic sites on the polymer chain. PEO in ethanol forms an opaque gel-like mixture with a partially crystalline structure. Addition of a small amount of water disrupts the gel: 5 wt % PEO in ethanol becomes a transparent solution with the addition of 4 vol % water. The phase behavior of PEO in mixed solvents have been studied using small-angle neutron scattering (SANS). PEO solutions (5 wt % PEO) which contain 4 vol % – 10 vol % (and higher) water behave as an athermal polymer solution and the phase behavior changes from UCST to LCST rapidly as the fraction of water is increased. 2 wt % PEO in water and 10 wt % PEO in ethanol/ water mixtures are examined to assess the role of hydration. The observed phase behavior is consistent with a hydration layer forming upon the addition of water as the system shifts from UCST to LCST behavior. At the molecular level, two or three water molecules can hydrate one PEO monomer (water molecules form a sheath around the

PEO macromolecule) which is consistent with the suppression of crystallization and change in the mentioned phase behavior as observed by SANS.

The clustering effect of aqueous PEO solution (M.W of PEO = 90,000 g/mol) is monitored as an excess scattering intensity at low- $Q$ . Clustering intensity at  $Q = 0.004 \text{ \AA}^{-1}$  is used for evaluating the clustering effect. The clustering intensity is proportional to the inverse temperature and levels off when the temperature is less than 50 °C. When the temperature is increased over 50 °C, the clustering intensity starts decreasing. The clustering of PEO is monitored in ethanol/ water mixtures. The clustering intensity increases as the fraction of water is increased. Based on the solvation intensity behavior, we confirmed that the ethanol/ water mixtures obey a random solvent mixing rule, whereby solvent mixtures are better at solvating the polymer than any of the two solvents.

The solution behavior of PEO in ethanol was investigated in the presence of salt ( $\text{CaCl}_2$ ) using SANS. Binding of  $\text{Ca}^{2+}$  ions to the PEO oxygens transforms the neutral polymer to a weakly charged polyelectrolyte. We observed that the PEO/ethanol solution is better solvated at higher salt concentration due to the electrostatic repulsion of weakly charged monomers. The association of the  $\text{Ca}^{2+}$  ions with the PEO oxygen atoms transforms the neutral polymer to a weakly charged polyelectrolyte and gives rise to repulsive interactions between the PEO/ $\text{Ca}^{2+}$  complexes. Addition of salt disrupts the gel, which is consistent with better solvation as the salt concentration is increased. Moreover, SANS shows that the phase behavior of PEO/ethanol changes from UCST to LCST as the salt concentration is increased.

**THERMODYNAMICS AND STRUCTURE OF POLY(ETHYLENE OXIDE) IN  
MIXTURES OF WATER AND ETHANOL**

By

Sang Hak Shin

Dissertation submitted to the Faculty of the Graduate School of the  
University of Maryland, College Park, in partial fulfillment  
of the requirements for the degree of  
Doctor of Philosophy  
2011

Advisory Committee:  
Professor Robert M. Briber, Chair/ Advisor  
Dr. Boualem Hammouda  
Professor Peter Kofinas  
Professor Mohamad Al-Sheikhly  
Professor Luz Martinez-Miranda

© Copyright by  
Sang Hak Shin  
2011

## Acknowledgements

I would like to thank my advisor, Prof. Robert M. Briber. Dr. Briber guided me how to approach scientific discovery, problem solving and technical communication.

I would like to thank my co-advisor Dr. Boualem Hammouda. Dr. Hammouda led me into a fascinating new scientific world.

I would like to thank my committee members, Prof. Peter Kofinas, Prof. Mohamad Al-Sheikhly, and Prof. Luz Martinez-Miranda for their advice.

I would like to thank SANS group at NCNR. Cedric Gagnon and Jeffrey Krzywon helped SANS instrumentation.

I am grateful to all of my group colleagues who have enriched my graduate experiences: Chris Metting, Ping-yen Hsieh, Xin Zhang, Won Seok Hwang and Joon Ho Roh. Also, I would like to thank Prof. Kofinas group members for the helpful group meetings.

Last, I would like to thank my wife, Eun Jung Shim, and all my family for their support and patience.

# Table of Contents

Acknowledgements	ii
Table of Contents	iii
List of Tables	iv
List of Figures	v
Chapter 1 Introduction	1
Chapter 2 Backgrounds and Review of Prior Work	3
2.1 Thermodynamics of polymer solutions: The Flory-Huggins theory	3
2.2 Aqueous PEO solution	10
2.2.1 The solvation of ether group polymer	10
2.2.2 Solvation and thermodynamics	12
2.2.3 Clustering of PEO in aqueous medium	18
Chapter 3 Experimental methods	24
3.1 Scattering Method	24
3.1.1 Neutron scattering	24
3.1.2 Scattering theory	26
3.1.3 Contrast variation in neutron scattering	36
3.1.4 Data from small-angle neutron scattering	38
3.1.5 Zero angle scattering and thermodynamics	40
3.1.6 The SANS instruments at the NCNR	44
3.2 Dynamic light scattering	46
3.3 Density measurements by the vibrating tube method	47
Chapter 4 Solvation and clustering of poly(ethylene oxide) in ethanol/ water mixtures	50
4.1 Introduction	50
4.2 Experimental	52
4.3 Morphology and structure of PEO in ethanol	54
4.4 Model function for SANS Data from PEO solution	57
4.5 Solvation and clustering of PEO in d-water	60
4.6 Solvation and clustering of PEO in d-ethanol/ d-water	64
4.7 Conclusions	69
Chapter 5 Phase behavior of poly(ethylene oxide) in ethanol/ water mixtures	71
5.1 Introduction	71
5.2 Experimental	71
5.3 Model function for SANS data	73
5.4 Thermodynamics of PEO in ethanol/ water mixtures	74
5.4.1 Phase behavior and spinodal temperature ( $T_{SP}$ )	74
5.4.2 Self consistency in the change of the phase behavior	79
5.5 Conclusions	86
Chapter 6 Salt effect on poly(ethylene oxide) in ethanol	88
6.1 Introduction	88
6.2 Experimental	89
6.3 Results and data analysis	90

6.4 Conclusions	101
Chapter 7 Conclusions	103
Chapter 8 Future Work	106
Bibliography	108

## List of Tables

Table 3.1 Scattering lengths and cross-sections of some common elements	37
Table 4.1 Sample preparation list	53
Table 5.1 Sample preparation for each PEO fraction	73
Table 5.2 Transition point from UCST to LCST ( $\phi_{water}^t$ )	86
Table 6.1 Sample preparation and visual observations	96

## List of Figures

- Figure 2.1 The Flory-Huggins lattice model: (A) mixing two solvent molecules, (B) mixing solvent and one polymer chain and (C) mixing two polymers (polymer blend). 9
- Figure 2.2 The phase diagram of a polymer blend with  $N_A = N_B = N$ . The binodal is the solid curve and the spinodal is the dashed curve. 10
- Figure 2.3 Schematic model for hydration of PEO 15
- Figure 2.4 Schematic contour map of PEO based on the electrostatic potential. (A) Contour map of the 3-D electrostatic potential of the PEO chain: Blue denotes the negative potential zone and brown is the positive potential zone induced along the PEO chain. (B) Blue denotes the negative potential zone induced by water oxygen and brown represents the positive potential zone. Red is oxygen which accounts for the electron rich regions. 16
- Figure 2.5 Simulation results for (A) the number of hydrogen bonds : the closed data set is for PEO-water (EO-W) and the open data set is for water-water (W-W) (B) the free energy calculated from simulation data 17
- Figure 2.6 Phase diagram for aqueous solutions of PEO. Experimental data are represented by symbols and theoretical curves are calculated using the same parameters. N is the degree of polymerization. 18
- Figure 2.7 Histogram of N(Rh) for aqueous PEO solution (0.025 wt %) 21
- Figure 2.8 End group effect on clustering: (A) SANS intensity and (B) clustering strength defined by  $A/(0.004)^m$  for varying chain end group. A and n are obtained from fitting of the SANS intensity 22
- Figure 2.9 SANS intensity for PEO in d-benzene with different chain ends. D-benzene is relatively hydrophobic compared to water. Clustering becomes stronger as chain ends become more hydrophilic. 23
- Figure 3.1 Elastic neutron scattering events and scattering from a fixed nucleus 34
- Figure 3.2 Geometry of scattering. 35

- Figure 3.3 Schematic illustration of scattering. Intensity is measured as a function of wave vector,  $Q$ . 35
- Figure 3.4 A system containing two phases with different scattering length densities  $\rho_1$  and  $\rho_2$ . 38
- Figure 3.5 (A) Schematics of the NG3 30m SANS instrument at NIST. There are 4 main instrument parts; (1) velocity selector, (2) beam collimation, (3) Sample (scattering event) and (4) 2D neutron area detector. The sample-to-detector maximum distance is 15 m. (B) Photograph of the NG3 30m SANS instrument. 45
- Figure 3.6 Schematic representation of the vibrating U-tube density meter. 49
- Figure 4.1 The PEO/ ethanol mixture changes from an opaque gel to a clear solution with the addition of 4% water. (A) The photograph shows that the solution becomes clear as the fraction of water in mixed-solvents becomes 0.04 (4 vol %). (B) SANS intensity from PEO solutions. Open circles represent SANS intensity for PEO (5 wt %) in pure ethanol. The high- $Q$  slope of polymer solution is  $-5/3$ . 52
- Figure 4.2 PEO gel in ethanol (A) the gel is opaque, (B) an optical micrograph, (C) WAXS data with crystalline peaks and (D) SANS data. 56
- Figure 4.3 Thermoreversible gel. PEO forms a gel through partial crystallization at room temperature and becomes a homogeneous solution at higher temperature ( $T > 40^\circ\text{C}$ ). 56
- Figure 4.4 Formation of the thermoreversible gel of PEO in ethanol. (A) DSC and (B) density measurements 57
- Figure 4.5 Typical SANS intensity of aqueous PEO solutions. The solvation intensity can be obtained from fitting the SANS intensity at high  $Q$  and the clustering behavior can be estimated from the low- $Q$  data. Here, the clustering is monitored in terms of a clustering strength,  $A/(0.004)^m$ . 59
- Figure 4.6 Typical SANS intensity for an aqueous PEO solution. The solvation intensity can be obtained from fitting intensity at high  $Q$  and the clustering can be estimated through the upturn intensity at low- $Q$ . Here, the clustering is monitored through a clustering strength,  $A/(0.004)^m$ . 62

Figure 4.7 (A) Solvation intensity, (B) clustering strength for PEO (5 wt %, 90,000 g/mol) in d-water as a function of temperature. 63

Figure 4.8 PEO solvation and clustering in water. Hydrogen bonding between water and the PEO oxygen atoms forms a hydration shell. Rearrangement of the hydrogen bond configurations as two hydrophobic ethylenes come together causes clustering. 63

Figure 4.9 SANS intensities for 5 wt % PEO in ethanol/ water mixtures as a function of water fraction. 67

Figure 4.10 (A) Solvation intensities for 5 wt % PEO in ethanol/ water mixtures at  $T = 45^{\circ}\text{C}$ . (B) Solvation intensities for 5 wt % PEO in ethanol/ water mixtures at various temperatures. 68

Figure 4.11 (A) Density of PEO in ethanol/ water mixtures as a function of water fraction. (B)  $1/C$  vs. density of PEO in d-ethanol/ d-water mixture. Measured density and solvation intensity show deviation from ideal mixing line. 68

Figure 4.12 Clustering intensity for 5 wt % PEO in ethanol/ water mixtures as a function of water fraction. 69

Figure 5.1 (A) SANS intensity of PEO in ethanol, which shows UCST behavior. (B) SANS intensity of PEO in water, which shows LCST behavior. 78

Figure 5.2 Extrapolation of  $1/I(0)$  vs.  $1/T$  determines the phase behavior. (A) for UCST and (B) for LCST. The intercept with the x-axis ( $1/T$  axis) gives the spinodal temperature. Error bars are smaller than the symbol size. 78

Figure 5.3 (A) Phase diagram with spinodal temperature. (B) Slopes taken from linear extrapolation of  $1/I(0)$  vs.  $1/T$ . 79

Figure 5.4 SANS intensities for (A) 2 wt %, (B) 5 wt % and (C) 10 wt % PEO (90K g/mol) in ethanol / water mixtures. 82

Figure 5.5 Plots of  $1/C$  vs.  $1/T$  (A) 2 wt %, (B) 5 wt % and (C) 10 wt % PEO in ethanol/water mixtures. Error bars are smaller than the symbol size. 83

Figure 5.6 Slopes vs. water fraction. (A) 2 wt %, (B) 5 wt % and (C) 10 wt % PEO in ethanol/water mixtures. The transition points from UCST to LCST were estimated by observing slope changes. 84

Figure 5.7 Variation of the spinodal temperature as function of (A) water fraction and (B) hydration level. Hydration level can be defined as '(number of water molecule)/(number of PEO monomer in solution)'. The lower region corresponds to the demixed phase and the solution changes to the mixed phase upon heating. 85

Figure 6.1 Complexation between cation and induced dipole of a neutral polymer. 97

Figure 6.2 (A) Picture of PEO/ethanol with varying salt concentration. (B) SANS intensity of PEO/ ethanol with varying  $\text{CaCl}_2$  concentration at 25 °C and (C) at 35 °C. 98

Figure 6.3 SANS intensity for PEO/ ethanol/  $\text{CaCl}_2$  solution at 45 °C. The forward scattering intensity decreases as the  $\text{CaCl}_2$  concentration increases. 99

Figure 6.4 (A) Solvation intensity as a function of salt concentration at 45 °C inset picture shows the correlation length. (B) Clustering strength as function of salt concentration. 99

Figure 6.5 Proposed model to describe solvation and clustering in the presence of salt. Cation can exist as two states: bound cation with PEO oxygen and unbound free solvated ion. Complexation between PEO oxygen and calcium ion (bound cation) reduce the solvation intensity (better solvation in the presence of salt). The PEO cluster is formed through cation sharing by multiple chains. Screening effect by counter ion (anion) was not observed in solvation intensity as a function of salt concentration. Chloride exists as free ion in ethanol solvents. Dashed arrows represent columbic repulsion. 100

Figure 6.6 (A) Plot of  $1/C$  vs.  $1/T$  with varying salt concentration. (Error bars are smaller than plot symbols) (B) slope from linear fitting of  $1/C$  vs.  $1/T$ . The phase behavior changes from UCST to LCST with addition of salt. 101

# Chapter 1

## Introduction

Poly(ethylene oxide) (PEO) is one of the most researched synthetic polymers due to its structural simplicity and diverse functionality. PEO is a unique polymer because it is soluble in both water and organic solvents (methanol etc.).<sup>1, 2</sup> Although the PEO monomer ( $\text{CH}_2\text{CH}_2\text{O}$ ) is relatively simple, PEO exhibits complex solution behavior.<sup>1-6</sup> The complexity of the solution behavior stems from the oxygen atom in the chain backbone. The methyl group is hydrophobic and the oxygen atom along the backbone mediates hydrophilic interactions. The presence of oxygen atoms along the backbone strongly influences the nature of the interactions and the thermodynamics when PEO is dissolved in various solvents.<sup>7, 8</sup> The interplay between the hydrophilic and hydrophobic interactions in PEO is relevant to the folding and unfolding of proteins. Consequently, PEO is often mentioned as a simple and tractable model for understanding biopolymers. Varied interactions with other molecules also enable PEO to be used in both energy and biological applications.<sup>9-13</sup>

PEO exhibits a rich phase behavior including crystalline and/or gel-like structures when dissolved in organic solvents.<sup>6, 14</sup> When dissolved in organic solvents, PEO exhibits different phase behavior than when dissolved in aqueous solution. When dissolved in alcohols (particularly ethanol or methanol which are of interest here) PEO exhibits an upper critical solution temperature (UCST) thermodynamic behavior. This implies that the solvation mechanism of PEO in alcohols is different from that of

PEO in water even though alcohol has a strong hydrogen bonding ability. The current understanding of PEO solutions in organic solvents is limited and more work is needed to fully explain the complex solution behavior. This thesis has been focused on the understanding of structure and thermodynamics of PEO in ethanol and water.

## Chapter 2

### Background and Review of Prior Work

#### 2.1 Thermodynamics of polymer solutions: the Flory-Huggins theory

The classical Flory-Huggins theory has been widely used to study the thermodynamics of polymers. This theory uses a lattice model based on the mean field approximation.<sup>15-18</sup> It assumes that solvent molecules and monomers (polymer segments) in a polymer chain each occupy one lattice site. The lattice sites are filled fully, one segment or one solvent molecule per site. The Flory-Huggins theory assumes that there is no volume change upon mixing. The connectivity of monomers within a polymer chain is considered although obeying random mixing.<sup>15, 16, 18</sup>

Consider the mixing of two species A and B with no volume change in the homogeneous phase region as shown in Figure 2.1 (A). The volume of each species is  $V_A$  and  $V_B$  respectively. The volume fractions after mixing are given by

$$\phi_A = \frac{V_A}{V_A + V_B} \text{ and } \phi_B = \frac{V_B}{V_A + V_B} = 1 - \phi_A \quad (2-1)$$

Here, the volume of species A is  $V_A = n_A * v_0$ . Here  $n_A$  is the number of molecule A and  $v_0$  is the volume of each lattice site.

The entropy  $S$  is determined by the number of states as<sup>15, 16, 18</sup>

$$S = k \ln \Omega \quad (2-2)$$

where  $k$  is the Boltzmann constant and  $\Omega$  denotes the number of ways to arrange molecules.

$n_A$  and  $n_B$  are the number of sites of each molecule and  $n$  is the total number of sites after mixing ( $n = n_A + n_B$ ). Here, we assume that each molecule is indistinguishable so that the number of states is the same for possible lattice sites. For a single molecule of species A, the entropy change upon mixing is given by

$$\Delta S_A = k \ln n - k \ln n_A = -k \ln(n_A / n) = -k \ln \phi_A > 0 \quad (2-3)$$

Also, the mixing entropy for species B is similarly

$$\Delta S_B = -k \ln \phi_B > 0 \quad (2-4)$$

The change of entropy on mixing is always positive because the volume fraction is always less than 1. The total entropy change is summed up over all molecules,

$$\Delta S_{mix} = n_A \Delta S_A + n_B \Delta S_B = -n_A \times k \ln \phi_A - n_B \times k \ln \phi_B = -nk(\phi_A \ln \phi_A + \phi_B \ln \phi_B) \quad (2-5)$$

or

$$\overline{\Delta S_{mix}} = \frac{\Delta S_{total}}{n} = -k(\phi_A \ln \phi_A + \phi_B \ln \phi_B) \quad (2-6)$$

$$\Delta S_{mix} = -n_A \times k \ln \phi_A - n_B \times k \ln \phi_B = -nk \left( \frac{\phi_A}{N_A} \ln \phi_A + \frac{\phi_B}{N_B} \ln \phi_B \right) \quad (2-7)$$

or

$$\overline{\Delta S_{mix}} = -k \left( \frac{\phi_A}{N_A} \ln \phi_A + \frac{\phi_B}{N_B} \ln \phi_B \right) \quad (2-8)$$

Eq (2-8) implies that the mixing entropy is dependent on the chain connectivity in polymeric systems. In polymer systems, the total number of translational degrees of freedom of the chains is much lower than the total number of segments because the degree of polymerization ( $N_A$  and  $N_B \gg 1$ ) is large. Therefore, the mixing entropy is extremely small and mixtures of polymers tend to phase separate.

Up to now, we have considered just the mixing entropy. But the change in free energy on mixing is a function of interaction energy as well as entropy. The Flory-Huggins model assumes no volume change on mixing and hence the free energy is the Helmholtz free energy. The energy difference on mixing per lattice site in binary mixtures is given as

$$\Delta U_{mix} = \frac{1}{2} nz\phi_A(1-\phi_A)(2u_{AB} - u_{AA} - u_{BB}) \quad (2-9)$$

or

$$\Delta \bar{U}_{mix} = \Delta U / n = \frac{1}{2} z\phi_A(1-\phi_A)(2u_{AB} - u_{AA} - u_{BB}) \quad (2-10)$$

where  $z$  is the coordination number of the lattice

$u_{ij}$  is a pair interaction energy between sites  $i$  and  $j$

The Flory-Huggins interaction parameter,  $\chi$ , is defined to represent the difference of interaction energies in the mixtures.<sup>15, 16</sup> The Flory-Huggins interaction parameter is given by

$$\chi \equiv \frac{z}{2} \frac{(2u_{AB} - u_{AA} - u_{BB})}{kT} \quad (2-11)$$

Using the Flory interaction parameter, we can write the energy of mixing per lattice site as

$$\Delta \bar{U}_{mix} = \frac{\chi\phi_A(1-\phi_A)}{kT} \quad (2-12)$$

Combining Eq (2-8) for entropy of mixing, we get the free energy of mixing per lattice site

$$\Delta\bar{F}_{mix} = \Delta\bar{U}_{mix} - T\Delta\bar{S}_{mix} = kT \left( \frac{\phi_A}{N_A} \ln \phi_A + \frac{(1-\phi_A)}{N_B} \ln(1-\phi_A) + \chi\phi_A(1-\phi_A) \right) \quad (2-13)$$

The first two terms are from the contribution of the mixing entropy and become very small for long chains. Miscibility, in this case, depends strongly on the interaction parameter. In practice, the volume change on mixing and the local packing can affect the Flory-Huggins interaction parameter through an additional temperature independent additive constant. The Flory-Huggins interaction parameter is often written as<sup>15, 16</sup>

$$\chi = A + \frac{B}{T} \quad (2-14)$$

The temperature independent constant  $A$  accounts for an entropic component, while last term ( $B/T$ ) is the classical enthalpic contribution. The value (magnitude and sign) of the constants  $A$  and  $B$  depend strongly on the specific chemical components and may depend weakly on chain length.

The phase behavior is estimated by considering the temperature dependence of the free energy of mixing. The binodal phase boundary is determined by the common tangent of the free energy at a specific composition. The tangent is given by the first derivative of the free energy with respect to volume fraction, referred as the chemical potential ( $\mu$ ), therefore the common tangent of the free energy at the compositions

$\phi'$  and  $\phi''$  the corresponding to the two equilibrium phases characterizes the binodal phase boundary

$$\left( \frac{\partial \Delta \bar{F}_{mix}}{\partial \phi} \right)_{\phi=\phi'} = \left( \frac{\partial \Delta \bar{F}_{mix}}{\partial \phi} \right)_{\phi=\phi''} \quad \text{or} \quad \mu_{\phi=\phi'} = \mu_{\phi=\phi''} \quad (2-15)$$

The binodal curve for symmetric blend ( $N_A = N_B$ ) is obtained by setting the first derivative of the free energy of mixing with respect to the concentration to be zero

$$\left( \frac{\partial \Delta \bar{F}_{mix}}{\partial \phi} \right) = kT \left[ \frac{\ln \phi_A}{N_A} + \frac{1}{N_A} - \frac{\ln \phi_B}{N_B} - \frac{1}{N_B} + \chi(1 - 2\phi_A) \right] \quad (2-16)$$

Which leads to:

$$\chi_{AB}^{binodal} = -\frac{1}{1-2\phi} \left[ \frac{\ln \phi_A + 1}{N_A} - \frac{\ln \phi_B + 1}{N_B} \right] \quad (2-17)$$

The phase boundary of a symmetric blend ( $N_A = N_B$ ) delimited by the binodal line is shown in Figure 2.2 (solid line) as a function of the volume fraction for component A.

The spinodal curve is located between the metastable and unstable regions. Spinodal curve can be obtained by setting the second derivative of the free energy of mixing with respect to volume fraction to zero,

$$\left( \frac{\partial^2 \Delta \bar{F}_{mix}}{\partial \phi^2} \right) = kT \left[ \frac{1}{N_A \phi_A} + \frac{1}{N_B \phi_B} - 2\chi \right] \quad (2-18)$$

which yields

$$\chi_{AB}^{spinodal} = \frac{1}{2} \left[ \frac{1}{N_A \phi_A} + \frac{1}{N_B \phi_B} \right] \quad (2-19)$$

The phase boundary of the spinodal region for symmetric polymer blend is shown in Figure 2.2 (dashed line).

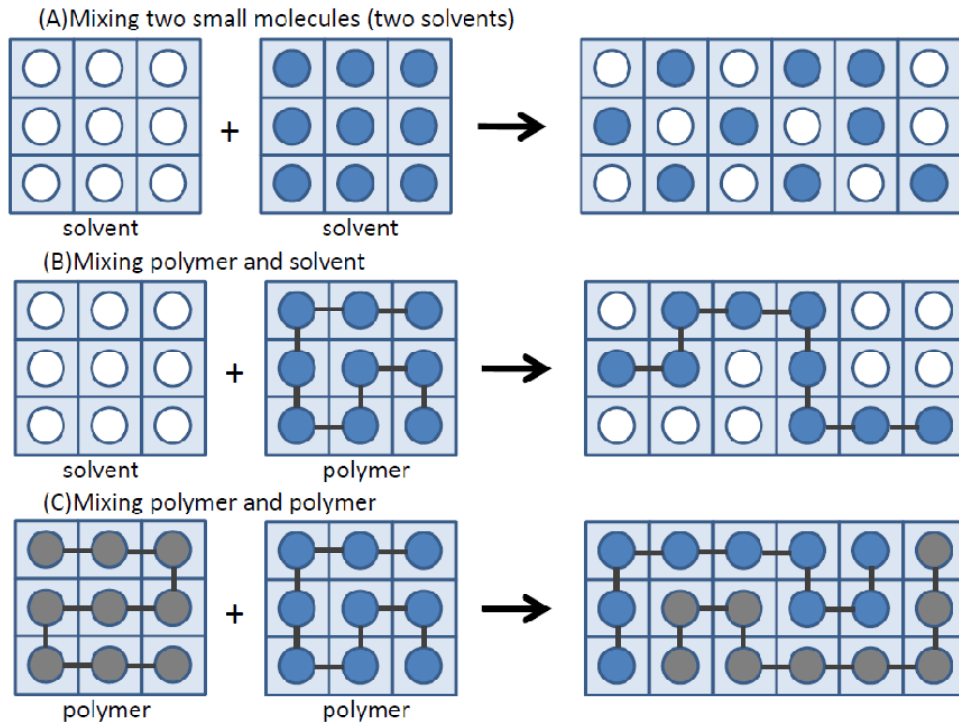


Figure 2.1 The Flory-Huggins lattice model: (A) mixing two solvent molecules, (B) mixing solvent and one polymer chain and (C) mixing two polymers (polymer blend).<sup>15, 16, 19</sup>

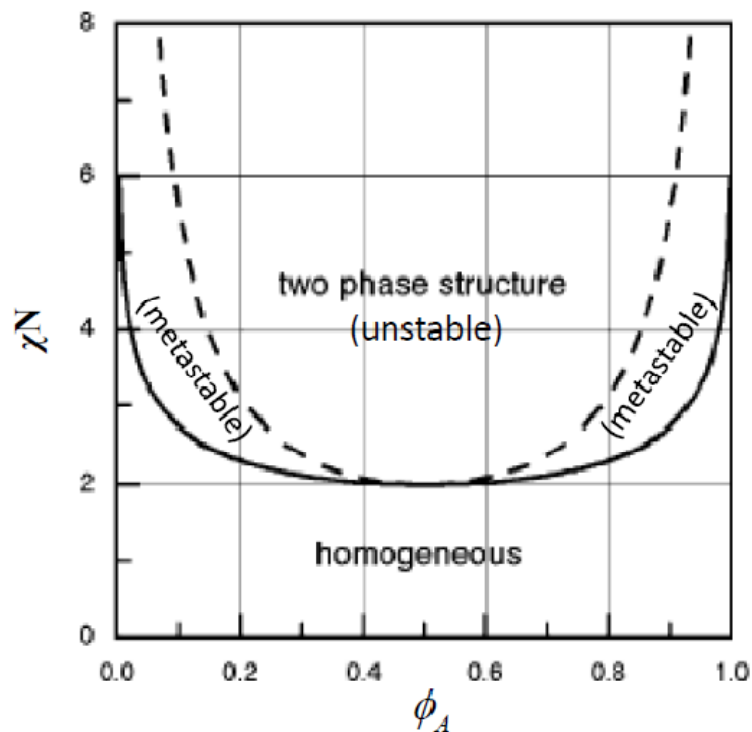


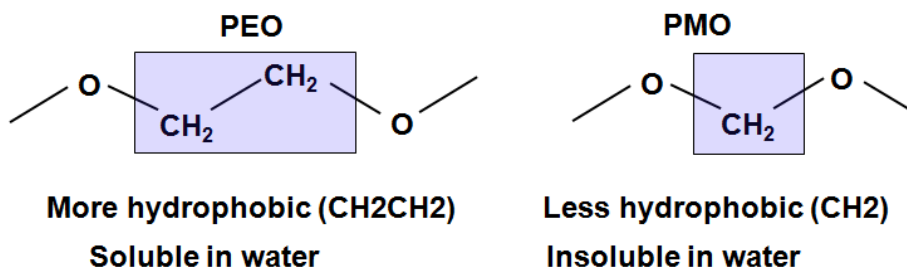
Figure 2.2 Phase diagram for a polymer blend with  $N_A = N_B = N$ . The binodal line is the solid curve and the spinodal line is dashed line.<sup>20</sup>

## 2.2 Aqueous PEO solution

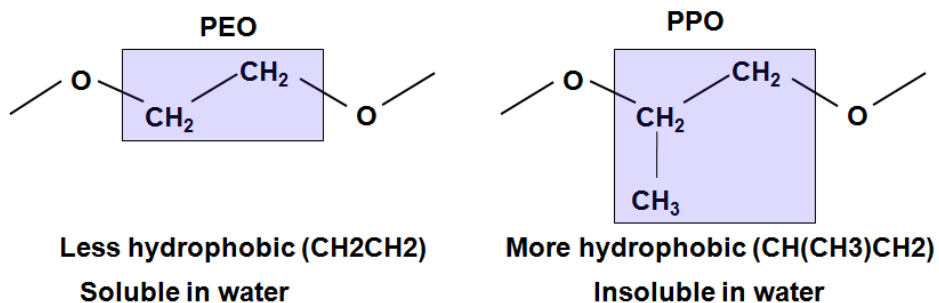
### 2.2.1 The solvation of ether group polymer in water

The solvation of PEO in water is believed to arise from hydrogen bonding between water and oxygen atoms in the PEO monomer. Hydrogen bonding involves a hydrophilic interaction. However, hydrogen bonding cannot explain PEO solvation in water when compared to other ether group polymers such as poly(methylene oxide) (PMO) or poly(propylene oxide) (PPO). Hydrocarbons (-CH<sub>2</sub>-) give rise to hydrophobic effect in water. Let's compare PEO with PMO. PEO has ethylene groups (CH<sub>2</sub>CH<sub>2</sub>) on the backbone while PMO has methylene groups (CH<sub>2</sub>) so one expects

that PEO is more hydrophobic than PMO. However, PEO dissolves in water but PMO does not.



Comparing PEO with PPO, PPO has one more methylene group than PEO which indicates that PPO is more hydrophobic than PEO. As expected, PPO does not dissolve well in water, PEO dissolves in water over a wide temperature range (0 °C – 100 °C) while PPO dissolves in water only over a narrow temperature range.



Based on such observations, the solvation of PEO in water cannot be explained using simple hydrogen bonding arguments. The solvation of molecules having both hydrophilic and hydrophobic sites should be explained in terms of both hydrophobic effects and hydrogen bonding. PEO solvation is believed to arise from the formation

of a hydration shell around the PEO chain. The hydration shell behaves as a protection sheath to prevent water from contacting the ethylene groups.

### **2.2.2 Solvation and thermodynamics**

As mentioned earlier, PEO is a widely researched synthetic water-soluble polymer. The monomer structure and dimensions are found to be key factors in understanding the solvation of ether group containing polymers in water.<sup>7, 21</sup> The distance between oxygen atoms along PEO chains in water is 2.85 Å and 4.85 Å for nearest and next-nearest neighbors respectively as measured by neutron/ X-ray diffraction and as calculated from molecular dynamics simulation.<sup>7, 22-24</sup> The distance between adjacent oxygen atoms in PEO single crystals as measured by X-ray diffraction is 2.88 Å and the distance between adjacent oxygen atoms in the liquid state PEO is 2.85 Å. The schematic model is shown in Figure 2.3.

Such similar dimensions in the liquid and solid states suggest that the structure of PEO in the liquid state may adopt a slightly distorted helical structure. Based on the solubility difference between the ether group containing polymers and the distance between oxygen-oxygen atoms in PEO and in water, a solvation model of PEO in water has been suggested to consist of polymer chains embedded into the hexagonally packed water structure via hydrogen bonding between PEO oxygen atoms and the hydrogen atoms of water. This structural solvation model describes the water cage around PEO chains and results in the formation of a hydration shell around the PEO chain. Two water molecules are needed to hydrate a PEO monomer based on the packing geometry. This is not sufficient to form a complete hydration shell around the

polymer chains unless each water molecule participates in the shell from neighboring chains. Figure 2.4 represents a schematic model for the electrostatic potential map of PEO chains used for predicting solvation via hydrogen bonding between hydrogen atoms in water and oxygen atoms in PEO. Simulation studies predicted that the highly negative electrostatic potential regions (in blue) are formed around ether oxygens (red) in PEO chains as shown in Figure 2.4 (A). Considering the dimensions in liquid state PEO, the solvated PEO chains in water are believed to form helical structures as discussed earlier. The contour map of negative potential along the chain estimated through simulation is shown in Figure 2.4 (B). Water molecules are believed to form a hydration shell along the negative potential region of PEO via hydrogen bonding although there is currently no experimental evidence for helical structures. The hydrogen bonding between water molecules and PEO rearranges the water molecules near the PEO chain to form a highly directional water structure, resulting in a loss of entropy; the negative entropic change comes from the loss of conformational freedom in forming the hydration shell around the PEO chain.

Generally, the strength of hydrogen bonding is sensitive to temperature. The strength of hydrogen bonding between water molecules becomes weaker as the temperature is increased and has been characterized by Raman or IR spectroscopy.<sup>25-</sup>  
<sup>28</sup> The hydration shell in PEO solution is disrupted at high temperature due to lower hydrogen bonding strength. Smith and coworkers studied hydrogen bonding between PEO and water using molecular dynamics simulations to extend the understanding on the phase behavior of aqueous PEO solutions. The simulation results showed the characteristics of a lower critical solution temperature (LCST).<sup>7, 28-31</sup> The number of

water molecules participating in hydrogen bonding with PEO was calculated and monitored as a function of temperature as shown in Figure 2.5. They observed a decrease in the number of water molecules participating in hydrogen bonding as the temperature increased. This decrease in the number of hydrogen bonds leads to a decrease in the solvation driving force. The estimated phase boundary was located around 450 K – 500 K depending on the PEO concentration.<sup>31-34</sup> A thermodynamic model for the PEO-water system has been developed by different researchers in an attempt to understand aqueous PEO solutions and the role of hydrogen bonding.<sup>21, 35-37</sup> A primitive model of a LCST system was introduced by Hirschfelder and coworkers which explained the formation of a LCST through short range ordered molecules when polar solvents (water or alcohol) are used.<sup>36</sup> Based on this idea, Wheeler developed a lattice model to describe the LCST and UCST behaviors.<sup>38</sup> Karlstrom constructed a thermodynamic model based on the Flory-Huggins theory, and adapted Hirschfelder's model (which used an attractive potential at short range and low temperature and a dominant repulsive long range force at increased temperatures) to explain the UCST and LCST behaviors.<sup>16, 18, 37, 38</sup>

A simple and successful description of hydrogen bonding between PEO and water was presented by Matsuyama et al.<sup>30</sup> They presented a molecular theory, incorporated a hydrogen bonding term in the Flory-Huggins theory to explain LCST behavior of PEO solutions. The theory showed that the hydrogen bond formation between PEO and water molecules can be the major cause of the miscibility gap and the system can exhibit a closed-loop phase behavior.<sup>39, 40</sup> Intramolecular interactions were ignored and the competition between inter- and intra-molecular hydrogen bonding effects was

not considered. The most advanced theory for the hydration of aqueous PEO has been presented by Dormindntova which accounted for both intermolecular and intramolecular hydrogen bonding.<sup>29</sup> The theory used a statistical thermodynamics concept and explained the hydration behavior by incorporating both enthalpic and entropic effects as a function of temperature. The calculated phase diagram showed excellent agreement with experimental data. The results of different experimental groups concerning the phase behavior of PEO in aqueous solutions are shown in Figure 2.6.<sup>29, 41-43</sup> As seen in Figure 2.6, there is a general agreement between the theoretical curves and experimental data. The shapes of the curves and the decrease in LCST (increase in UCST) with increase degree of polymerization  $N$  are consistent with experimental observations.

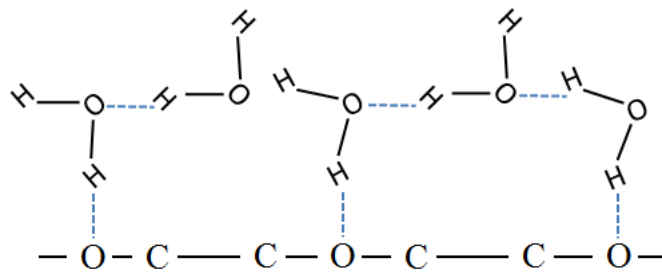


Figure 2.3 Schematic for hydration of PEO based on geometric dimension.<sup>7</sup>

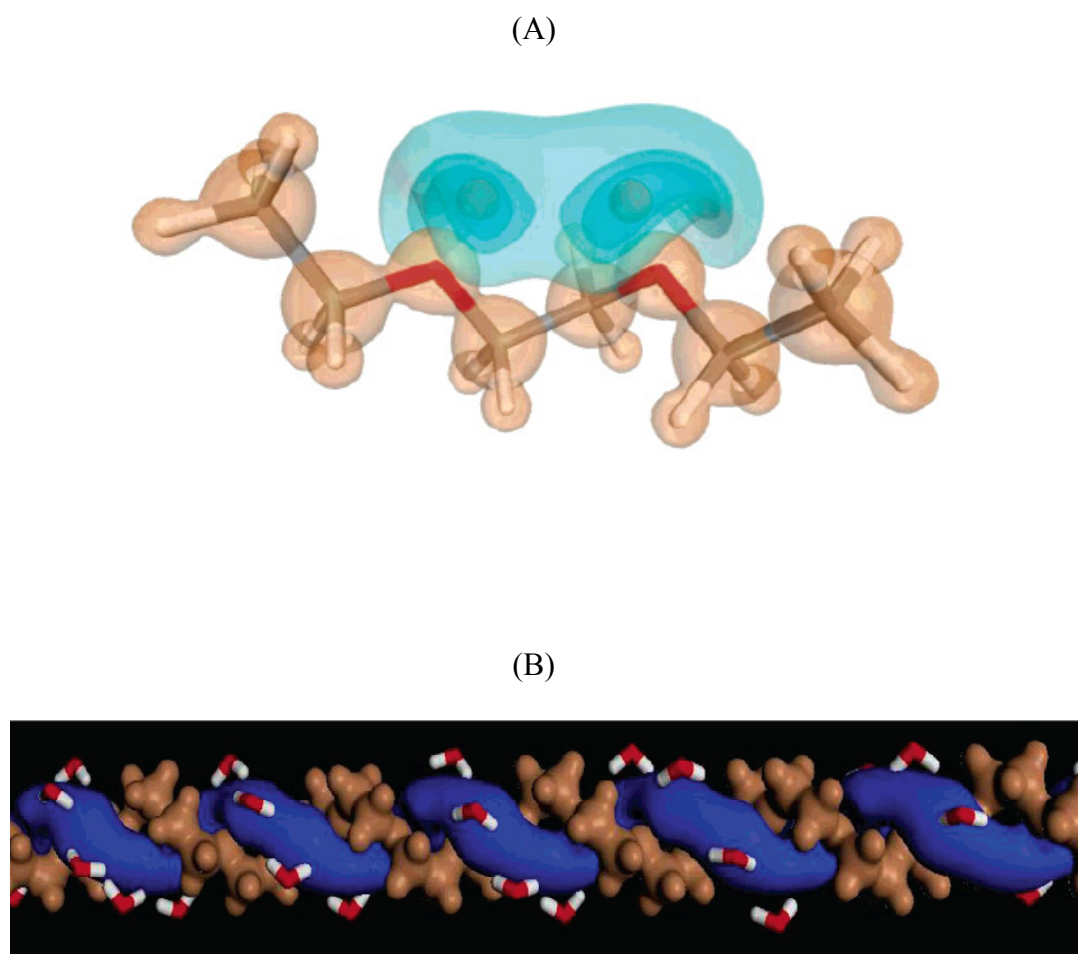


Figure 2.4 Schematic contour map of PEO based on the electrostatic potential. (A) Contour map of 3-D electrostatic potential of PEO chain: Blue denotes the negative potential zone and brown is the positive potential zone induced by the PEO chain. (B) Electrostatic potential induced by water oxygen and brown represents positive potential zones. Red is oxygen which accounts for the electron rich region.<sup>44</sup>

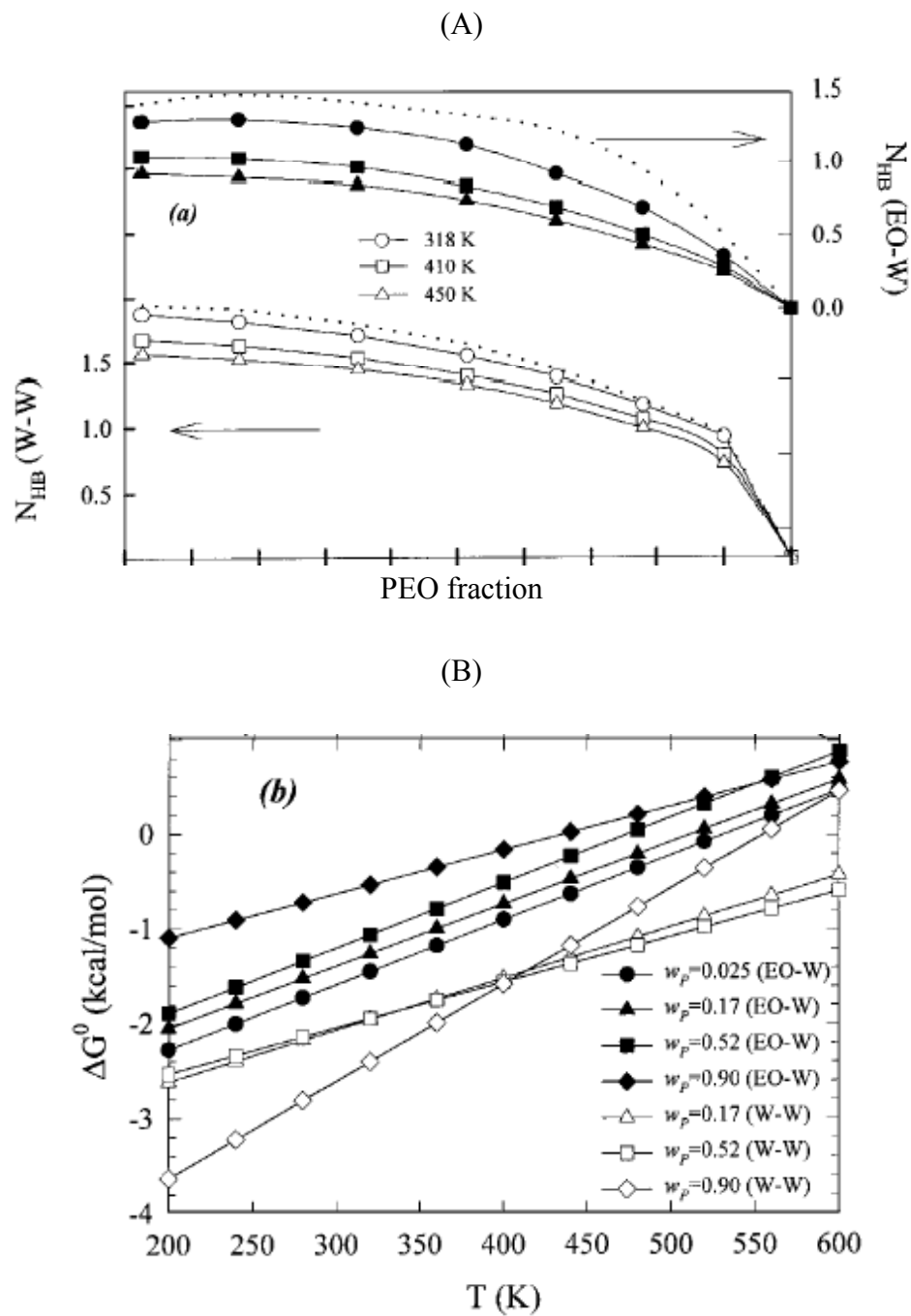


Figure 2.5 Simulation results (A) showing the number of hydrogen bonds : closed symbols are for PEO-water (EO-W) and open symbols are for water-water(W-W) (B) free energy calculated from the simulation data.<sup>31</sup>

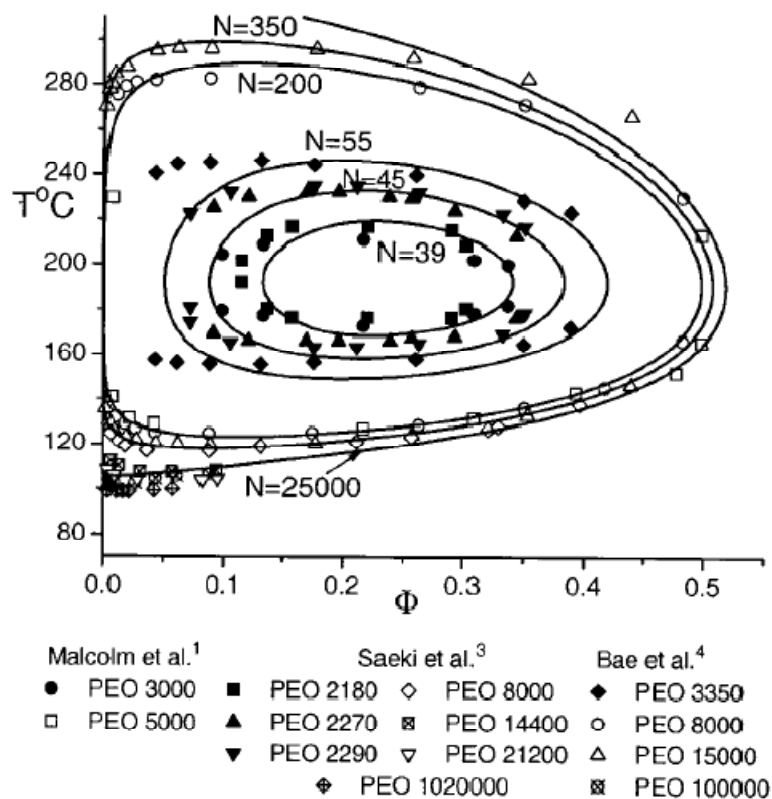


Figure 2.6 Phase diagram for aqueous solutions of PEO. Experimental data are represented by symbols and theoretical curves are all calculated using the same parameters.  $N$  is the degree of polymerization.<sup>29</sup>

### 2.2.3 Clustering of PEO in aqueous medium

The clustering (or aggregation) has been observed in water soluble polymers and there is interest in understanding its origin and identification.<sup>45-47</sup> Aggregation has been found in various water soluble polymer systems including neutral polymers (e.g. PEO) and polyelectrolyte solutions.<sup>48</sup> Light/X-ray/neutron scattering, dynamic light

scattering (DLS) and gel permeation chromatography (GPC) have been used to identify PEO clustering in aqueous solutions.<sup>4, 49, 50</sup>

Devanand et al. studied impurity effects on aggregation behavior of PEO in water using dynamic light scattering of dilute aqueous PEO solutions.<sup>51</sup> They measured the hydrodynamic radius and diffusion coefficient as a function of molecular weight after filtration with 0.2  $\mu\text{m}$  pore size filter and did not find any evidence for aggregation. This result implied that impurities such as dust can be a possible origin of aggregation. Poverari et al confirmed the coexistence of single chain and clusters and filtration effect with a 0.22  $\mu\text{m}$  filter.<sup>52</sup> Clusters are removed by filtration but begin to reform spontaneously with time. Ho et al. measured the hydrodynamic radii of aqueous PEO solutions before and after filtration with a 0.1  $\mu\text{m}$  filter using dynamic light scattering.<sup>50</sup> The experimental results are shown in Figure 2.7. The hydrodynamic radius distribution for an unfiltered aqueous PEO solution, Figure 2.7 (A), exhibited the two distinct peaks representing the hydrodynamic radii of single chains and aggregated chains respectively. They confirmed the disappearance of the aggregation peak after filtration in Figure 2.7 (B). The aggregation peak, however, reappeared after one day as shown in Figure 2.7 (C). This confirmed that the filtration eliminates clustering in aqueous PEO solution but clusters reform over time.

One possible origin of the clustering in aqueous PEO solutions is chain end group effect. Hammouda et al. performed systematic experiments varying chain ends in aqueous PEO solutions.<sup>53</sup> They measured SANS intensities of aqueous PEO solutions with different chain ends:  $\text{CH}_3\text{O-PEO-OCH}_3$ ,  $\text{HO-PEO-OCH}_3$  and  $\text{HO-PEO-OH}$ . The  $\text{CH}_3\text{O-}$  chain end is relatively hydrophobic whereas  $\text{HO-}$  end group is hydrophilic.

All samples exhibited clustering behavior in water regardless of end group as shown in Figure 2.8 (A). The magnitude of clustering is defined by an intensity at  $Q = 0.004 \text{ \AA}^{-1}$  which is obtained from fitting the SANS data. The magnitude of clustering depends on the type of chain end as shown in Figure 2.8 (B). PEO having hydrophobic end groups on both ends exhibits the largest clustering magnitude whereas PEO with hydrophilic end groups shows the lowest clustering. From these observations, it is concluded that chain end effects are one of the causes of PEO clustering even though chain ends are only a small fraction of the polymer. This explanation becomes clearer for the case of other kinds solvents such as methanol and benzene. Benzene is a strongly hydrophobic solvent compared to water or methanol. The SANS intensity of PEO in benzene is shown in Figure 2.9. Clustering is clearly affected by changing polymer chain end groups. When both chain ends are hydrophilic (HO) high clustering intensity was observed. The clustering intensity, however, disappears completely in the case of hydrophobic groups ( $\text{CH}_3\text{O}-$ ) on both ends.

A practical application of PEO aggregation is found in liquid drag reduction. Small quantities of dissolved polymers (e.g., PEO) can reduce considerably the frictional drag exerted by a liquid.<sup>46, 47, 54</sup> The mechanism of drag reduction is still not well understood.

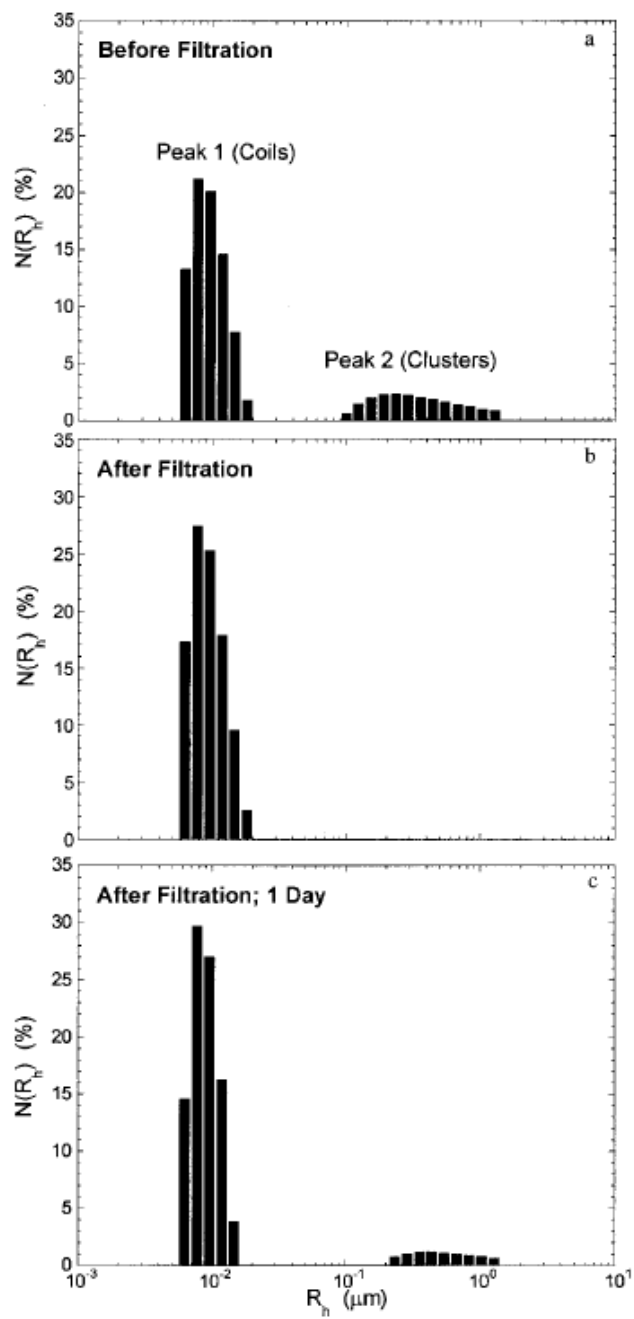


Figure 2.7 Histogram of  $N(R_h)$  for aqueous PEO solution (0.025 wt %).<sup>50</sup>

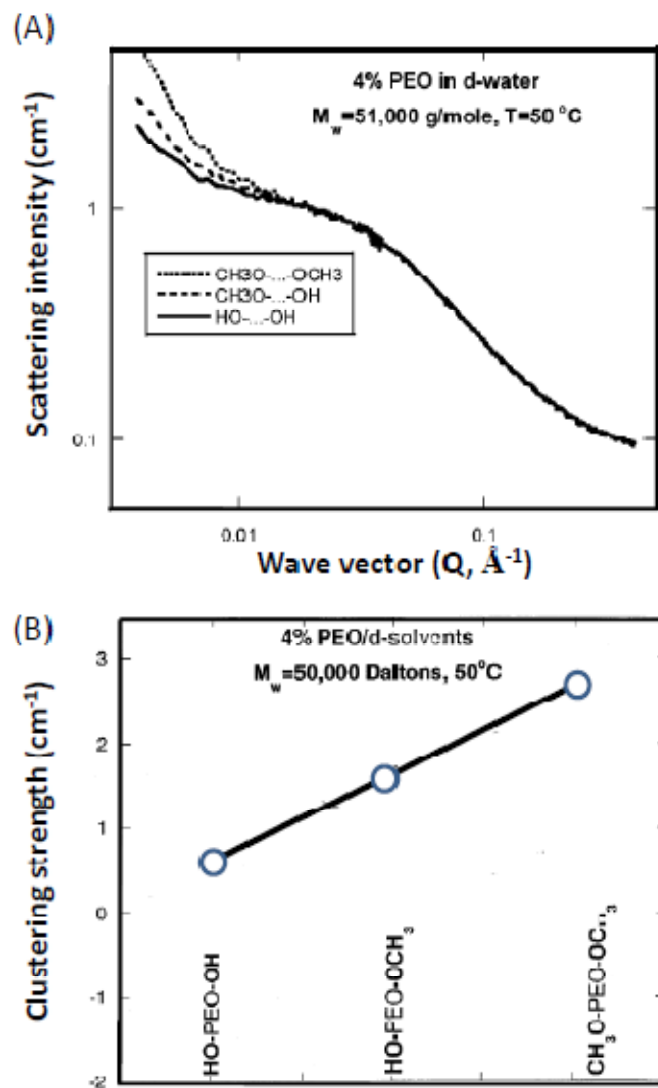


Figure 2.8 End group effect on clustering: (A) SANS intensity and (B) clustering strength defined by  $A/(0.004)^n$  with varying chain end group.  $A$  and  $n$  are obtained from fitting SANS intensity.<sup>53</sup>

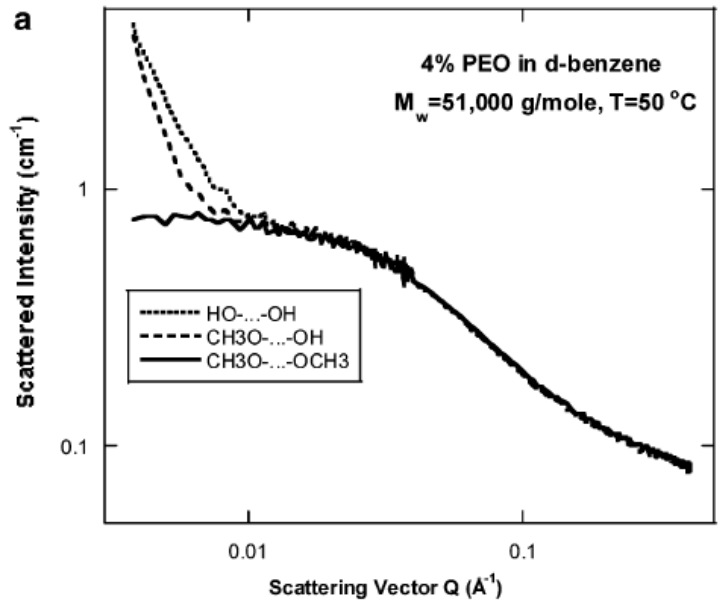


Figure 2.9 SANS intensity of PEO in d-benzene with different chain ends. D-benzene is relatively hydrophobic compared to water. The clustering magnitude becomes higher as chain end becomes more hydrophilic.<sup>53</sup>

## Chapter 3

### Experimental methods

#### 3.1 Scattering method

Scattering techniques are widely used as tools for characterizing the microscopic structure in condensed matter, including polymers and biomolecules and soft matter in general.<sup>17, 48</sup> Light scattering is a relatively simple and convenient technique. It is also possible to probe complex systems using X-ray and neutron scattering in user facilities. Choosing a scattering technique depends on the probed system (size scale and materials). For small-angle scattering, the probed length scale is in the range of 10 Å - 1000 Å.<sup>17, 48, 55</sup> Scattering arises from variations in the refractive index of samples in the case of light, from fluctuations in the electron density in the case of X-rays and in the neutron scattering length, in the case of neutrons. While the theoretical basis of scattering remains the same, the choice of radiation is dependent on the presence of contrast. In this work neutron scattering was used because the scattering contrast could be enhanced through the use of deuterium-labeled species. The summary given in this chapter is similar to the discussion found in Squire and Hammouda.<sup>17, 56</sup>

##### 3.1.1 Neutron scattering

Neutron scattering has been used for a long time. This technique gained prominence when the 1994 Nobel Prize in physics was awarded to Bertram Brockhouse and Clifford Schull for their pioneering work in neutron scattering. Due to their penetrating power, isotope sensitivity and magnetic moment, neutrons have been used extensively to study both hard crystalline materials and soft matter such as biological and synthetic polymer systems. Soft materials have relevant length scales that are larger than the atomic length scale. Their study has become widely possible by the advent of 'cold' neutron sources that produce neutrons with longer wavelengths, (lower velocities) compared to 'thermal' neutrons.

At first, neutron probes are non-destructive due to their lower kinetic energy compared to X-rays. One of the differences of fundamental importance between X-rays and neutrons is the respective energies. Whereas the energy of an X-ray photon used for materials characterization is of order of 10 keV, the kinetic energy of a thermal neutron is of order of 10 meV. Kinetic energies from atomic and molecular motions are around 20 meV. Thus, when X-rays are scattered by matter even when there is an exchange of energies between the motion of atoms and the X-ray photon, the energy of the photon is affected. This is very important for most fragile, soft matter and biological systems. X-rays interact strongly with samples and can cause radiation damage, particularly in soft materials.

Neutrons can distinguish between isotopes, since neutron scattering lengths vary in a non-systematic manner. This is because neutrons interact with atomic nucleus while X-rays interact with the electron cloud. Isotopic labeling can be used to probe structural information in detail. The advantage and uses of isotopic labeling will be

discussed in terms of varying the scattering length density later. Moreover, due to the high penetrating ability of neutrons they can be employed to study thick samples which cannot be studied with X-rays.

### 3.1.2 Scattering theory

Neutron scattering occurs either through interactions with the nucleus (called nuclear scattering) or through interactions between the neutron's magnetic moment and unpaired electrons (called magnetic scattering). A scattering experiment measures the intensity of scattered waves by the sample. In an elastic scattering experiment, the incident and scattered waves have the same energy, and information on the time averaged structure of the sample can be obtained. When the scattering is inelastic, the change in energy of the neutron is used to obtain information about the sample dynamics. In this work, we are concerned with structure determination and hence focus on elastic scattering only.

Neutron scattering results from the strong nuclear forces between the nucleus and the incident neutrons. The range of nuclear forces between the neutron and the nucleus (interaction potential) is on the order of  $10^{-15}$  m which is much shorter than the wavelength of the neutron. The nucleus is treated as a fixed point. A schematic of the scattering process is shown in Figure 3.1. Scattering depends on the interaction potential,  $V(r)$ , between the neutron and the nucleus (separated by distance  $r$ ) from a quantum mechanical viewpoint. The potential is very short range and falls rapidly to zero at within a distance of  $10^{-14}$  m -  $10^{-15}$  m, which is much shorter than the

wavelength of a neutron which is on the order of 1 Å ( $10^{-10}$  m).<sup>17, 56</sup> As a result the nucleus acts as a point scatterer and diffraction theory can be applied.

Take the origin to be at the position of nucleus, and the x-axis to be along the direction of  $k$ , the wave vector of the incident neutrons as shown in Figure 3.1.<sup>56</sup> The incident neutron beam can be represented by a plane wave with wavefunction

$$\psi_{inc} = \exp(ikx) \quad (3-1)$$

where  $x$  is the distance from the nucleus along the neutron propagation direction and  $k$  is the wavenumber defined by  $2\pi/\lambda$ . The scattered wave is spherically symmetric as a result of scattering from nucleus which is a point scatterer. Then the scattered wave can be represented by the wavefunction

$$\psi_{sc} = -\frac{b}{r} \exp(ikr) \quad (3-2)$$

where  $b$  is the nuclear scattering length of the nucleus and represents the interaction between the neutron and the nucleus. The minus sign corresponds to a positive value of  $b$  for a repulsive potential.

The quantity  $b$ , appearing in Eq (3-2), is known as the scattering length. In general, the scattering length is a complex number. The imaginary component represents neutron absorption for nuclei. The neutron absorption becomes important for nuclei that have a high absorption coefficient such as boron and cadmium. The imaginary part of the scattering length is generally very small and is usually treated as

a real quantity. The value of scattering length depends on the particular nucleus and varies in a nonsystematic manner across the periodic table, and depends on the spin state of the nucleus-neutron system. It also varies between isotopes of the same element. A useful example of this is the difference between hydrogen and deuterium ( $\text{H}({}^1\text{H})$  and  $\text{D}({}^2\text{H})$  respectively). Hydrogen has a coherent scattering length of  $-3.74 \times 10^{-5} \text{ \AA}$  and deuterium  $6.67 \times 10^{-5} \text{ \AA}$ .<sup>56</sup> Thus the scattering length of a molecule which includes hydrogen can be changed by replacing hydrogen with deuterium. This technique of contrast variation using isotopes is one of the advantages of neutron scattering over X-ray and light scattering. The scattering lengths of some elements are shown in Table 3.1.

In a typical elastic scattering experiment, the number of scattered neutrons in a particular direction is counted as shown in Figure 3.2. When the distance from the detector to the sample,  $r$ , is large, then the probability of a neutron being scattered into a solid angle  $d\Omega$ , is defined as a differential scattering cross section (in the direction  $\theta, \varphi$ )

$$\frac{d\sigma}{d\Omega} = \frac{\textit{number of neutrons scattered per second in } d\Omega}{\textit{number of incident neutrons per second}} \quad (3-3)$$

and is equivalent to the effective area that the nucleus presents to the incident neutron in the direction  $d\Omega$ . The total scattering cross section is obtained by integrating over all solid angles

$$\sigma = \int \frac{d\sigma}{d\Omega} = 4\pi b^2 \quad (3-4)$$

so that  $\sigma$  has the dimension of area. Physically, the cross-section represents the effective area presented by the target nucleus to the incident neutrons. As mentioned previously, the scattering length of a target nucleus depends not only on nucleus, but also on its spin state.

The value of the scattering length of a single element depends on the isotope and the spin state. If the value of  $b$  varies due to the presence of isotopes and/ or varying nuclear spin states and the value of  $b_i$  occurs with relative frequency  $f_i$ , with  $\sum_i f_i = 1$ , then the average value for  $b$  and  $b^2$  can be defined as

$$\bar{b} = \sum_i f_i b_i \quad \bar{b}^2 = \sum_i f_i b_i^2 \quad (3 - 5)$$

Here, we assume that there is no correlation between the values of  $b$  for any two nuclei. As a result of the distribution of scattering lengths, the total cross section separates into two components: a coherent part and an incoherent part. The total cross section is a sum of two components

$$\sigma_{total} = \sigma_{coh} + \sigma_{incoh} \quad (3 - 6)$$

The coherent cross section,  $\sigma_{coh}$ , represents scattering that can produce interference from correlations between nuclear positions. Thus coherent scattering cross section provides structural information. The incoherent scattering involves scattering from individual nuclei. Thus incoherent cross section does not contain structural information. The two forms of scattering are related to the mean and variance of the scattering length

$$\sigma_{coh} = 4\pi\langle b \rangle^2 \quad \sigma_{incoh} = 4\pi(\langle b^2 \rangle - \langle b \rangle^2) \quad (3-7)$$

The brackets,  $\langle \rangle$  denotes the ensemble average of the quantity within the brackets. Only the coherent part of the scattering cross section contributes to the scattering signal while the incoherent part contributes to a  $Q$ -independent background to the scattering. As photons do not have any spin, there is no strict analog in X-ray or light scattering with the incoherent scattering of neutrons.

As discussed previously, neutron scattering is a powerful technique for probing soft matter due to the power of the deuterium labeling method and the low neutron kinetic energy compared with other scattering techniques.<sup>17, 48</sup> A schematic of the neutron scattering process is shown in Figure 3.3 and its instrumental components are shown in Figure 3.5. The small-angle neutron scattering technique was introduced to study the structure of large length scales found in high molecular weight materials and materials with nanoscale structure for which the probing length scale is much larger than atomic dimensions. Small-angle neutron scattering (SANS) is used to determine the large scale structure of macromolecules such as molecular

conformations, morphology and supra-molecular structure. Scattering data are expressed as function of wave vector,  $Q = (4\pi/\lambda)\sin\theta/2$ , defined by the difference between incident wave vector and scattered wave vector as shown in Figure 3.3. In a typical experiment, scattering is the result of interference of waves scattered by multiple scattering units/atoms that compose the sample. For coherent scattering, the amplitudes of the scattered waves are added and the measured scattering intensity is the square of the resulting amplitude. Consider the scattering from two points separated by a distance  $r$  as shown in Figure 3.1. An incoming wave with wave vector  $k_0$  scatters off points O and P such that the scattered beam is in the direction given by  $k_1$  as shown in Figures 3.1 and 3.3. In complex notation, a scattered wave can be written as  $e^{i\delta}$ , where the phase  $\delta$  is  $2\pi/\lambda$  times the distance traveled from an arbitrary reference point. With a path difference of  $r$ , the phase difference between the waves scattered from the two points is given by

$$\delta = \frac{2\pi}{\lambda} r \cdot (k_0 - k_1) \quad (3-8)$$

Then the scattering amplitude in the direction  $k_1$  from the two point scatterers is given by

$$A(Q) = \sum b(r) e^{iQ \cdot r} \quad (3-9)$$

$Q$  is the scattering wave vector and  $b(r)$  is the bound scattering length of the scattering objects at  $r$ . The bound scattering length assumes that the target molecules are fixed and there is negligible energy transfer from the neutron. In terms of a macroscopic view, the number of scatterers is large and the sum can be replaced by an integral

$$A(Q) = \int d^3r \rho(r) e^{iQ \cdot r} \quad (3-10)$$

where  $\rho(r)$  is the scattering length density (SLD) which describes the scattering length per unit volume and the integral is over the volume of the object. The scattering length density of a molecule composed of  $N$  known elements can be calculated as

$$\rho = \sum_i^N \frac{b_i}{\bar{V}_i} \quad (3-11)$$

where  $\bar{V}_i$  is the volume of component  $i$ .

The scattering intensity,  $I(Q)$ , is the absolute square of the scattering amplitude

$$I(Q) = A^* A = \iint d^3r_1 d^3r_2 \rho(r_1) \rho(r_2) e^{iQ \cdot (r_1 - r_2)} \quad (3-12)$$

Since the double integral involves only the relative distance,  $|r_1 - r_2|$ , between every pair of points in the probing object, the integration can be divided into two steps: (1) integrate over all points with equal relative distances, and (2) integrate over all

possible relative distances. The magnitude of integration over all points with equal relative distances is a measure of correlations between the scattering length densities at all points in the sample separated by a distance  $r$  ( $r$  is constant distance)

$$\overline{\rho(r)^2} = \int d^3r \rho(r_1)\rho(r_2) \quad (3-13)$$

We can represent the scattering intensity with Eq (3-13) as

$$I(Q) = \frac{1}{V} \iint d^3r \overline{\rho(r)^2} e^{iQ \cdot r} \quad (3-14)$$

Let's consider a simple scattering system such as a spherical particle dispersed in a solvent medium. If this system is assumed to be incompressible, the coherent scattering intensity can be modeled as

$$I(Q) \approx P(Q)S(Q) \quad (3-15)$$

where  $P(Q)$  is the single particle form factor which represents the interference of neutrons scattered from different parts of the scattering object, and  $S(Q)$  is the inter-particle structure factor which accounts for scattering from different objects. Note that  $P(Q = 0)$  goes to 1 and  $P(Q = \infty)$  goes to 0. Generally,  $S(Q = \infty)$  goes to 1 due to correlation decay and  $S(Q)$  has a peak corresponding to the average particle inter-distance (the so-called coordination shell) in the case of concentrated systems where

the inter-particle distance is of the same order of magnitude as the particle size. The inter-particle distance is much larger than the particle size for dilute systems for which  $S(Q)$  is not expected to have a peak.

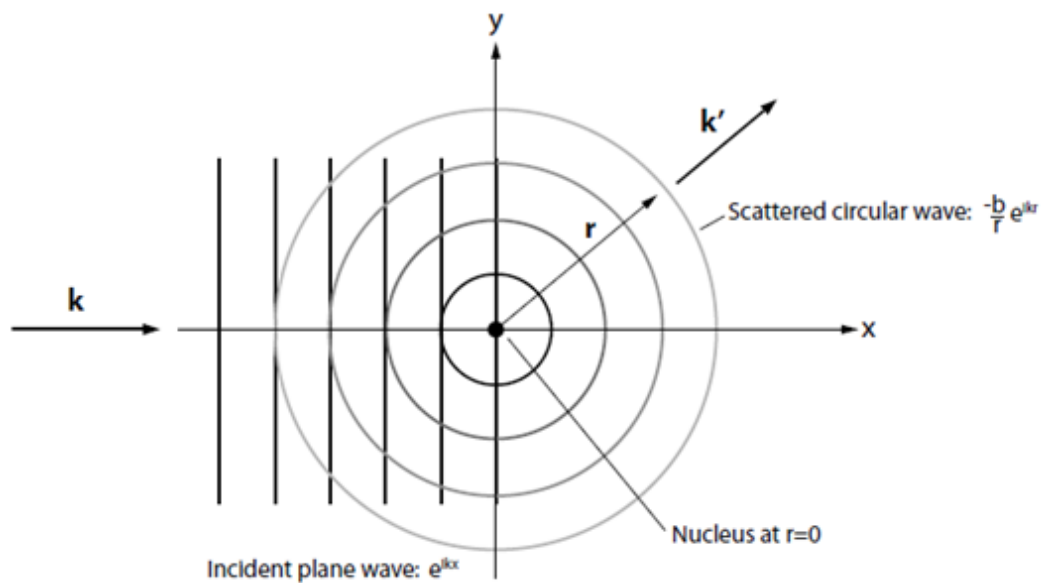


Figure 3.1 Elastic neutron scattering from a fixed nucleus.<sup>56</sup>

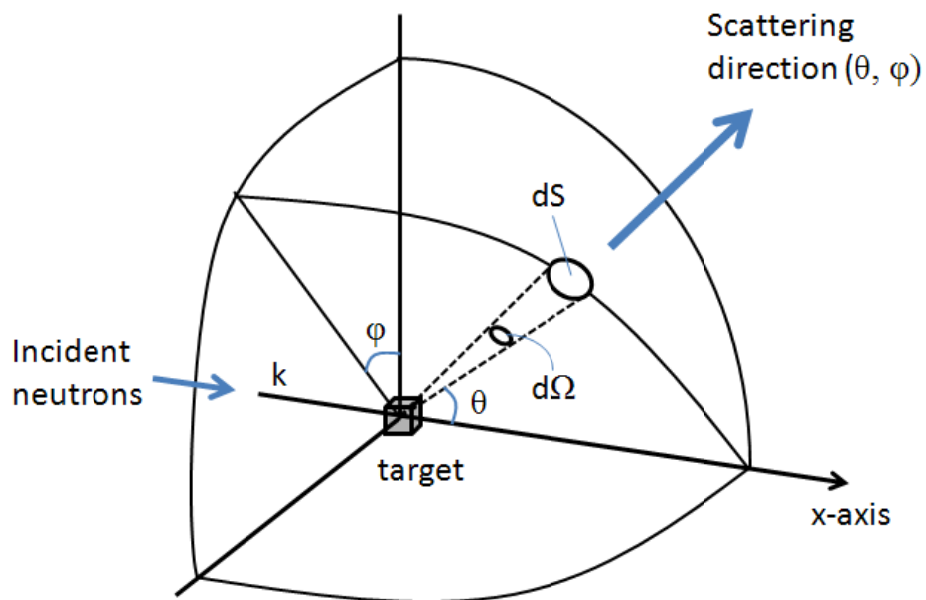


Figure 3.2 Geometry of scattering.<sup>56</sup>

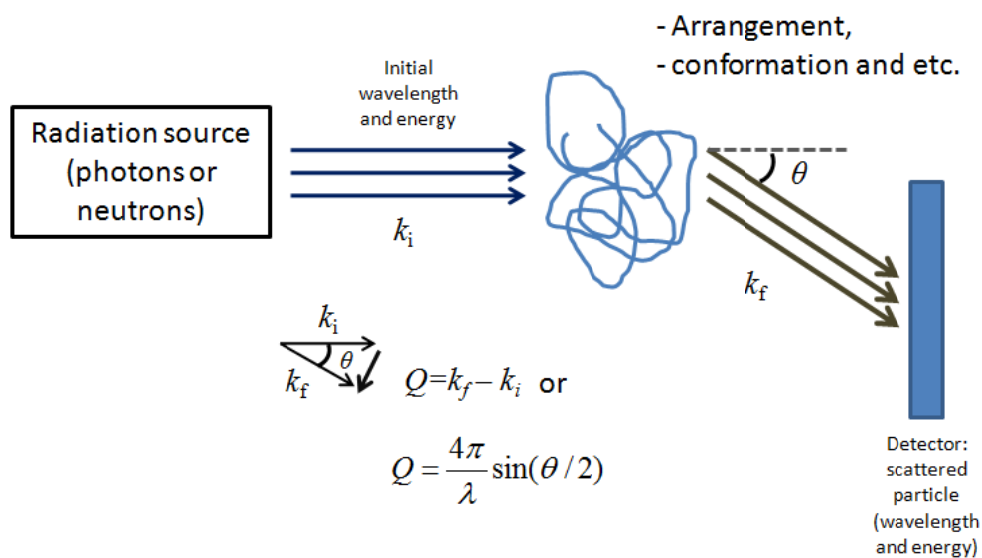


Figure 3.3 Schematic illustration of scattering. Intensity is measured as a function of wave vector,  $Q$ .<sup>17, 56</sup>

### 3.1.3 Contrast variation in neutron scattering

Consider a system composed of two phases with different scattering length densities  $\rho_1$  and  $\rho_2$  as shown in Figure 3.4 and assume that the system is incompressible. The total volume  $V$  is the sum of each volume ( $V = V_1 + V_2$ ). Then Eq (3-12) and (3-14) are divided into two sub volumes

$$I(Q) = \frac{1}{V} \left| \int_{V_1} dr_1 \rho_1 e^{iQ \cdot r} + \int_{V_2} dr_2 \rho_2 e^{iQ \cdot r} \right|^2 = \frac{1}{V} \left| \int_{V_1} dr_1 \rho_1 e^{iQ \cdot r} + \rho_2 \left( \int_V dr e^{iQ \cdot r} - \int_{V_1} dr_1 \rho_1 e^{iQ \cdot r} \right) \right|^2 \quad (3-16)$$

The above equation is reduced to (after removing the zero value terms),

$$I(Q) = \frac{1}{V} (\rho_1 - \rho_2)^2 \left| \int_{V_1} dr_1 e^{iQ \cdot r} \right|^2 = \frac{1}{V} \Delta\rho^2 \left| \int_{V_1} dr_1 e^{iQ \cdot r} \right|^2 \quad (3-17)$$

where the difference in scattering length densities contains some material properties (density, composition) as well as radiation properties (scattering lengths), while the integral term describes the spatial arrangement of the material. The difference in scattering length densities is called the contrast factor. Eq (3-17) leads to the Babinet principle which shows that two identical systems except for the interchange of their scattering length densities gives rise to the same coherent scattering although the incoherent term may be different. Thus it is important when designing SANS experiments to consider the appropriate use of contrast variation in order to determine the sample structure. Contrast variation often uses the partial deuteration method.

The deuteration method consists in replacing hydrogen by deuterium and therefore changing the scattering length density. Assuming a binary polymer mixture of identical chains with one deuterated (D) and the other protonated (H), the two polymers exhibit contrast due to the difference in their neutron scattering lengths,  $b_D$  and  $b_H$ . Assume that the volumes of D and H are the same. When the volume fractions of polymers are denoted  $\phi_D$  and  $\phi_H$  respectively, then the scattering intensity is given by:

$$I(Q) = \frac{N}{V} (b_D - b_H)^2 \phi_D \phi_H P(Q) S(Q) \quad (3-18)$$

The above equation is similar to Eq (3-15) but scaled by the difference in scattering length densities squared and by the compositions.

Table 3.1 Scattering lengths and cross-sections of some common elements<sup>56</sup>

Element	$b$ ( $10^{-12}$ cm)	$\sigma_{\text{coh}}$ (barns)	$\sigma_{\text{incoh}}$ (barns)
Hydrogen	-0.374	1.760	79.70
Deuterium	0.667	5.597	2.04
Carbon	0.665	5.590	0.00
Nitrogen	0.930	11.100	0.00
Oxygen	0.580	4.230	0.00
Sodium	0.363	1.660	1.62
Phosphorous	0.513	3.310	0.00
Chlorine	0.958	11.530	5.90

unit: 1 barn =  $10^{-18}$  m<sup>2</sup>

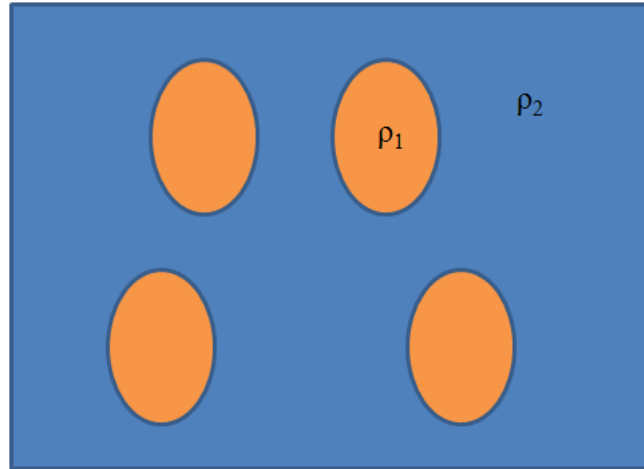


Figure 3.4 A system containing two phases with different scattering length densities  $\rho_1$  and  $\rho_2$ .<sup>17</sup>

### 3.1.4 Data from small-angle neutron scattering

Small-angle scattering provides information on the system where the length scale is much larger than the atomic dimensions so that it yields materials properties such as density and composition. One of the simplest analysis methods is to look at the limiting values of  $I(Q)$ . In the limit of  $Q \rightarrow 0$ , we are looking at the scattering objects on a length scale much larger than the objects. For an isotropic system the phase factor can be replaced by its orientational average as follows

$$\langle e^{iQ \cdot r} \rangle = \frac{\sin Qr}{Qr} \quad (3-15)$$

The factor  $Qr$  approaches 0 in the limit  $Q \rightarrow 0$ . The above equation can be approximated

$$\langle e^{iQ \cdot r} \rangle = \frac{\sin Qr}{Qr} = 1 - \frac{1}{3}(Qr)^2 \dots \quad (3-16)$$

The scattering intensity can be expressed as

$$I(Q) \cong \frac{1}{V} \left( \int_V \rho(r) dr \right)^2 \left[ 1 - \frac{1}{3}(QR_g)^2 \right] \text{ or } I(Q) \cong I(0)e^{-\frac{1}{3}(QR_g)^2} \quad (3-17)$$

where  $R_g^2 = \frac{\int \rho(r)r^2 dr}{\int \rho(r) dr}$  ( $R_g$  is the radius of gyration) and  $I(0)$  is proportional to the contrast factor. This is the Guinier approximation. The radius of gyration can be obtained from the slope of  $\ln I(Q)$  vs.  $Q^2$ .

SANS data contain information about the fractal dimension from the Porod plot.<sup>16, 17, 48</sup> The Porod region corresponds to a probed range smaller than the scattering objects ( $Q \ll 1/D$ ) so that the scattering radiation is probing the local scale structure. At high- $Q$ , the scattering intensity can be approximated as

$$I(Q) = \frac{A}{Q^n} + B \quad (3-18)$$

where  $A$  is a fitting variable,  $B$  is the incoherent background and  $n$  is called the Porod exponent.  $\text{Log}(I)$  vs.  $\text{Log}(Q)$  yields information about the fractal dimensions of the objects. A Porod slope  $n = 1$  is obtained for scattering from rigid rods; a slope  $n = 4$  represents a smooth surface for the scattering particle; whereas a slope  $n$  between 3 and 4 characterizes rough interfaces of surface fractal dimension  $D$  with  $n = 6 - D$ .

We can apply the Porod law to polymer chains to understand excluded volume interaction (or solvent quality). The Porod slope  $n$  is related to the excluded volume parameter  $\nu$  as its inverse  $n = 1/\nu$ . A slope  $n = 2$  is a signature of Gaussian chains in a dilute environment (theta condition), a slope  $n = 5/3$  is for fully swollen coils, a signature of good solvent, and a slope  $n = 3$  is for collapsed polymer coils which is a signature of poor solvent. A slope between 2 and 3 is for “mass fractals” such as branched systems (gels) or networks.

### **3.1.5 Zero angle scattering and thermodynamics**

The measured SANS intensity also contains information about the thermodynamics of the system from the zero angle scattering intensity (sometimes termed the forward scattering intensity). A simple derivation from statistical mechanics shows that the density or concentration fluctuations depend on thermal properties.<sup>15-19, 57</sup> From the grand canonical ensemble, the standard deviation of density and concentration fluctuations can be written as a function of temperature and thermodynamic parameters as<sup>18, 57</sup>

$$\sigma_N^2 = \overline{N^2} - \bar{N}^2 = kT \left( \frac{\partial \bar{N}}{\partial \mu} \right)_{V,T} \quad (3-19)$$

where  $\mu$  is the chemical potential.

The density and concentration fluctuations are related to the forward scattering intensity. Simple extrapolation of the scattering intensity to  $Q = 0$  produces  $I(0) \approx \sigma_N^2$  and we have  $I(0) \approx kT \left( \frac{\partial \bar{N}}{\partial \mu} \right)_{V,T}$ . The inverse of  $\left( \frac{\partial \mu}{\partial \bar{N}} \right)_{V,T}$  is called as the exchange chemical potential which is equivalent to the second derivative of the free energy.

Consider a multicomponent polymer. The Flory interaction parameter  $\chi$ , discussed in Chapter 2, can be determined in homogeneous single phase blends (or mixtures) by measuring the composition fluctuations using light, X-ray or neutron scattering. Generalization to the case of a simple binary polymer blend at equilibrium with average composition  $\bar{\phi}$  and consider a small volume segment containing  $n$  total monomers with  $n_A = \phi n$ . A small fluctuation in composition  $\delta\phi$  can occur spontaneously in a small volume at equilibrium:

$$\delta\phi \equiv \phi - \bar{\phi} \quad (3-20)$$

The free energy of mixing in this small volume,  $\Delta F_{mix}$ , can be expanded in a power series of the fluctuations:

$$\Delta F_{mix}(\phi) = \Delta F_{mix}(\bar{\phi}) + \frac{\partial \Delta F_{mix}}{\partial \phi} \delta\phi + \frac{1}{2!} \frac{\partial^2 \Delta F_{mix}}{\partial \phi^2} (\delta\phi)^2 + \dots \quad (3-21)$$

Here, we introduced the exchange chemical potential by implementing  $\delta n_A$  instead of  $\delta\phi$ .

$$\delta n_A = n \delta\phi \quad (3-22)$$

$$\frac{\partial \Delta F_{mix}}{\partial \phi} \delta\phi = \frac{\partial \Delta F_{mix}}{n \partial \phi} n \delta\phi = \frac{\partial \Delta F_{mix}}{\partial (n\phi)} \delta(n\phi) = \frac{\partial \Delta F_{mix}}{\partial n_A} \delta n_A \quad (3-23)$$

The exchange chemical potential is the change in free energy of mixing arising from the exchange of one A monomer by one B monomer. The change in free energy in the system,  $\delta F$ , arising from this fluctuation is the sum of the free energy change in the small volume containing  $n$  monomers ( $= \Delta F_{mix}(\phi) - \Delta F_{mix}(\bar{\phi})$ ) and the free energy change in the rest of the blend ( $\frac{\partial \Delta F_{mix}}{\partial n_A} (-\delta n_A)$ ):

$$\delta F = \Delta F_{mix}(\phi) - \Delta F_{mix}(\bar{\phi}) + \frac{\partial \Delta F_{mix}}{\partial n_A} (-\delta n_A) \quad (3-24)$$

The typical free energy change is of the order of the thermal energy,  $kT$ . Using Eq (3-21), Eq (3-24) yields

$$\langle (\delta\phi)^2 \rangle \approx kT \left( \frac{\partial^2 \Delta F_{mix}}{\partial \phi^2} \right)^{-1} = \frac{kT}{n} \left( \frac{\partial^2 \Delta \bar{F}_{mix}}{\partial \phi^2} \right)^{-1} \quad (3-25)$$

This relation indicates that composition fluctuation is a thermodynamic function. The last term involving the normalized free energy per lattice site clearly shows that thermally driven composition fluctuations diminish as the volume increases due to the increase of  $n$ .

The total fluctuation is the superposition of density fluctuations and concentration fluctuations as

$$I(0) \sim \langle (\delta N)^2 \rangle + \langle (\delta\phi)^2 \rangle \quad (3-26)$$

Where the first term is the contribution from density fluctuations and the second term is the contribution from concentration fluctuations. Concentration fluctuations arise from the change on mixing hence the forward scattering intensity has information on the thermodynamics of mixing. Combined with the Flory-Huggins theory, the forward scattering intensity of a two-component polymer system (such as a polymer solution or a polymer blend) can be written as

$$\frac{1}{I(0)} \sim \frac{1}{S(0)} = \frac{1}{kT} \left( \frac{\partial^2 \Delta \bar{F}_{mix}}{\partial \phi^2} \right) = \frac{1}{N_A \phi} + \frac{1}{N_B (1 - \phi)} - 2\chi \quad (3-27)$$

where  $N_A$  is the degree of polymerization of A

$\chi$  is Flory-Huggins interaction parameter

$\phi$  is the volume fraction of component A.

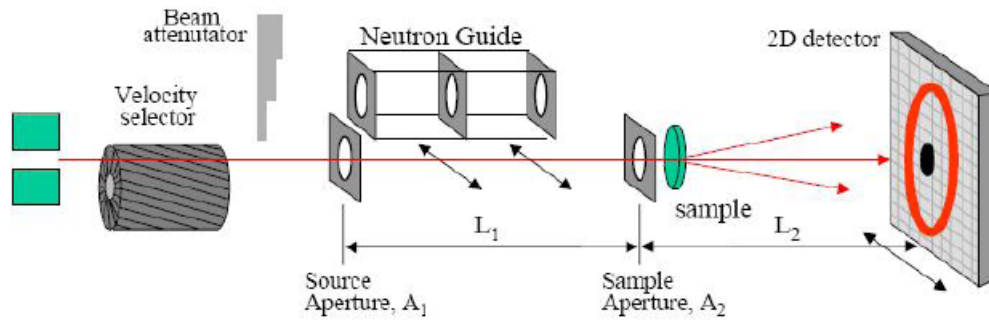
The forward scattering intensity is used to predict the phase behavior of polymeric systems. The second derivative of the free energy approaches 0 as the phase boundary is approached-which yields the spinodal condition. Physically, the forward scattering intensity becomes infinite at the spinodal condition.

### **3.1.6 SANS instruments at NCNR**

SANS measurements have been carried out using the NG3 and NG7 30m SANS instruments at the National Institute of Standards and Technology Center for Neutron Research (NCNR), shown in Figure 3.5.<sup>17, 55</sup> The range of wavelengths for the SANS instruments is from 5 Å to 20 Å. It covers a scattering vector ( $Q$ ) range from 0.0001 Å<sup>-1</sup> to 0.6 Å<sup>-1</sup>, which corresponds to d-spacings from 6,000 Å down to 10 Å. SANS instruments at the NCNR use velocity selectors to select a portion of the neutron spectrum.

In order to obtain small angles, good collimation and high resolution area detectors are needed. Good collimation is achieved through the use of long neutron flight paths before the sample.

(A)



(B)

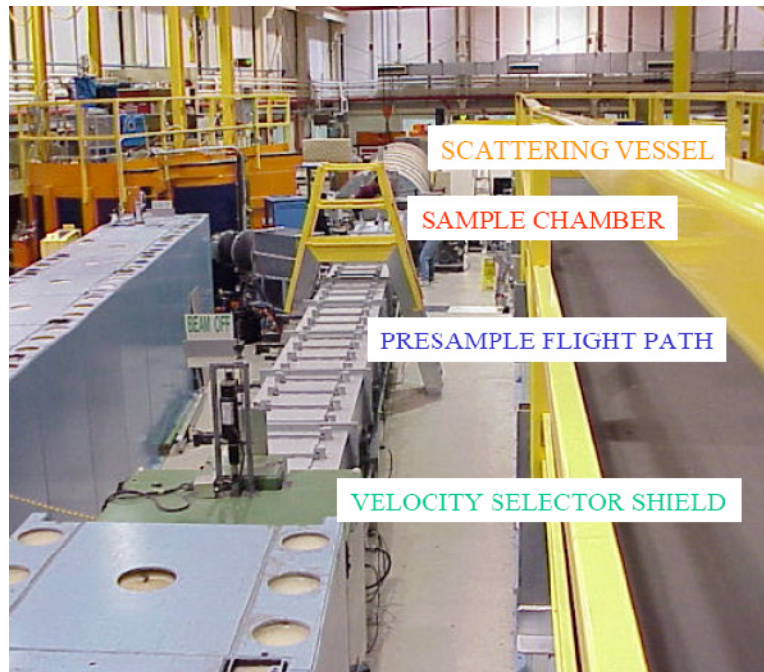


Figure 3.5 (A) Schematics of the NG3 30m SANS instrument at NIST. There are 4 main instrumental parts; (1) velocity selector, (2) beam collimation, (3) Sample (scattering event) and (4) 2D area detector. The sample-to-detector maximum distance is 15 m. (B) Photograph of the NG3 30m SANS instrument.<sup>17, 55</sup>

### 3.2 Dynamic light scattering

The dynamic light scattering (DLS) technique has been used to probe the clustering behavior of PEO by monitoring the hydrodynamic radius. DLS has a complementary role in that it probes structural relaxations and dynamics. In particular, DLS probes the dynamic motion of particles in a fluid. This method can give a reliable estimate of particle size under certain conditions such as dust free sample preparation. In a DLS experiment, the fluctuating intensity of light scattered from the sample is recorded at a particular angle  $\theta$  ( $\theta$  is  $90^\circ$  in our case). The fluctuations are then correlated to yield the intensity autocorrelation function  $g^{(2)}(q, \tau)$  vs. correlation time  $\tau$ :

$$g^{(2)}(q, \tau) = \frac{\langle I(q, t)I(q, t + \tau) \rangle}{\langle I(q, t) \rangle^2} \quad (3-28)$$

where  $\tau$  is the correlation time and  $q = \frac{4\pi n}{\lambda} \sin(\theta/2)$ . The measured intensity autocorrelation function  $g^{(2)}(q, \tau)$  can be converted into an electric field autocorrelation function  $g^{(1)}(q, \tau)$  through the Siegert relation:

$$g^{(2)}(q, \tau) = 1 + f |g^{(1)}(q, \tau)|^2 \quad (3-29)$$

Here,  $f$  is the coherence factor that depends on the instrumental geometry. For a dilute solution of monodisperse spherical particles, the electric-field autocorrelation

function is a single exponential whose time decay is determined by the translational diffusion coefficient of the particle  $D$ :

$$g^{(1)}(q, \tau) = \exp(-Dq^2\tau) \quad (3-30)$$

From the measured diffusion coefficient, the particle size can be obtained by the Stokes-Einstein equation:

$$D = \frac{kT}{6\pi\eta R_h} \quad (3-31)$$

where  $k$  is the Boltzmann constant and  $\eta$  the viscosity of the solvent (assumed to be a Newtonian liquid). The size obtained from DLS is the hydrodynamic radius of the particle  $R_h$ .

### **3.3 Density measurement technique by the vibrating tube method**

The density of a material is the ratio of its mass to its volume and can be used to directly monitor the state of the material.<sup>58</sup> Density measurements were used to monitor the crystallization as it is a first order phase transition as defined by a discontinuous change in the specific volume. Density measurements involve precise measurements of the mass and/or volume or the use of an indirect method for measuring physical quantities that are related to the density. High precision density measurements are possible since the introduction of a practical model of the

mechanical oscillator. It is a well established method for measuring the density of fluids and complex fluids with high precision. The vibrating U-tube method is one of the most common density measurement methods and uses a mechanical oscillator.<sup>58-60</sup> The volume of the tube is fixed and the mass is measured by measuring the vibration frequency of the U-tube. The frequency of U-tube oscillations depends on the vibrating mass  $m$  and spring constant  $k$  as

$$f = \frac{1}{2\pi} \sqrt{\frac{k}{m}} \quad (3-32)$$

Volume of the U-tube is controlled by the stationary vibrations of the oscillator. If the oscillator is filled, a constant volume participates in the oscillation. Since the same volume is involved, a precise measurement of the mass yields the density with high precision. This method can be used even for flowing liquids, which enables industry to monitor the density of a product.

The vibrating U-tube is driven by an electro-mechanical system that uses a magnet and coil assembly. The coil creates an oscillating magnetic field that acts (pushes) on the magnet and therefore on the tube periodically. A feedback amplifier is used to maintain the oscillation at the resonant frequency. The mechanical oscillation of the tube is transformed into an alternating voltage of the same frequency and then to a calibrated digital signal of the density. The calibration is performed using substances of precisely known densities.

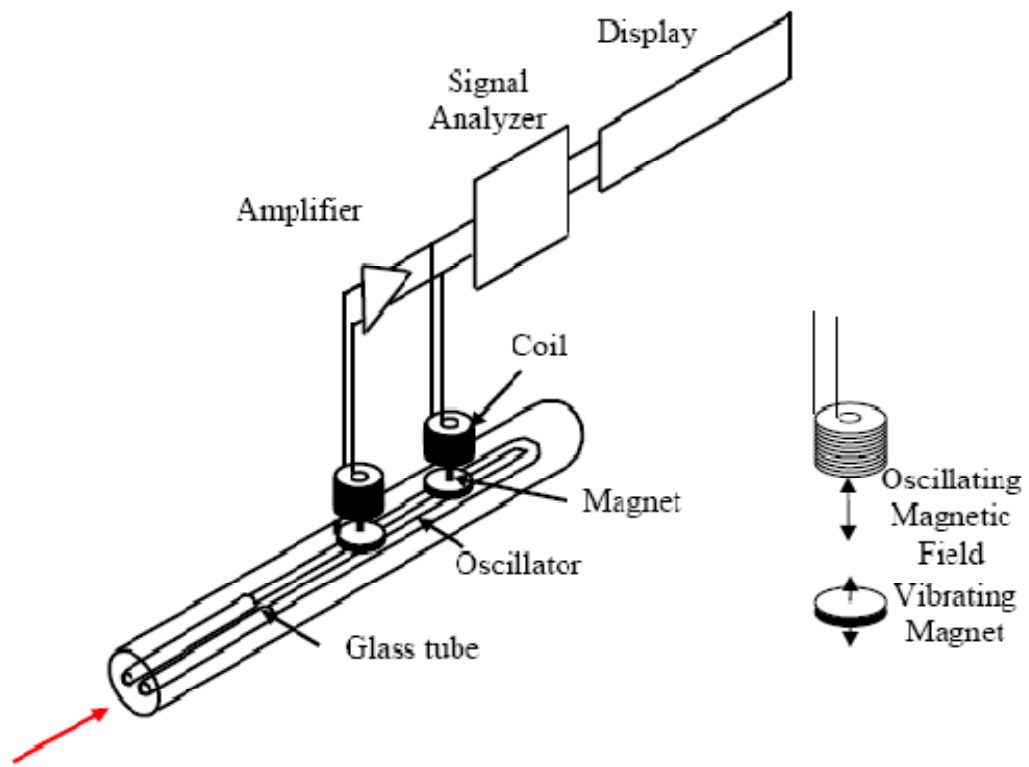


Figure 3.6 Schematic representation of the vibrating U-tube density meter. (Antonpaar, <http://www.antonpaar.com>)

## Chapter 4

### Solvation and clustering of poly(ethylene oxide) in ethanol/water mixture

#### 4.1 Introduction

As mentioned in a previous section, the diverse range of PEO solution behavior is due to the interplay of hydrophobic and hydrophilic sites along the polymer backbone. When dissolved in water, PEO is characterized by both hydrophilic interactions (hydrogen bonding of water molecules to the oxygen atoms on the polymer) and hydrophobic interactions (the  $\text{CH}_2\text{CH}_2$  groups repel water).<sup>3, 7, 30</sup> This can be compared to other ether group polymers such as poly(propylene oxide) (PPO,  $-\text{CH}(\text{CH}_3)\text{CH}_2-$ ) or poly(methylene oxide) (PMO,  $-\text{CH}_2\text{O}-$ ) which do not dissolve readily in water over a wide temperature range. A significant difference between PEO and these other ether group polymers (PPO and PMO) is the size of the alkyl group.

When PEO is dissolved in ethanol, it forms a paste-like gel (opaque) at room temperature.<sup>6</sup> It is an unusual phase behavior although the hydrogen-bonding capability of ethanol is relatively small compared to methanol or water. We confirmed that the origin of this gelation is partial crystallization. The gel structure and morphology will be discussed in detail in the following chapters. Furthermore, a very interesting phenomenon is observed when mixed solvents are used. The solution

becomes clear when a small amount of water is added to the PEO/ethanol mixture. Figure 4.1 (A) shows the solution change as the water fraction is varied. PEO in pure ethanol is opaque but PEO in ethanol (96 vol %)/ water (4 vol %) mixture is clear. These PEO solutions were studied using neutron scattering to examine molecular properties. Besides measuring the radius of gyration of the polymer chain in solution, neutron scattering is a powerful technique to identify the solvent quality and interactions between molecules.<sup>15, 16, 19, 20</sup> The SANS data are shown on a log-log scale in Figure 4.1 (B). The SANS intensity for PEO in ethanol exhibits a stacked lamellar crystal structure. The intensity increases at low  $Q$  and displays oscillations at intermediate  $Q$  due to the formation of PEO lamellae which are of higher density than amorphous PEO. The slope of the SANS intensity at high  $Q$  of a PEO solution with a small amount of water (4 vol % water in solvent) is  $-5/3$  as shown in Figure 4.1 (B) which is a signature of good solvent.

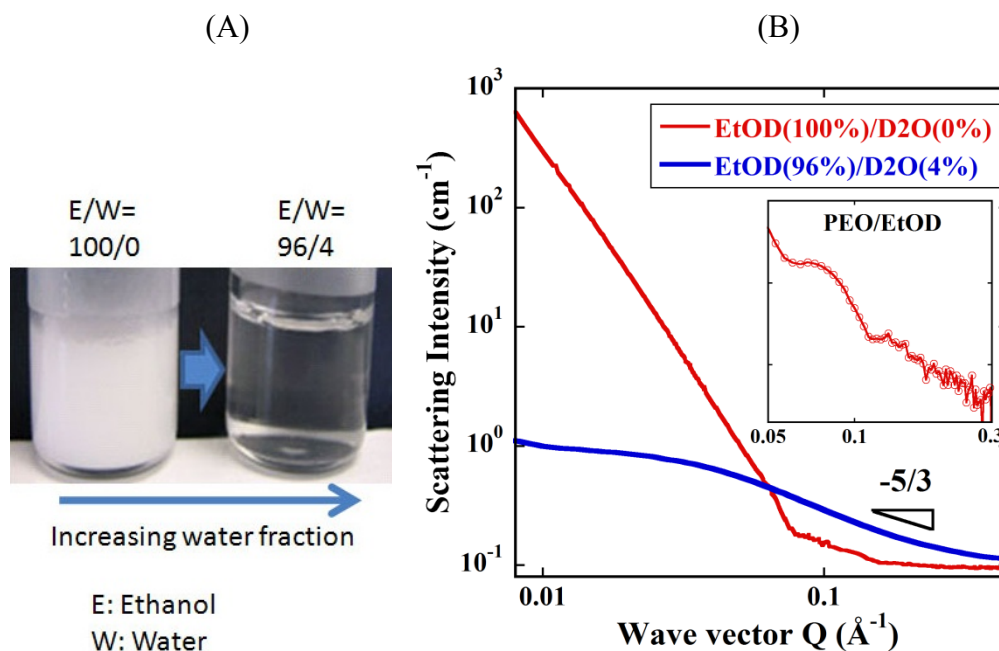


Figure 4.1 The PEO/ ethanol mixture changes from an opaque gel to a clear solution with the addition of 4 vol % water. (A) Photograph shows that the solution becomes clear as the fraction of water in mixed-solvents becomes 0.04 (4 vol %). (B) SANS intensity from PEO solutions. Red circle in inset picture represents SANS intensity for PEO (5 wt %) in pure ethanol. The slope for the polymer solution at high  $Q$  is  $-5/3$ .

## 4.2 Experimental

PEO (h-PEO,  $\text{HO}-(\text{CH}_2\text{CH}_2\text{O})_n-\text{CH}_3$ ) of molecular weight  $M_w = 90,000$  g/mol ( $M_n = 83,000$  g/mol) was purchased from Polymer Source, Inc. and used without further purification. Anhydrous deuterated ethanol ( $\text{C}_2\text{D}_5\text{OD}$ , d-ethanol) and deuterated water ( $\text{D}_2\text{O}$ , d-water) were purchased from Cambridge Isotope Laboratories Inc. and used without further purification. Protonated polymer/deuterated solvent were used to enhance contrast and lower background in neutron experiments. The mass fraction of PEO was fixed at 5 wt %. The volume fraction of

water in total solvents (d-ethanol + d-water) was varied from 0 vol % to 100 vol % as shown in Table 4.1. When PEO is first mixed with ethyl alcohol, there is no observable change for 10 hours at room temperature. Heating is required to dissolve PEO in d-ethanol. PEO/ ethanol mixture becomes a clear solution after 2 hours at 60 °C. PEO/ d-ethanol/ d-water mixture was held at 60 °C water bath for 3 hours. All samples were prepared with the same thermal processing time (3 hours). After fully dissolving the PEO, samples were quenched and held at room temperature in a 1 mm standard SANS cell for several hours. Samples #01 – #04 (water fraction  $\leq 3$  vol %) became an opaque gel while samples #05 – #11 (water fraction  $\geq 4$  vol %) became a clear solution.

Table 4.1 Sample preparation

Sample #	# 01	# 02	# 03	# 04	# 05	# 06	# 07	# 08	# 09	# 10	# 11
h-PEO*						0.05					
d-ethanol	100	99	98	97	96	90	70	50	30	10	0
d-water	0	1	2	3	4	10	30	50	70	90	100

Small-angle neutron scattering (SANS) measurements were carried out using the 30m SANS instrument (NG-3 and NG-7) at the National Institute of Standards and Technology Center for Neutron Research (NCNR).<sup>55</sup> SANS configurations used a neutron wavelength ( $\lambda$ ) = 6 Å with  $\Delta\lambda/\lambda = 0.15$ . Three detector configurations were used: 1m, 4m and 13m. The wave vector ( $Q$ ) range using the 3 configurations is  $0.0034 \text{ \AA}^{-1} - 0.4421 \text{ \AA}^{-1}$ . Samples were prepared and measured in 1 mm quartz cells.

The measured scattering data were reduced for scattering from the empty cell, incoherent scattering, detector dark current, detector sensitivity, sample transmission, and thickness.<sup>17, 55, 61</sup> The reduction procedure was performed with SANS data reduction package provided by NCNR.<sup>61</sup> The data after standard reduction were placed on an absolute scale using direct beam measurement and circularly averaged to produce  $I(Q)$  vs.  $Q$  plots. Sample #11, PEO/d-water sample was measured at temperature range of 15 °C – 90 °C. Sample #01 – #10 which have ethanol were measured at  $T = 25$  °C, 45 °C, 55 °C and 65 °C.

Wide-angle X-ray scattering (WAXS) was used to confirm the crystal structure of PEO in ethanol. PEO/ethanol and ethanol samples were measured to confirm the origin of gelation. The ethanol sample was used for background subtraction. The wave vector range was  $0.4 \text{ \AA}^{-1} - 3.5 \text{ \AA}^{-1}$ .

Density was measured using an Anton Parr 3000 which used vibrating U-tube. Data was measured over a temperature range of 10 °C – 65 °C. A homogeneous solution was injected into the tube and equilibrated at  $T = 65$  °C for 10 min. The density was measured every 5 °C upon cooling from 65 °C to 10 °C followed by heating from 10 °C to 65 °C. An equilibration time of 5 min was used before each measurement.

### **4.3 Morphology and structure of PEO in ethanol**

PEO forms a opaque gel structure in ethanol. (Figure 4.1 (A)) The origin of this gel is the partial crystallization of PEO chains. This gel can be characterized by wide-angle X-ray scattering or with optical microscopy as shown in Figure 4.2 (B) and (C).<sup>62, 63</sup> Indexing the observed WAXS peaks is shown in Figure 4.2 (C). The

observed peaks, (120) and (112) or (032), agreed with the PEO crystallographic data. The SANS intensity having microcrystalline structure exhibits an upturn at low- $Q$  and a weak peak around  $Q = 0.01 \text{ \AA}^{-1}$  which corresponds to the lamellar stack periodicity as shown in Figure 4.2 (D).

As mentioned, the origin of the gelation of PEO in ethanol solutions is thermoreversible partial crystallization. The thermoreversible gelation through crystallization is shown in Figure 4.3. Thermoreversible gelation induced through crystallization has been identified by DSC (differential scanning calorimeter) and density measurements. The processes of crystallization and melting of PEO forms a hysteresis loop observed in the DSC as shown in Figure 4.4 (A). The first order phase transition (crystallization) is manifested through a discontinuous change in the specific volume or specific density. We can confirm the crystallization process by monitoring the density with varying temperature. The discontinuous density change upon heating and cooling are observed in PEO/ ethanol mixture as shown in Figure 4.4 (B).

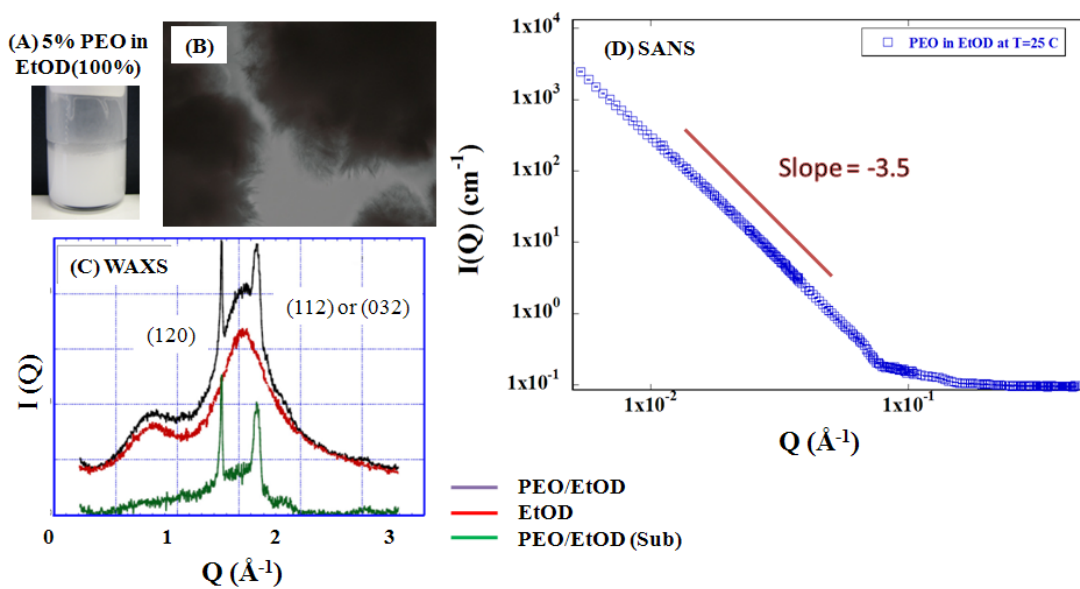


Figure 4.2 PEO gel in ethanol. (A) the opaque gel, (B) optical micrography, (C) WAXS data with crystalline peaks and (D) SANS data.

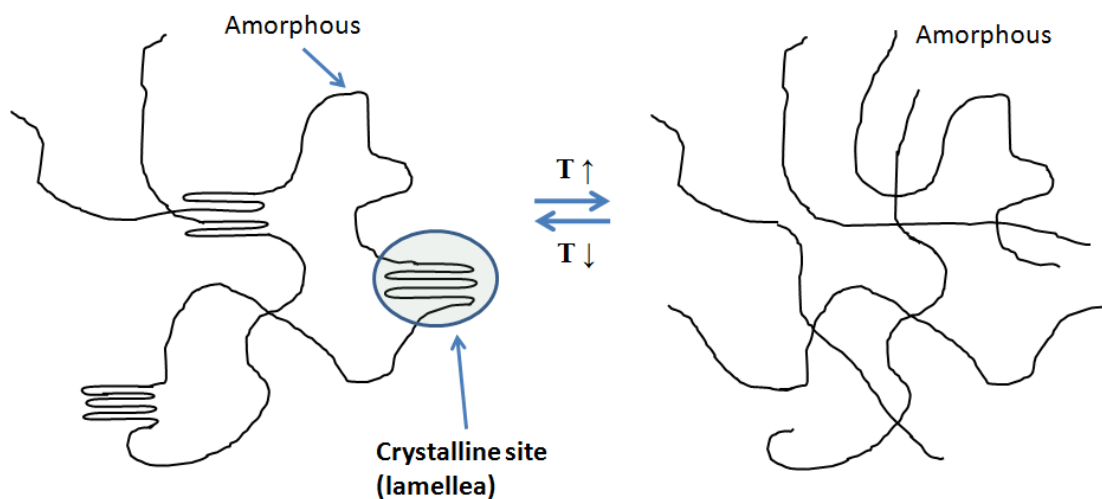


Figure 4.3 Thermoreversible gel. PEO forms a gel through partial crystallization at room temperature and becomes a homogeneous solution at higher temperature ( $T > 40$  °C).

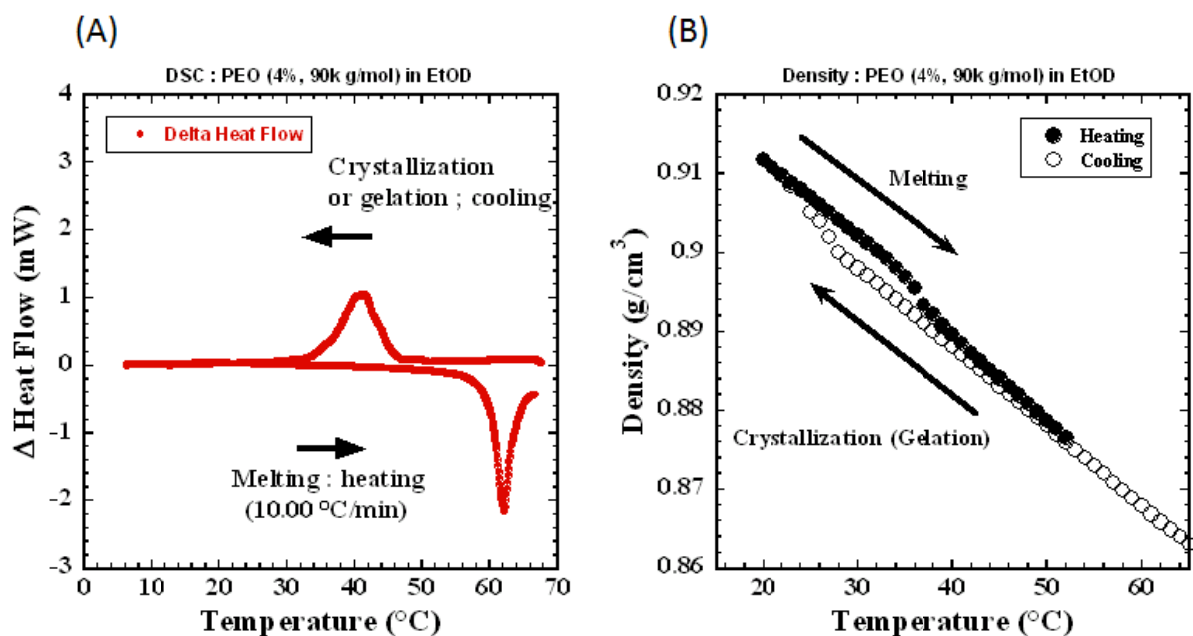


Figure 4.4 Formation of a thermoreversible gel for PEO in ethanol. (A) DSC and (B) density measurements.

#### 4.4 Model function for SANS from PEO solution

The SANS profile of an aqueous PEO solution can be divided into two regions; the upturn in the low- $Q$  region (signature of clustering), and scattering at high- $Q$ .<sup>5</sup> A typical SANS data set for an aqueous PEO solution is shown in Figure 4.5. Generally, polymer solutions (such as an aqueous PEO solution) can be fit with a Lorentzian-like function in the high- $Q$  region with three floating variables (scale factor, correlation length and Porod exponent) and Porod scattering in the low- $Q$  region to describe clustering. PEO in ethanol at elevated temperatures (over 40 °C) exhibits the features of a polymer in a good solvent, similar to aqueous PEO

solutions, so the Lorentzian-like function can be directly applied to fit the SANS scattering intensity to monitor solution behavior such as solvation and clustering. As a result, a simple generic functional form that incorporates these two features is used to fit the SANS data. The SANS intensity ( $I(Q)$ ) is fit to the form:

$$I(Q) = \frac{A}{Q^m} + \frac{C}{1+(QL)^n} + B \quad (4-1)$$

The two multiplicative factors  $A$  and  $C$ , the correlation length  $L$ , the incoherent background  $B$  and the two exponents  $m$  and  $n$  are used as fitting parameters. The quantities  $C$  and  $n$  from the fitting function represent the solvation behavior (high- $Q$ ) and the quantities  $A$  and  $m$  represent the clustering behavior. The first term describes Porod scattering from clusters (long range behavior) and the second term is a Lorentzian-like function describing scattering from the polymer chains (short range behavior). This second term characterizes the polymer/solvent interactions and therefore the chain solvation characteristics at the molecular level.

Here we will monitor clustering behavior with a clustering strength defined by

$$\text{Clustering strength or clustering intensity} = \frac{A}{(0.004)^m} \quad (4-2)$$

where  $A$  and  $m$  are obtained from fitting SANS intensity with Eq (4-1).

The solvation behavior can be discussed with correlation length and forward scattering intensity ( $I(0)$ ). Forward scattering intensity combined based on Flory-

Huggins theory provides thermodynamics information such as phase behavior or spinodal temperature. The detailed thermodynamics will be discussed in Chapter 5. Furthermore the forward scattering intensity will be used here because it can be obtained directly from Eq (4-1). For now consider the solvation between solvent molecules and the PEO monomer and ignore the clustering effect for convenience. The forward scattering intensity from Eq (4-1) is given by

$$I(Q=0) = \frac{C}{1+(0*L)^n} = C \quad (4-3)$$

$C$  is directly related to the solvation between PEO and solvent.  $C$  is termed the solvation intensity.

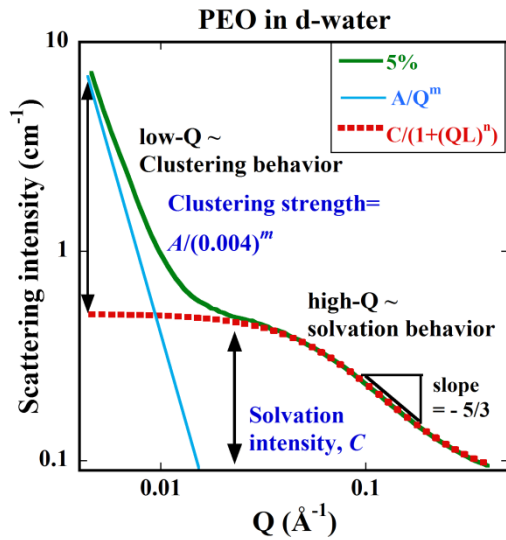


Figure 4.5 Typical SANS intensity of aqueous PEO solutions. The solvation intensity can be obtained from fitting the SANS intensity at high- $Q$  and the clustering behavior can be estimated from the low- $Q$  data. Here, the clustering is monitored in terms of a clustering strength,  $A/(0.004)^m$ .

## 4.5 Solvation and clustering of PEO in d-water

Consider the clustering behavior of PEO in water with varying temperature and PEO concentration. The SANS intensity of aqueous PEO solution exhibits an upturn in the low- $Q$  region which is the signature of clustering at relatively large length scales as shown in section 2.2. Here we will study the clustering and solvation behavior to understand the effect of water on PEO in ethanol/ water mixtures. As discussed in section 4.4, PEO solutions can be characterized by two distinctive scattering features: Chain scattering at high- $Q$  and clustering scattering through an upturn at low- $Q$ . The SANS intensity was fit to the form of Eq (4-1). The solvation characteristics will be measured in terms of a solvation intensity  $C$  and the clustering behavior will be monitored with a clustering strength defined by Eq (4-2).

The SANS data for an aqueous PEO solution (5 wt % PEO, MW = 90K g/mol) are shown in Figure 4.6 with varying temperature from 10 °C to 90 °C. Aqueous PEO solutions exhibit a lower critical solution temperature (LCST): the scattering intensity increases as temperature increases. The forward scattering intensity is directly proportional to the composition fluctuations. The increase in SANS intensity upon heating is a signature of LCST behavior. Parameter  $C$  obtained from fitting the SANS intensity represents the solvation behavior and is proportional to the composition fluctuations. Higher solvation intensity originates from larger concentration fluctuations in the system. The solvation characteristics can be understood by monitoring the solvation intensity ( $C$ ). Higher values of  $C$  indicate less efficient solvation. The dependence of  $C$  on temperature gives the solvation characteristics as well as the phase behavior. The data points (filled squares) in Figure 4.7 (A) are the

values of  $C$  from the SANS data fits; these increase with increasing temperature which is the signature of LCST behavior. Moreover the spinodal temperature obtained from the extrapolation of  $1/C$  vs.  $1/T$  for 5 % PEO in d-water is estimated to be around  $99.8 \text{ }^\circ\text{C}$  ( $\pm 8 \text{ }^\circ\text{C}$ ). (Inset in Figure 4.7 (A)) These result implied that the PEO solvation in water arises from hydrogen bonds between water and PEO oxygen. The strength of hydrogen bonds is proportional to the inverse of temperature: the strength of hydrogen bond decreases as temperature increase. Simulation results by Smith et al. are consistent with SANS result shown in Figure 4.6 and 4.7 (A).<sup>31</sup> The number of hydrogen bonds calculated from MD simulations decrease as temperature increases.

The clustering strength of PEO defined by Eq (4-2) decreases with increasing temperature as shown in Figure 4.7 (B). The magnitude of the clustering intensity is almost constant in the temperature range of  $10 \text{ }^\circ\text{C}$  –  $50 \text{ }^\circ\text{C}$  and starts to decrease rapidly at  $T = 60 \text{ }^\circ\text{C}$ . The trend of the clustering intensity is opposite to the trend of the solvation intensity as a function of temperature. The clustering intensity becomes higher at lower solvation intensity which indicates that the formation of clusters is enhanced in the better solvated state.

The hydrophilic interaction (hydrogen bond) and the hydrophobic effect can be applied in order to explain the origin of PEO clustering and solvation in water. The solvation of PEO in water was explained in terms of hydrogen bonds between PEO and water as shown in Figure 2.3, while the possible origin of PEO clustering is a hydrophobic interaction between water and ethylene groups in PEO. The hydrophobic effect arises from the tendency of water to exclude hydrophobic molecules such as

the ethylene group.<sup>64, 65</sup> Water molecules participated in PEO solvation gives rise to a rearrangement of water molecules around the PEO chain. The hydrogen bonds are partially reconstructed by building a water ‘cage’ around the PEO chain (sheath layer) and the hydrophobic groups (CH<sub>2</sub>CH<sub>2</sub>) come together to reduce the contact with water. Therefore, the hydrophobic effect and hydrogen bonding in the presence of water can cause clustering and solvation simultaneously. A schematic of hydrophobic hydration of PEO is shown in Figure 4.8.

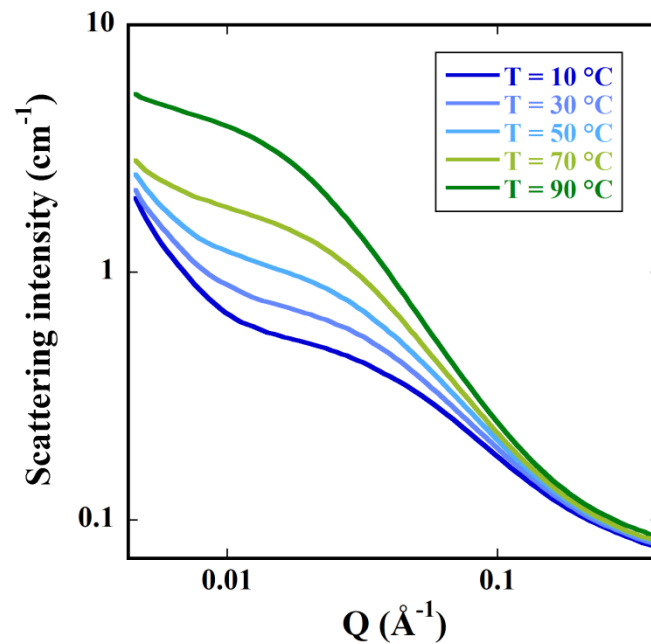
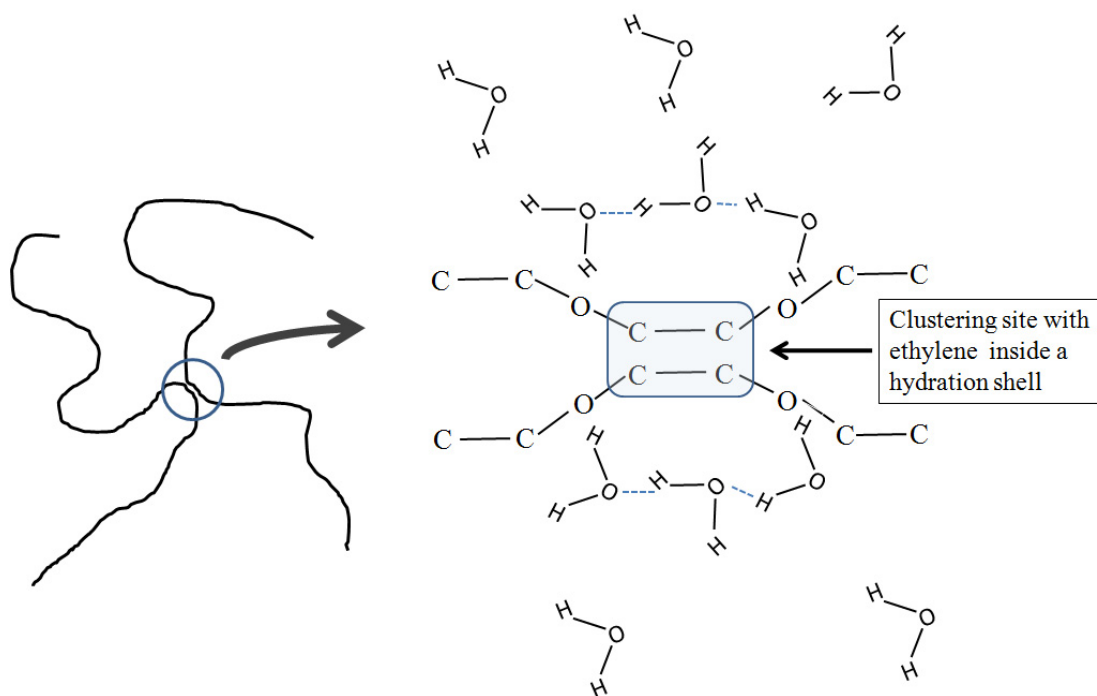
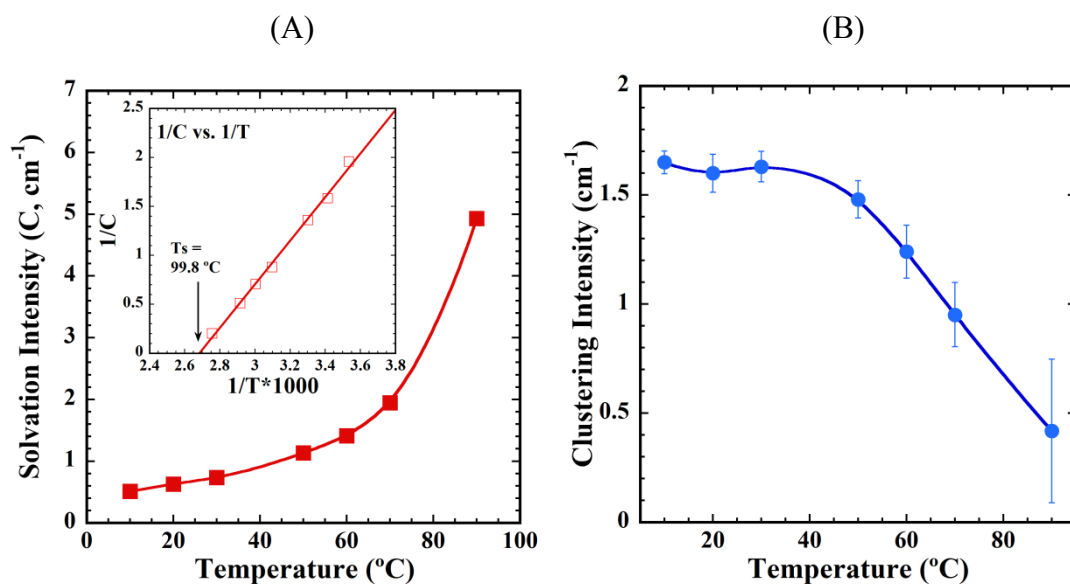


Figure 4.6 Typical SANS intensity for an aqueous PEO solution. The solvation intensity can be obtained from fitting intensity at high- $Q$  and the clustering can be estimated through the upturn intensity at low- $Q$ . Here, the clustering is monitored through a clustering strength,  $A/(0.004)^m$ .



## 4.6 Solvation and clustering of PEO in d-ethanol/ d-water mixtures

We observed that PEO forms an opaque gel in d-ethanol at room temperature due to PEO crystallization but becomes a transparent solution when a small amount of water is added. Addition of a small amount of water suppresses the crystallization of the PEO chains. The water interaction can change the solution behavior of PEO in ethanol as the water fraction is increased. Consider the effect of water on the solution characteristics of PEO in ethanol as a function of water fraction. The solvation intensity and clustering intensity from fitting the SANS was discussed at Section 4.4. Here we will use results of homogeneous solutions to observe solution properties. The PEO (5 wt %, MW = 90K g/mol) in ethanol becomes homogeneous above  $T = 45\text{ }^{\circ}\text{C}$  regardless of the water fraction. SANS intensities measured at  $T = 45\text{ }^{\circ}\text{C}$  to avoid crystallization. SANS intensities for 5 wt % PEO in d-ethanol/ d-water mixtures as a function of water fraction at  $T = 45\text{ }^{\circ}\text{C}$  are shown in Figure 4.9. The slope at high- $Q$  is  $-5/3$ , the signature of a good solvent.

The solvation intensities of PEO in ethanol/ water mixtures were obtained from fitting the SANS data at  $T = 45\text{ }^{\circ}\text{C}$  are shown in Figure 4.10 (A). Furthermore we measured SANS for  $55\text{ }^{\circ}\text{C}$  and  $65\text{ }^{\circ}\text{C}$  to estimate temperature effect. The obtained solvation intensities are plotted as a function of water fraction and temperature and are shown in Figure 4.10 (B). The temperature effect (phase behavior) will be discussed in a later chapter. The solvation intensity for PEO in pure water is lower than that of PEO in pure ethanol at  $45$ ,  $55$  and  $65\text{ }^{\circ}\text{C}$ . Increasing the water fraction in total solvent mixtures enhances the solvation state of the PEO. The dependence of solvation intensity on water fraction is not monotonic but shows a parabolic shape

with solvent composition as shown in Figure 4.10. When the ratio of ethanol:water is 70:30, 50:50 and 30:70 the solvation intensity is lower than that of pure water. The ethanol and water mixture exhibits a synergistic cosolvent effect where the mixed solvent is more effective at dissolving PEO than the pure components. Experimentally, 30 vol % of water in ethanol/ water mixtures is the most effective solvent.

The parabolic pattern of the solvation intensities implies non-ideal mixing which is characterized by a deviation from linear dependence (ideal random mixing). Non-ideal mixing can be confirmed by measuring the solution density. The density of PEO in d-ethanol/ d-water mixture is measured as a function of water fraction as shown in Figure 4.11 (A). The solid straight lines in Figure 4.11 (A) and (B) represent ideal mixing for PEO in ethanol/water mixtures. The specific volume of PEO is  $38.94 \text{ cm}^3/\text{mol}$ , for ethanol it is  $58.3 \text{ cm}^3/\text{mol}$  and for water it is  $18.07 \text{ cm}^3/\text{mol}$ . The large difference in molecular size might be one reason for the non-ideal mixing behavior. Random mixing is related to the effective packing due to the difference in molecular size. Compare the variation of the inverse of the solvation intensity for PEO to the variation of the density as a function of water fraction. The inverse of the solvation intensity increases rapidly when a small amount of water is added. The change in the solution density shows almost ideal mixing behavior in this composition range. The large increase of the inverse solvation intensity without a large change in density means that the solution behavior is driven by specific interactions between the water and PEO not by a volumetric effect. This large increase in the inverse solvation intensity can be explained through hydrogen bonding between water and PEO. The

difference in solvent volumes and specific interactions such as hydrogen bonding probably accounts for the deviation from ideal mixing.

Consider the effect of temperature on solvation intensity, which will be discussed in more detail in Chapter 5. The solvation intensity of PEO in ethanol decreases with increasing temperature, which is the signature of UCST phase behavior, while the solvation intensity of PEO in water increases with increasing temperature, the signature of LCST phase behavior. When the water fraction is 4 vol % – 10 vol % in solvent mixtures the magnitude of the solvation intensity is small compared to the pure solvent cases. We observed a change in phase behavior from UCST to LCST as the water fraction increases by monitoring change of the solvation intensity as a function of water fraction and as a function of temperature.

Clustering of PEO in ethanol is small enough to ignore it compared to PEO in water. As expected, the clustering intensity increases as the water fraction is increased. The low- $Q$  scattering is varied as a function of water fraction as shown in Figure 4.9. The results on the clustering behavior from fitting the SANS data are shown in Figure 4.12 as a function of water fraction. The clustering intensity is small enough to be ignored when the water fraction is less than 10 %. The clustering intensity levels off when the water fraction exceeds 50 %. The clustering strength clearly depends on the water fraction in solvent mixtures. The probable origin of PEO clustering is a hydrophobic effect between the water and ethylene groups in PEO as discussed in section 4.5. Introduction water into PEO/ethanol solutions gives rise to hydrophobic effect as well as hydrogen bonding. The hydrophobic interaction of ethanol is very small as compared with water.<sup>66</sup> Denote the change of free energy from hydrophobic

effect which arises from sticking ethylene ( $\text{CH}_2\text{CH}_2$ ) groups as  $\Delta G^{\text{HI}}$ .  $\Delta G^{\text{HI}}$  per one ethylene group ( $\text{CH}_2\text{CH}_2$ ) is -1.7 Kcal/mol in water and -0.32 Kcal/mol in ethanol at  $T = 10^\circ\text{C}$ .<sup>66-68</sup> Thus the tendency to form clusters is greater in water than in ethanol. The hydrophobic interaction is spontaneous. ( $\Delta G < 0$ , spontaneous) The ordered water structure from hydrogen bond between water and PEO ether oxygen form a shield layer for salvation and lower free energy through associating ethylene molecules to form clusters. The hydrophobic interaction is not the only reason for clustering. Hydrophobic interaction in water increases as temperature increases so that the clustering intensity should increase, which is opposite to our observation.

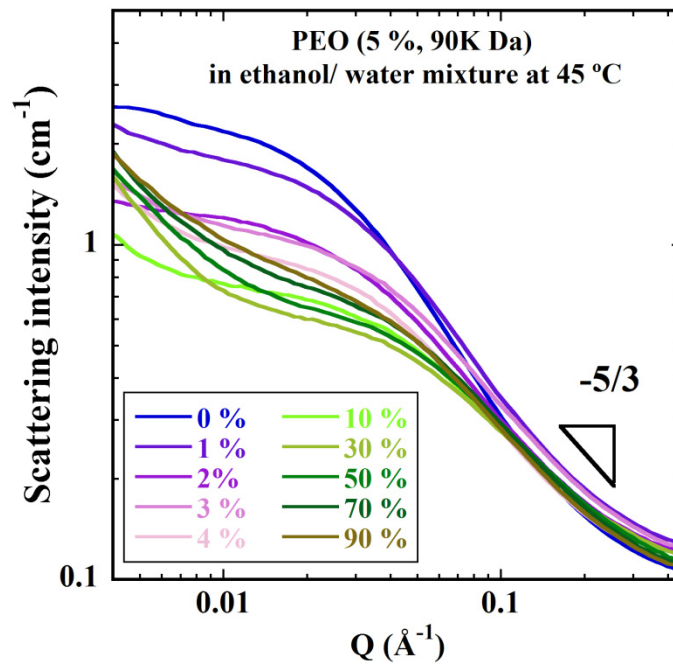


Figure 4.9 SANS intensities for 5 % PEO in ethanol/ water mixtures as a function of water fraction.

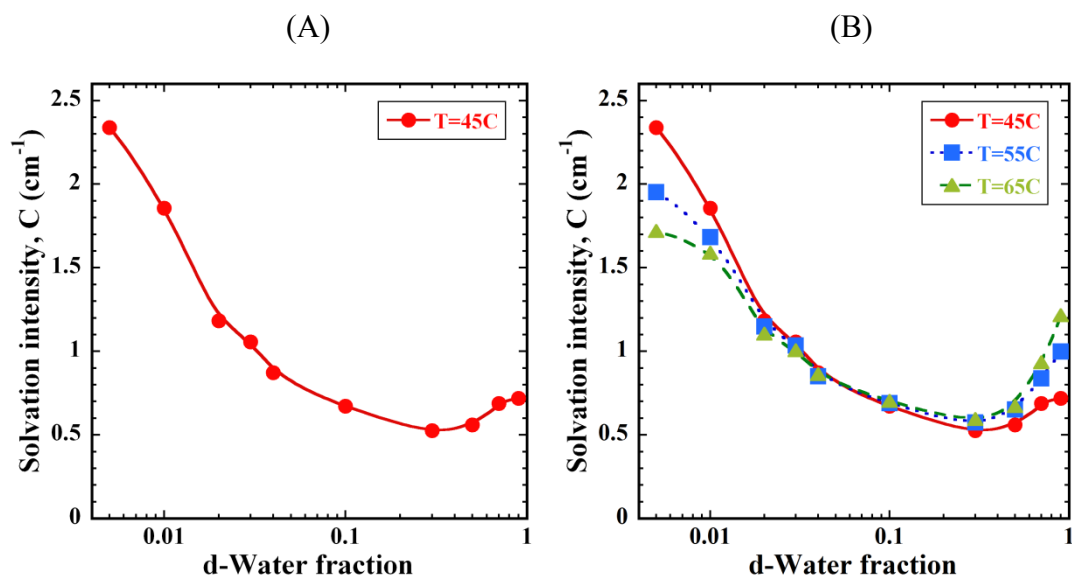


Figure 4.10 (A) Solvation intensities for 5 % PEO in ethanol/ water mixtures at  $T = 45^\circ\text{C}$ . (B) Solvation intensities for 5 % PEO in ethanol/ water mixtures at various temperatures. Errors are smaller than plot symbols.

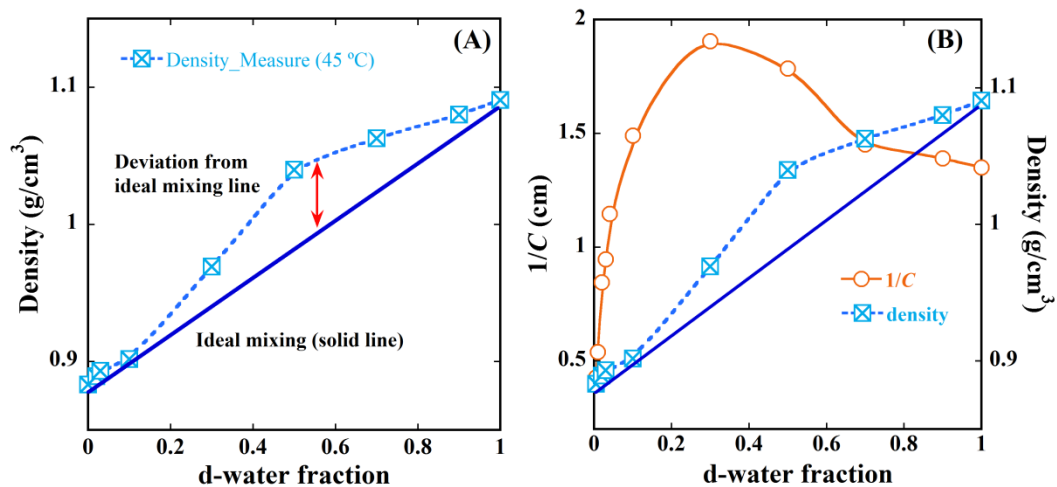


Figure 4.11 (A) Density of PEO in ethanol/ water mixtures as a function of water fraction. (B)  $1/C$  vs. density of PEO in d-ethanol/ d-water mixture. Measured density and solvation intensity shows deviation from ideal mixing line.

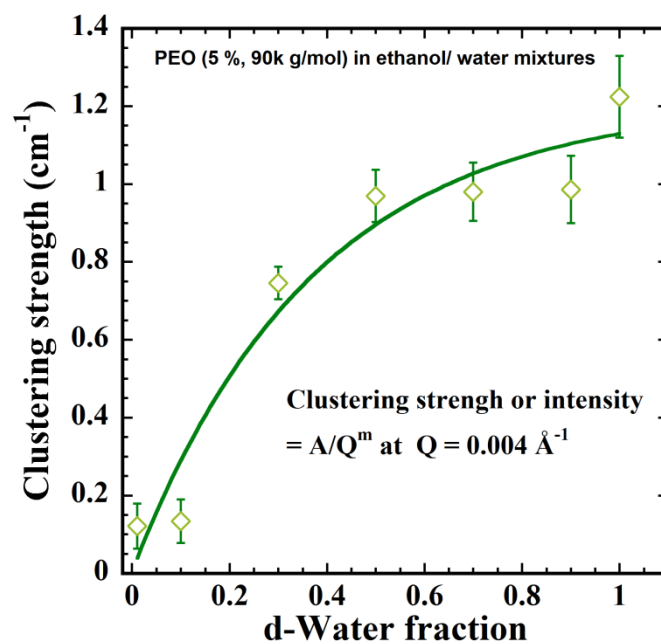


Figure 4.12 Clustering intensity for 5 % PEO in ethanol/ water mixtures as a function of water fraction at 45 °C.

## 4.7 Conclusions

High- $Q$  SANS scattering has been used to probe the local solvation and low- $Q$  scattering for clustering. The clustering intensity is proportional to the water fraction in water/ ethanol mixtures. The clustering intensity approaches a plateau value as the temperature is decreased or the water fraction is increased. The spontaneous tendency of clustering can be explained in terms of free energy of hydrophobic interaction. The solvation intensity shows a parabolic variation with ethanol/ water composition. Cosolvent mixtures make ethanol/water more effective solvating agent for PEO than pure solvents (water and ethanol).

The water molecules participating in hydrogen bonding with the polymer form a shield layer around the chain to prevent contact between water and ethylene groups. The interaction between ethylene and water is a hydrophobic effect, which causes aggregation. Hydrogen bonding between water and the ether oxygen and the hydrophobic effect can be induced by adding water to PEO in ethanol, resulting in lower solvation intensity (i.e. better effective solvation) and higher clustering.

## Chapter 5

### Phase behavior of poly(ethylene oxide) in ethanol/ water mixtures

#### 5.1 Introduction

In Chapter 4, the solvation behavior as a function of water fraction was discussed. PEO in water exhibits LCST behavior, while PEO in ethanol exhibits UCST behavior. We can determine the phase behavior of the system by observing the SANS intensity as a function of temperature. Figure 5.1 (A) shows SANS data of PEO in ethanol. The SANS intensity decreases as temperature increases, a signature of UCST phase behavior. SANS intensity for PEO in water, however, increases as the temperature increases as shown in Figure 5.1 (B). In this section we will discuss the phase behavior of PEO/ ethanol/ water mixtures in order to understand the effect of different solvents on the phase behavior.

#### 5.2 Experimental

PEO (h-PEO, HO-(CH<sub>2</sub>CH<sub>2</sub>O)<sub>n</sub>-CH<sub>3</sub>) of molecular weight  $M_w = 90,000$  g/mol ( $M_n = 83,000$  g/mol) was purchased from Polymer Source, Inc. and used without further purification. Anhydrous deuterated ethanol (C<sub>2</sub>D<sub>5</sub>OD, d-ethanol) and deuterated water (D<sub>2</sub>O, d-water) were purchased from Cambridge Isotope Laboratories Inc. and used without further purification. Protonated polymer/

deuterated solvent were used to enhance the contrast and lower background in neutron experiments. When PEO is first mixed with ethyl alcohol, a gradual change is observed over time at room temperature. Applying heat helps dissolve PEO in ethyl alcohol. Three different PEO fraction (2, 5 and 10 wt % PEO) were measured. PEO solutions were prepared with different composition ratios of solvent mixtures and fixing the h-PEO (2, 5 and 10 wt %) fraction. The water fraction was varied from 0 vol % to 100 vol % in for each PEO concentration as in Table 5.1. Before further experiment, PEO solution samples were cooled at 20 °C over 1 hour for equilibration before SANS experiments.

Small-angle neutron scattering (SANS) measurements were carried out using the 30m SANS instrument (NG-3 and NG-7) at the National Institute of Standards and Technology Center for Neutron Research (NCNR).<sup>55</sup> SANS configurations used a neutron wavelength ( $\lambda$ ) = 6 Å with  $\Delta\lambda/\lambda = 0.15$ . Three detector configurations were used: 1m, 4m and 13m. The wave vector ( $Q$ ) range using the 3 configurations is 0.0034 Å<sup>-1</sup> - 0.4421Å<sup>-1</sup>. Samples were prepared and measured in 1 mm quartz cells. The measured scattering data were reduced for scattering from the empty cell, incoherent scattering, detector dark current, detector sensitivity, sample transmission, and thickness.<sup>17, 61</sup> The reduction procedure was performed with SANS data reduction package provided by NCNR.<sup>61</sup> The data after standard reduction were placed on an absolute scale using direct beam measurement and circularly averaged to produce  $I(Q)$  vs.  $Q$  plots. The SANS intensity was measured in the temperature range 20 °C – 65 °C.

Table 5.1 Sample preparation for each PEO fraction

		2 wt % PEO									
<b>d-ethanol</b>		100	99.2	98.4	98	96.2	90	74	40	0	
<b>d-water</b>		0	0.8	1.6	2	3.8	10	26	60	100	

		5 wt % PEO										
<b>d-ethanol</b>		100	99	98	97	96	90	70	50	30	10	0
<b>d-water</b>		0	1	2	3	4	10	30	50	70	90	100

		10 wt % PEO										
<b>d-ethanol</b>		100	97	96	94	92	91	88	70	50	30	0
<b>d-water</b>		0	3	4	6	8	9	12	30	50	70	100

### 5.3 Model function for SANS data

The SANS data for a PEO solution can be fit with a Lorentzian-like function in the high- $Q$  region with three floating variables (scale factor, correlation length and Porod exponent) to monitor the solvation behavior. Note that the clustering intensity at low- $Q$  is not considered. As a result, a simple generic functional form is used to fit the SANS data:

$$I(Q) = \frac{C}{1+(QL)^n} + B \quad (5-1)$$

The parameter  $L$  is a correlation length for the polymer chains. The quantities  $C$  and  $n$  represent the solvation behavior (high- $Q$ ).  $B$  is the background. The zero angle scattering intensity can be obtained directly from Eq (5-1):

$$I(Q=0) = \frac{C}{1+(0*L)^n} = C \quad (5-2)$$

$C$  is directly related to the solvation between PEO monomers and solvent molecules.  $C$  is termed as the solvation intensity.

## **5. 4 Thermodynamics of PEO in ethanol/ water mixtures**

The addition of a small amount of water to PEO solutions in ethanol changes the system entirely. As shown in the SANS data in Figure 4.1 (B), the intensity for PEO in mixed solvents shows classical polymer solution behavior with a slope of -5/3, which is the signature of a good solvent. The water fraction used in mixed solvents is 4 vol % of the total solvent content and is enough to completely suppress the crystallization process. Here we will focus on the role of water in the solution behavior of PEO in ethanol/water mixtures. As a first step, we undertook a series of SANS experiments to probe the phase behavior of PEO in ethanol/ water mixtures.

### **5.4.1 Phase behavior and spinodal temperature ( $T_{SP}$ )**

The relation between the SANS intensity and thermodynamics provides a method to measure (or estimate) the thermodynamics of mixing such as the phase behavior and the spinodal temperature. The important quantity is the value of  $C$  in the fitting function (the zero angle scattering ( $I(0)$ ) in Eq (5-1) and (5-2). From section 3.1.4, the forward scattering intensity is related to the thermodynamics as  $I(0)$  or  $C \sim kT(\partial^2 \Delta F / \partial \phi^2)^{-1}$ .<sup>15, 16, 19, 48</sup> The second derivative of the free energy is a measure of concentration fluctuations so that the fitting value  $C$  represents the interactions between monomers and solvent molecules. As noted previously, we have termed  $C$  the solvation intensity. As a result, monitoring of the variation of  $C$  with temperature allows for the determination of the phase behavior (UCST or LCST), SANS is also a useful method to determine the spinodal temperature ( $T_{SP}$ ). The zero angle intensity ( $I(0)$ ) from SANS is used to estimate the spinodal temperature through extrapolation. The interaction parameter ( $\chi$ ) from the Flory-Huggins theory depends on temperature, generally as  $\chi \sim 1/T$ , and  $|\chi_{SP} - \chi|$  is proportional to the inverse of the zero angle scattering intensity ( $I(0)$  or  $C$ ),<sup>16, 48</sup>

$$|\chi_{SP} - \chi| \sim 1/I(0) \text{ or } 1/C \quad (5-3)$$

where  $\chi_{SP}$  denotes the value of spinodal Flory-Huggins  $\chi$  parameter at the spinodal. Thus, the temperature dependence of  $I(0)$  combined with the Flory-Huggins theory gives:

$$1/I(0) \sim |1/T - 1/T_{SP}| \quad (5-4)$$

The SANS intensity becomes infinite at the spinodal ( $I(0) \rightarrow \infty$  as  $T \rightarrow T_{SP}$ ) due to infinite fluctuations and  $T_{SP}$  can be obtained from extrapolation of  $1/I(0)$  vs.  $1/T$ .

The extrapolation equation based on Eq (5-4) is

$$\frac{1}{I(0)} = \frac{1}{C} = h + k \frac{1}{T} \quad (5-5)$$

where  $h$  and  $k$  are variables for fitting. Here, the extrapolated spinodal temperature is

$$T_{SP} = -\frac{k}{h} \quad (5-6)$$

Note that the spinodal temperature is a second order phase transition estimated from the scattering intensity measured in the homogeneous phase. The sign of the slope ( $k$ ) can be used to determine the phase behavior. A negative sign indicates a UCST and a positive sign indicates an LCST. Note that the phase separation temperature or spinodal temperature estimated here is a second order phase transition.

Samples were prepared over the range of from 0 vol % water (pure ethanol) to 100 vol % water (pure water) at a fixed PEO concentration (5 wt % hPEO MW = 90,000 g/mol). Protonated PEO and deuterated solvents were used to enhance the neutron scattering contrast. The result of the extrapolation is shown in Figure 5.2 (A) and (B).

The sign of the slopes in Figure 5.2 (A) are negative which means that the phase behavior is an UCST but the slopes in (B) are positive which is a signature of a LCST behavior. The addition of a small amount of water (4 vol % water) to the solvent mixture, increases the slope in Figure 5.2 (A) and changes  $T_{SP}$  from 0 °C to -200 °C as shown in Figure 5.3 (A). The dramatic change in the solution state from opaque (in pure ethanol) to transparent solution (ethanol (96 %)/ water (4 %)) is consistent with the suppression of crystallization of the PEO and a change in the thermodynamic phase behavior. The phase diagram showing the spinodal temperatures is presented in Figure 5.3 (A) which shows a divergence between 4 vol % and 10 vol % of water. The exact transition point from UCST to LCST cannot be determined precisely as a function of water fraction exactly but we estimate a transition at approximately 6 vol % water by monitoring the slope as shown in Figure 5.3 (B). The slope of Eq (5-5) is almost zero when the water fraction is 4 vol % – 30 vol % because the scattering intensity is independent of temperature. This means that the PEO solutions with a water fraction of 4 vol % – 30 vol % are an athermal system. The spinodal temperature of an athermal solution is physically unrealistic because the spinodal temperature is estimated by data in homogeneous state which is far from any phase boundary. In summary, the addition of a small amount of water dramatically changes the properties of PEO/ethanol solutions; (1) opaque mixtures become transparent and the quality of the solvent changes from poor to good, (2) there is a transition in the phase behavior from UCST to LCST and (3) there is a suppression of the crystallization process observed at room temperature (as discussed in Chapter 4).

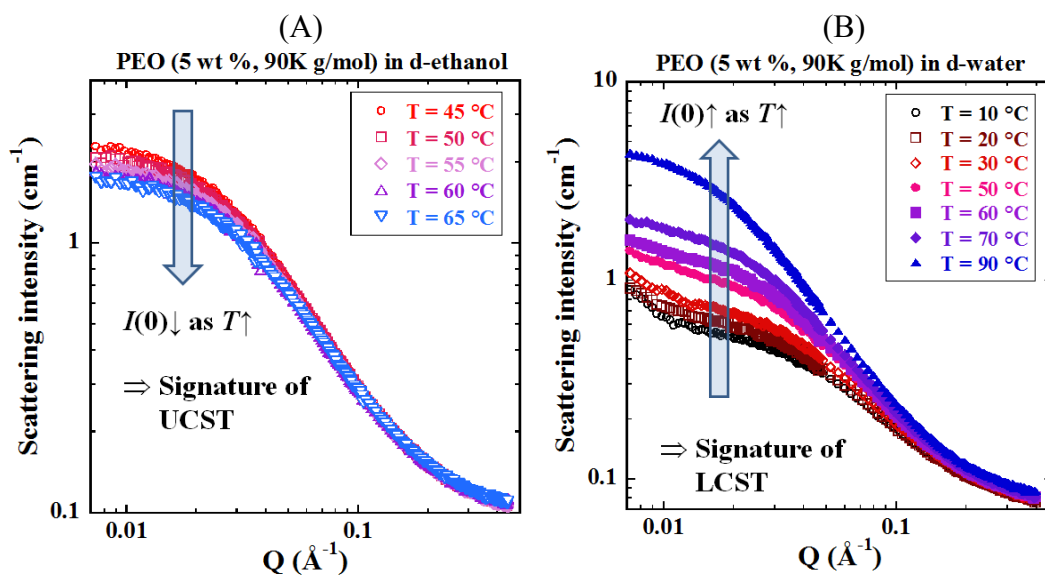


Figure 5.1 (A) SANS intensity of PEO in ethanol, which shows UCST behavior. (B) SANS intensity of PEO in water, which shows LCST behavior.

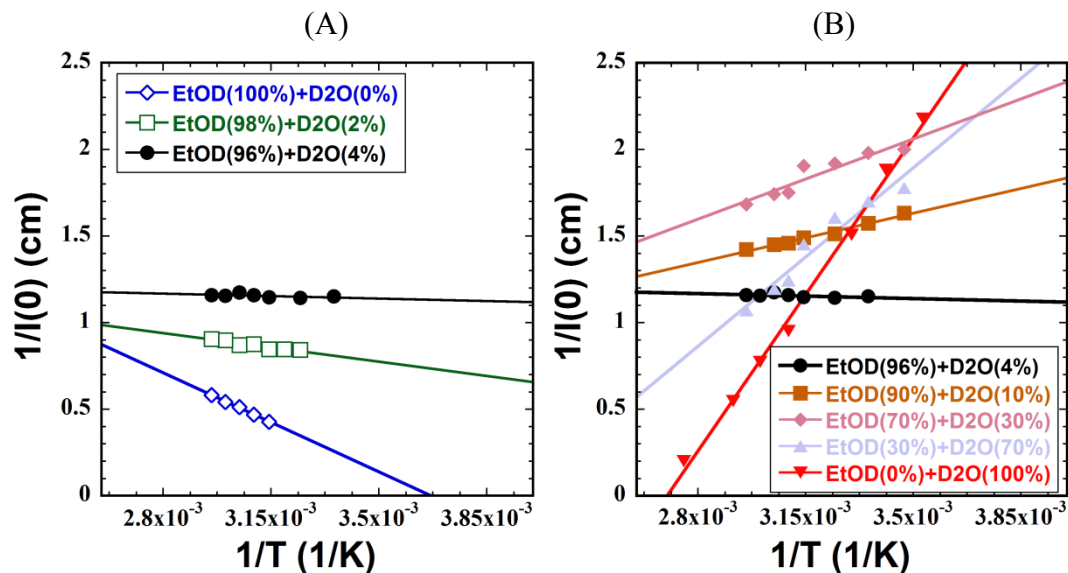


Figure 5.2 Extrapolation of  $1/I(0)$  vs.  $1/T$  determines the phase behavior. (A) for UCST behavior and (B) LCST behavior. The intercept with the x-axis ( $1/T$  axis) gives the spinodal temperature. Errors bars are smaller than the plot symbol size.

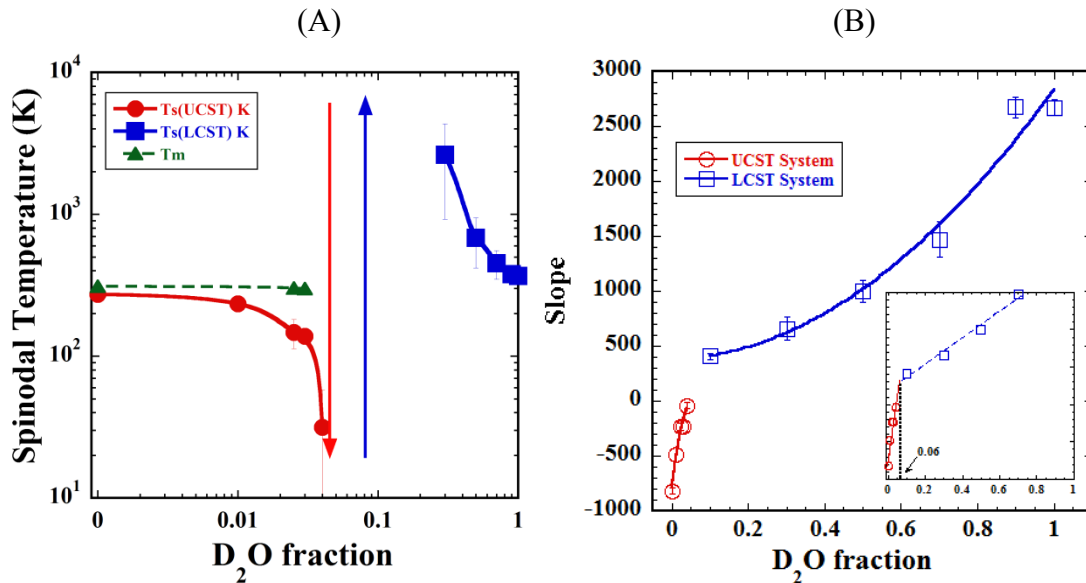


Figure 5.3 (A) Plot of spinodal temperature vs. water fraction. (B) Slopes taken from linear fit of  $1/I(0)$  vs.  $1/T$ .

#### 5.4.2 Self consistency in the change of the phase behavior

As shown in the previous section, adding water dramatically changes the solvation properties of PEO/ethanol mixtures. We choose 2 wt %, 5 wt % and 10 wt % PEO to probe the phase behavior as the water fraction is varied from 0 vol % to 100 vol % in order to examine the effect of varying polymer concentration. SANS intensities were measured as shown in Figure 5.4. We observed the suppression of crystallization and obtained a solvation intensity by fitting the SANS data with Eq (5-1). The gel becomes a homogeneously clear solution and the ethanol/water mixtures become a good solvent as identified by the slope ( $-5/3$ ) at high- $Q$  when the water fraction is 3.8 vol % water for 2 wt % PEO (Figure 5.4 (A)), 4 vol % water for 5 wt % PEO (Figure 5.4 (B)) and 8 vol % water for 10 wt % PEO solution (Figure 5.4 (C))

respectively at 20 °C. Furthermore, SANS intensities were measured as a function of temperature from 15 °C to 65 °C to monitor phase behavior and the role of water. Increasing the temperature suppresses the crystallization when the water fraction is not enough to fully hydrate the PEO chain. The PEO gel changed into a homogeneous solution upon heating although the water fraction is not enough to fully hydrate entire PEO molecules.

The solvation intensities,  $C$ , obtained from fitting SANS data of homogeneous solutions were used to monitor the phase behavior and spinodal temperature. Plots of  $1/C$  vs.  $1/T$  are shown in Figure 5.5 for each case. We can observe that the sign changes from negative (UCST) to positive (LCST) in each case. The transition from UCST to LCST is consistent with the disruption of the PEO gel. The transition point from UCST to LCST can be estimated by monitoring change in the slope ( $k$ ) obtained from fitting equation, Eq (5-1). Slopes are plotted as a function of water fraction in order to estimate a transition point in Figure 5.6. Abrupt changes in slope are observed for each case (2 wt %, 5 wt % and 10 wt % PEO content) as the water fraction is increased. In the UCST region, the slopes approach zero even though the change in the water fraction is very small. A slope of zero indicates a transition from UCST to LCST behavior. The rapid approach to the transition is due to the strong interaction between water and PEO. In the LCST region (positive slope) the magnitude of slope change is much smaller than in the UCST region. The magnitude of the slope around the transition point is small. Therefore the solution is not sensitive to the change in temperature around the transition point from UCST to LCST behavior. If we denote the transition point from UCST to LCST of water fraction in

total solvent as  $\phi_{water}^t$ . The intersection of the lines of slope in the UCST and LCST regions (as shown in Figure 5.6) can be used to estimate the transition point ( $\phi_{water}^t$ ) from UCST to LCST. The estimated transition points,  $\phi_{water}^t$ , are 0.03 for 2 wt % PEO solution, 0.06 for 5 wt % PEO solution and 0.08 for 10 wt % PEO solution respectively.

The spinodal temperatures can be obtained by extrapolations of Eq (5-6). The spinodal temperatures for all cases are extremely low when a small amount of water is used:  $\phi_{water} = 0.02$  (2 wt % PEO), 0.04 (5 wt % PEO) and 0.08 (10 wt % PEO). The spinodal temperatures are plotted as a function of water fraction in Figure 5.7 (A). The plot of the spinodal temperatures as a function of water fraction exhibits a divergence as the water fraction approaches the transition point from UCST to LCST as shown in Figure 5.7 (A). The diverging spinodal temperature means that the solution becomes athermal around the transition point. To understand the role of water, we define a new variable, the hydration level ( $\zeta$ ) which is defined as the ratio of the (number of water molecules)/(number of PEO monomers) assuming that all water molecules contribute to PEO hydration. The spinodal temperature decreases in a self-consistent manner as a function of hydration level with varying PEO concentration as shown in Figure 5.7 (B). The calculated water fraction at the transition points from UCST to LCST ( $\phi_{water}^t$ ) are shown in Table 5.2. The spinodal temperature decreases as a function of hydration level and diverges as the hydration level approaches 2 – 3 in the UCST region. This number implies that two or three

water molecules are required to hydrate one PEO monomer as discussed in section 2.2.

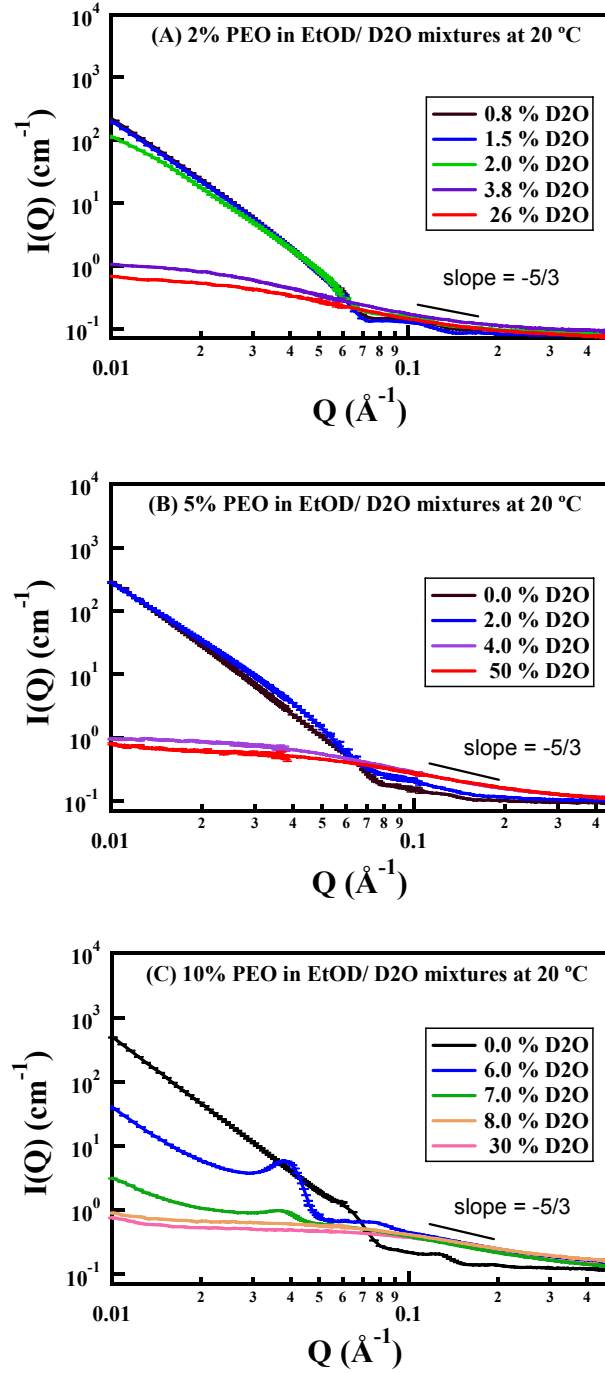


Figure 5.4 SANS intensities for (A) 2 wt %, (B) 5 wt % and (C) 10 wt % PEO (90k g/mol) in ethanol / water mixtures.

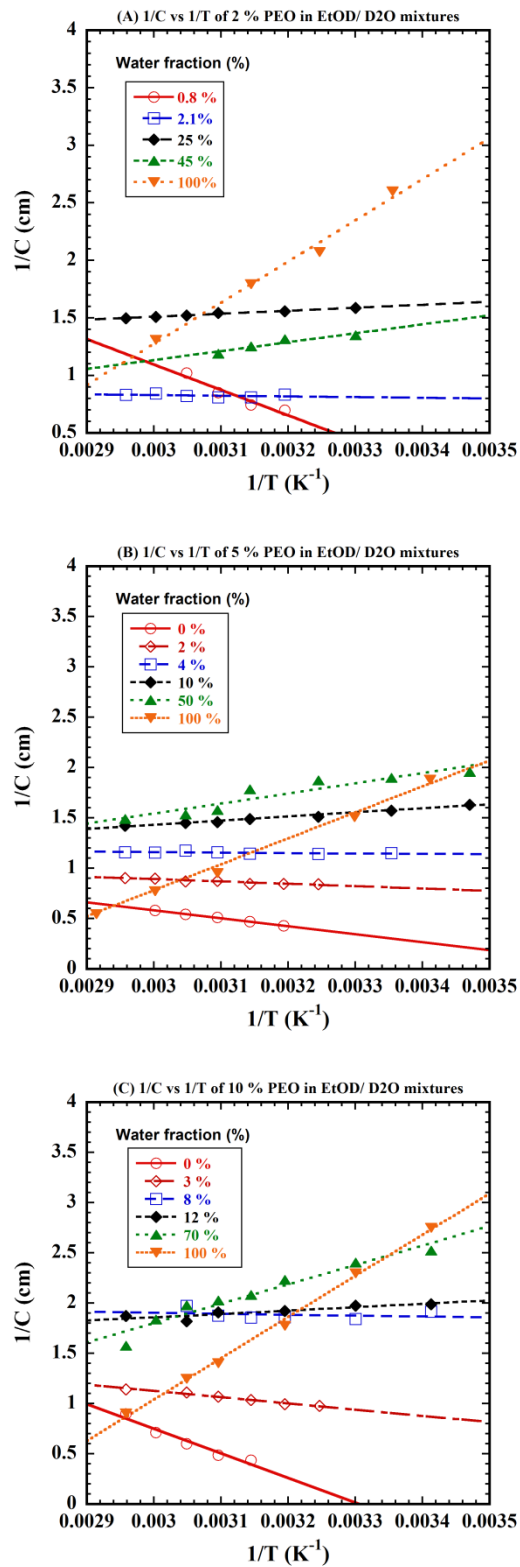


Figure 5.5 Plots of  $1/C$  vs.  $1/T$  (A) 2 wt %, (B) 5 wt % and (C) 10 wt % PEO in ethanol/ water mixtures. Errors are smaller than plot symbols.

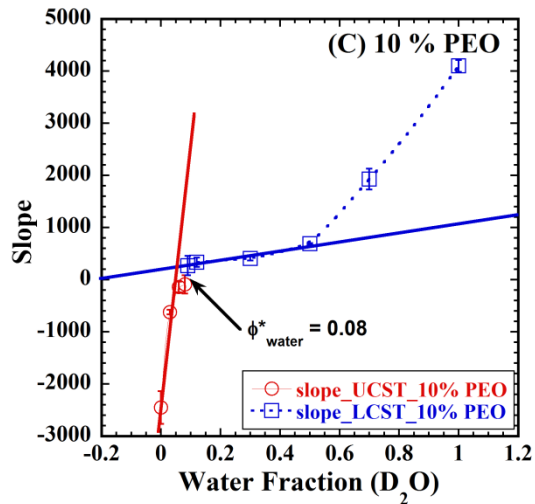
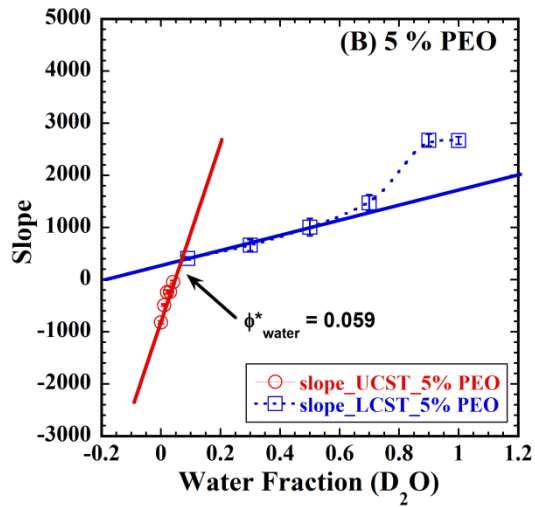
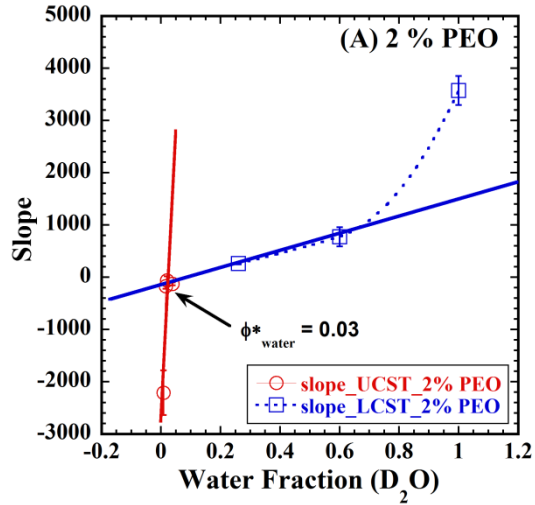


Figure 5.6 Slopes from Figure 5.5 vs. water fraction. (A) 2 wt %, (B) 5 wt % and (C) 10 wt % PEO in ethanol/water mixtures. The transition points from UCST to LCST were estimated by observing slope changes.

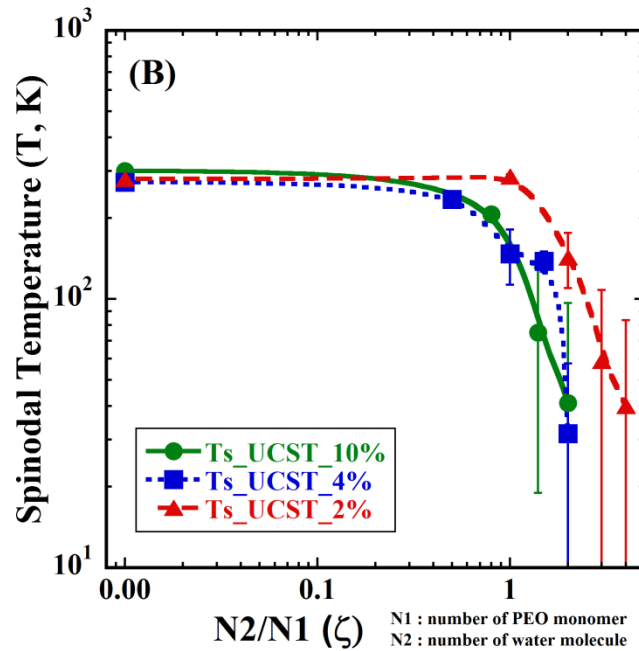
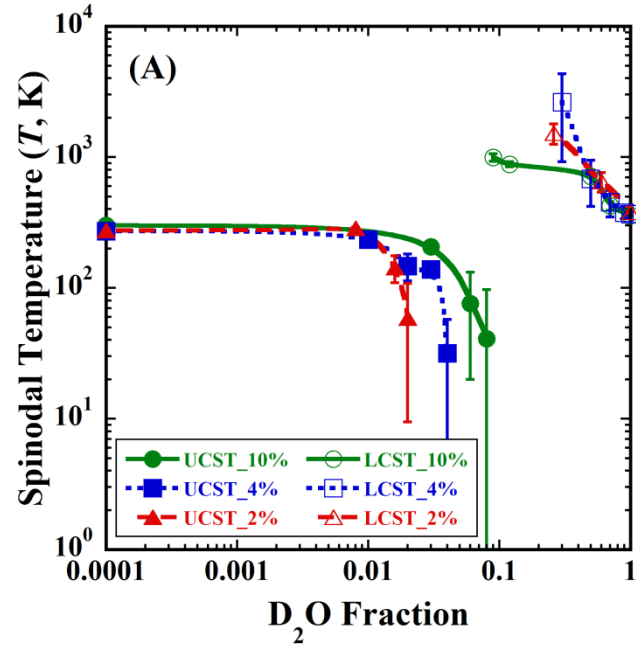


Figure 5.7 Variation of the spinodal temperature as function of (A) water fraction and (B) hydration level. Hydration level can be defined as (number of water molecule)/(number of PEO monomer in solution). The lower region corresponds to the demixed phase and the solution changes to the mixed phase upon heating.

Table 5.2 Transition point from UCST to LCST ( $\phi_{water}^t$ )

<b>PEO (90k)</b>	<b>2 %</b>	<b>5 %</b>	<b>10 %</b>
Water Fraction	0.03	0.059	0.08
Hydration level ( $\zeta$ )	3.9	3.2	1.99

## 5.5 Conclusions

The solvation of PEO in water is believed to be due to the formation of a hydration layer around the PEO chains to shield the contact between CH<sub>2</sub>CH<sub>2</sub> groups and the water molecules.<sup>7, 69</sup> Experimental results show that water molecules play a critical role in solvating PEO. Hydrogen bonding between water and the ether oxygens on the polymer is believed to be strong enough to solvate PEO at small amounts of water in ethanol/water mixtures. A small amount of water forms hydration shell effectively to prevent the contact between water and ethylene group. At the molecular level, two or three water molecules can hydrate one PEO monomer (water molecules form a sheath around the PEO macromolecule) which results in the suppression of crystallization and change in the phase behavior observed by SANS. This observation strongly support previous hypothesis based on dimensional estimation.<sup>7</sup> The extrapolated spinodal temperature and phase behavior of PEO solutions with different PEO concentrations (2 wt % PEO and 10 wt % PEO) in water/ethanol mixtures are used to assess the role of hydration. The observed phase behavior is consistent with a hydration layer forming upon the addition of water and the system shifting from UCST to LCST behavior. The amount of water necessary to

form a hydration layer around PEO chains varies in a self-consistent manner as the PEO concentration increases from 2 wt % to 10 wt %. This conclusion agrees with a previous simulation study and estimates.<sup>31, 33, 70, 71</sup>

## Chapter 6

### Salt effect in PEO/ ethanol

#### 6.1 Introduction

Ions in solution bind to oppositely charged groups via electrostatic interactions. In certain cases ions can bind to non-ionic water-soluble polymers such as poly(ethylene oxide) although it is a neutral.<sup>72-76</sup> The binding between a salt ion and a neutral polymer is of fundamental relevance to many technological and biological applications.<sup>3,72,77</sup> For example, the ionic binding with the ether oxygen of PEO has been studied for polyelectrolyte for rechargeable battery technology.<sup>72, 78</sup> PEO is also used in many consumer products (soap, cosmetic) and medical products.<sup>79-85</sup>

The formation of complexes between ions and PEO in alcohol has been demonstrated by NMR measurements.<sup>76</sup> The magnitude of the NMR peak shift is proportional to the degree of polymerization; higher peak shift was observed at larger molecular weight. The complexation changes the solution properties of PEO in alcohol.<sup>76</sup> Pseudo-polyelectrolyte behavior has been demonstrated by SANS measurements. SANS data of PEO/d-methanol in the presence of a monovalent salt (KI) exhibited a peak at low- $Q$  which is a characteristic of polyelectrolyte solutions.<sup>73,</sup><sup>74</sup> The peak was observed in the SANS data for PEO/methanol/KI (or LiClO<sub>4</sub>) at low concentration of salts and occurred due to binding between ether oxygen and K<sup>+</sup> ion. The scattering intensity decreased in the binding regime as the salt concentration was

increased. The peak, however, disappeared as the salt concentration was increased because of screening by opposite ion. These phenomena can be understood by salt-in (polyelectrolyte peak) and salt-out (increase of scattering intensity) in the presence of salt. The scattering intensity increases as function of monovalent salt concentration in the screening regime.

PEO with divalent cations ( $\text{Ca}^{2+}$ ,  $\text{Mg}^{2+}$ ) exhibits unusual behavior compared to the PEO/monovalent system.<sup>47, 54, 86, 87</sup> There are no extensive studies on the solution behavior of PEO in the multivalent ion although a wide range of applications. Here we will examine the solution behavior of PEO in deuterated ethanol in the presence of divalent salt using small-angle neutron scattering. The divalent cation  $\text{Ca}^{2+}$  from  $\text{CaCl}_2$  was used.

## 6.2 Experimental

PEO (h-PEO,  $\text{HO}-(\text{CH}_2\text{CH}_2\text{O})_n-\text{CH}_3$ ) of molecular weight  $M_w = 90,000$  g/mol ( $M_n = 83,000$  g/mol) was purchased from Polymer Source, Inc. and used without further purification. Anhydrous deuterated ethanol ( $\text{C}_2\text{D}_5\text{OD}$ , d-ethanol) were purchased from Cambridge Isotope Laboratories Inc. and used without further purification. Protonated polymer/ deuterated solvent were used to enhance contrast and lower background in neutron experiments. The mass fraction of PEO was fixed as 5 wt %. When PEO is first mixed with d-ethanol, there is no observable change for 10 hours at room temperature. Heating process is required to dissolve PEO in d-ethanol. PEO/ d-ethanol become clear solution after 2 hours in 60 °C. PEO/ d-ethanol mixture

was processed at 60 °C water bath over 3 hours. Anhydrous CaCl<sub>2</sub> (Aldrich) was used as divalent salt. CaCl<sub>2</sub> was added into PEO/ d-ethanol and salt solutions were heated at 60 °C for 2 hour. The salt concentration (CaCl<sub>2</sub>) was varied from 0.00M to 1.00M. An additional concentration of 3.0M CaCl<sub>2</sub> was also examined as an extreme case as shown in Table 6.1. We examined the solubility of CaCl<sub>2</sub> in ethanol up to 4.5M CaCl<sub>2</sub> in ethanol. 4.5M CaCl<sub>2</sub> in ethanol is homogeneous solution.

Small-angle neutron scattering (SANS) measurements were carried out using the 30m SANS instrument (NG-3 and NG-7) at the National Institute of Standards and Technology Center for Neutron Research (NCNR).<sup>55</sup> SANS configurations used a neutron wavelength ( $\lambda$ ) = 6 Å with  $\Delta\lambda/\lambda = 0.15$ . Three detector configurations were used: 1m, 4m and 13m. The wave vector ( $Q$ ) range using the 3 configurations is 0.0034 Å<sup>-1</sup> – 0.4421 Å<sup>-1</sup>. Samples were prepared and measured in 1 mm quartz cells. The measured scattering data were reduced for scattering from the empty cell, incoherent scattering, detector dark current, detector sensitivity, sample transmission, and thickness.<sup>17, 61</sup> The reduction procedure was performed with SANS data reduction package provided by NCNR.<sup>61</sup> The data after standard reduction were placed on an absolute scale using direct beam measurement and circularly averaged to produce  $I(Q)$  vs.  $Q$  plots. SANS intensities were measured in the temperature range of 25 °C – 65 °C to understand the thermal behavior of the polymer solution.

### 6.3 Results and analysis

PEO forms a gel in ethanol at room temperature due to partial crystallization of the PEO. We have shown that the gel structure is disrupted by adding small

amounts of water to the PEO/ethanol solution. 4 vol % d-water is sufficient to totally disrupt the gel structure. In this chapter, we describe experiments to examine the effect of salt on PEO/ethanol solutions. Positively charged ions can bind with the oxygen atom in the PEO chain through Coulombic interactions between the  $\text{Ca}^{2+}$  cation and the induced oxygen dipole as shown in Figure 6.1. We will study the effect of complexation between the cation and the induced oxygen dipole. The goal is to understand the effect of salt on the solution behavior of PEO in ethanol.

Disruption of the PEO gel in d-ethanol is observed by adding divalent salt,  $\text{CaCl}_2$ . Up to 0.1M  $\text{CaCl}_2$  there is no observable visual change in the opaque gel at room temperature (25 °C) as shown in Figure 6.2 (A). The ratio of the number of  $\text{Ca}^{2+}$  ions per PEO monomer in 0.1M solution at 5 wt % PEO concentration is 0.088. When the salt concentration is 0.25M there is an observable change and the gel appears to be partially disrupted. The gel becomes totally disrupted when the salt concentration reaches 0.5M  $\text{CaCl}_2$ . After disruption the solution appears clear as shown in Figure 6.2 (A). The ratio of salt to PEO molecules and the visual observations are summarized in Table 6.1. The SANS data for PEO/ d-ethanol as a function of salt concentration ( $\text{CaCl}_2$ ) are shown in Figure 6.2 (B) at  $T = 25\text{ }^\circ\text{C}$  and Figure 6.2 (C) at  $T = 35\text{ }^\circ\text{C}$ . When the salt concentration was varied up to 0.1 M there is no significant change in the scattering intensity at 25 °C. The fractal dimension of the gel can be characterized by the Porod exponent, obtained from a Porod plot ( $I \sim Q^m$ , where  $m$  is the Porod exponent). The slope obtained from SANS data in the low- $Q$  region ( $Q < 0.1\text{ \AA}^{-1}$ ) for the opaque PEO gel is approximately -3.2. This implies the surface roughness of the core crystalline region in these samples is intermediate between a

smooth surface ( $m = -4$ ) and rough surface ( $m = -3$ ). Adding salt suppresses the crystallization process and disrupts the gel structure. When the salt concentration is 0.25M an isolated opaque gel is formed at 25 °C. Bragg scattering peaks appear in the SANS data for 0.25M CaCl<sub>2</sub> at 25 °C which were not observed at lower salt concentrations. The SANS intensity for a homogeneous PEO solution at 25 °C (PEO in ethanol at high CaCl<sub>2</sub> concentrations, concentration of CaCl<sub>2</sub> > 0.5M) follows classical polymer solution behavior. The slope at high- $Q$  for the homogeneous PEO/salt solution in d-ethanol is -5/3, the signature of a good solvent, when the salt concentration exceeds 0.5M at 25 °C. The disruption of the PEO/ethanol gel is observed at elevated temperatures. PEO/ethanol with 0.25M CaCl<sub>2</sub> becomes a homogeneous solution at 35 °C as shown in Figure 6.2 (C). A decrease of the dissolution temperature of PEO is observed by adding CaCl<sub>2</sub>. The SANS intensity for PEO in ethanol with 0.25M CaCl<sub>2</sub> at  $T = 35$  °C also exhibits classical polymer solution behavior with a slope of -5/3 at high- $Q$  as shown in Figure 6.2 (C).

The gel structure has totally disappeared even in 0.00M CaCl<sub>2</sub> solution if the temperature is over 45 °C. The SANS data for PEO in ethanol, as a function of salt concentration at 45 °C, is shown in Figure 6.3. SANS intensity for PEO/ethanol/CaCl<sub>2</sub> in the homogeneous state exhibits excess scattering at low- $Q$ . The excess SANS intensity at low- $Q$  is likely due to aggregation behavior in solution. The SANS data for PEO in d-ethanol with salt at 45 °C can be analyzed in the same manner as was done for the aqueous PEO solutions in chapter 4. The Eq (4-1) describes clustering by upturn at low- $Q$  region and chain scattering at high- $Q$  region.

We have examined the solution behavior of PEO in ethanol as a function of salt concentration in the homogeneous phase. The addition of salt changes the solution behavior of PEO in d-ethanol even in the homogeneous region as shown in Figure 6.3. Disruption of the gel arises from bonding between cations ( $\text{Ca}^{2+}$ ) and oxygen atoms on the PEO chain as described in Figure 6.1. The zero angle scattering intensity is a measure of concentration fluctuations in system as discussed in Section 4.5. Ignoring the low- $Q$  clustering effect, we can use the fitting parameter  $C$  as the zero angle scattering intensity by setting  $Q$  as 0 in Eq (4-1):  $I(0) = C/(1+(0 \cdot L)^n) = C$ . The value of solvation intensity,  $C$ , decreases as a function of salt concentration as shown in Figure 6.4 (A). This implies better solvation with increasing salt concentration: the solution containing salt is better solvated than without salt. The inset of Figure 6.4 (A) shows the correlation length as a function of salt concentration. The correlation length decreases with increasing salt concentration. The decrease of the correlation length is consistent with the solution being better solvated at higher salt concentrations. Binding of  $\text{Ca}^{2+}$  ions to the PEO oxygens transforms the neutral polymer into a weakly charged polyelectrolyte as shown in Figure 6.1.<sup>75, 88</sup> The binding sites on PEO behave as positively charged sites and mediate repulsive interaction between sites as demonstrated in Figure 6.5. The interaction between PEO/salt complex and ethanol is more attractive than that of PEO and ethanol. These interactions from electrostatic repulsion repel the PEO chains each other. The solvation intensity decreases rapidly with increasing salt concentration when the salt concentration is less than 0.25M. The value of solvation intensity levels off when the salt concentration exceeds 0.25M. This leveling off may be due to screening by the

oppositely charged ions ( $\text{Cl}^-$ ) in solution at relatively high salt concentration.  $\text{Cl}^-$  (counter ion), however, do not screen repulsive charge interactions effectively. Effective screening increases the solvation intensity but there is no significant increase of solvation intensity. Increase of solvation intensity is a signature of onset screening but the solvation intensity of PEO/ethanol/salt does not increase even in very high salt concentration. It is unusual that screening by counter ion is not appeared even in high salt concentration. We could not observe any increase of solvation intensity up to 3.00M  $\text{CaCl}_2$ . Another possibility for leveling off of the solvation intensity at higher salt concentration may arise from cations being shared by multiple oxygens on the PEO chain.

The clustering behavior in the solutions can be monitored through the magnitude of the upturn in the low- $Q$  region of the scattering. The magnitude of the upturn at low- $Q$  for PEO/ d-ethanol solutions is relatively small compared to aqueous PEO solutions but a dependence on salt concentration is observed. The first term at Eq (4-1),  $A/Q^m$ , describes the low- $Q$  SANS intensity and can be used to monitor the clustering behavior. We will use the value of the intensity at  $Q = 0.004 \text{ \AA}^{-1}$  ( $A/(0.004^m)$ ),  $A$  and  $m$  are obtained from fitting the SANS intensity with Eq (4-1). The clustering intensity is observed to increase as a function of increasing salt concentration as shown in Figure 6.4 (B).

The clustering intensity becomes higher at lower solvation intensity. Here we suggest a model to describe the salt effect on solvation and clustering of PEO in ethanol. Consider the binding between the cation and ether oxygen on the PEO chain. As discussed above, the decrease of solvation intensity of PEO in ethanol with added

salt arises from the repulsive force induced through the binding of the cation ( $\text{Ca}^{2+}$ ) to the ether oxygen. The population of PEO monomer bound with cations increase as salt concentration increases. Therefore solvation intensity decreases as a function of salt concentration and levels off when the salt concentration is 0.25M: The ratio of  $\text{Ca}^{2+}$  to ether oxygens in this solution is 1/5, which indicates that one cation can complex with multiple PEO oxygens. Therefore one cation acts as an anchoring site for the PEO. The cations anchoring model is represented in Figure 6.5. The cations anchoring model can explain both the clustering and solvation behavior for PEO/ethanol as function of salt concentration. The cations are not shared by PEO oxygen at low concentration ( $\text{CaCl}_2 < 0.1\text{M}$ ). The cations transform the neutral polymer into a weakly charged polymer through complexation at low salt concentration and lower the solvation intensity. The cations shared by multiple monomers to form clusters after 0.2M of  $\text{CaCl}_2$ .

In order to analyze the salt effect on the phase behavior, SANS intensities were measured as a function of temperature. The solvation intensity,  $C$ , obtained from the SANS data was used to estimate the spinodal temperature from Flory-Huggins theory as discussed in section 5.1.1. A plot of  $1/C$  vs.  $1/T$  is shown in Figure 6.6 (A). The slope of  $1/C$  vs.  $1/T$  increases as the salt concentration increases. The magnitude of the slope taken from the  $1/C$  vs.  $1/T$  plot is shown in Figure 6.6 (B). The sign of this slope changes from negative to positive, which indicates a change in phase behavior from UCST (negative) to LCST (positive). Addition of salt ( $\text{CaCl}_2$ ) to PEO/ d-ethanol disrupts the gel structure and changes the thermodynamic behavior from UCST to LCST. The value of slope at higher salt concentrations, 0.2M – 1.0M, levels off as

salt concentration increases. This implies that the excess salt beyond 0.25M CaCl<sub>2</sub> does not continue to change the thermodynamic behavior of PEO/ethanol, which is consistent with the observed behavior for solvation and clustering.

Table 6.1 Sample preparation and visual observations

<b>PEO concentration in EtOD</b>	<b>Salt concentration (M, mol/L)</b>	<b>Salt (mol)/PEO monomer (mol)</b>	<b>Visual observations at 25 °C</b>
<b>5 wt %</b>	<b>0.00</b>	<b>0</b>	<b>opaque (gel)</b>
	<b>0.04</b>	<b>0.035</b>	<b>opaque (gel)</b>
	<b>0.10</b>	<b>0.088</b>	<b>opaque (gel)</b>
	<b>0.25</b>	<b>0.22</b>	<b>start of a disrupted gel (isolated gel)</b>
	<b>0.50</b>	<b>0.44</b>	<b>totally disrupted gel (homogeneous)</b>
	<b>1.00</b>	<b>0.88</b>	<b>totally disrupted gel (homogeneous)</b>
	<b>3.00</b>	<b>2.64</b>	<b>totally disrupted gel (homogeneous)</b>

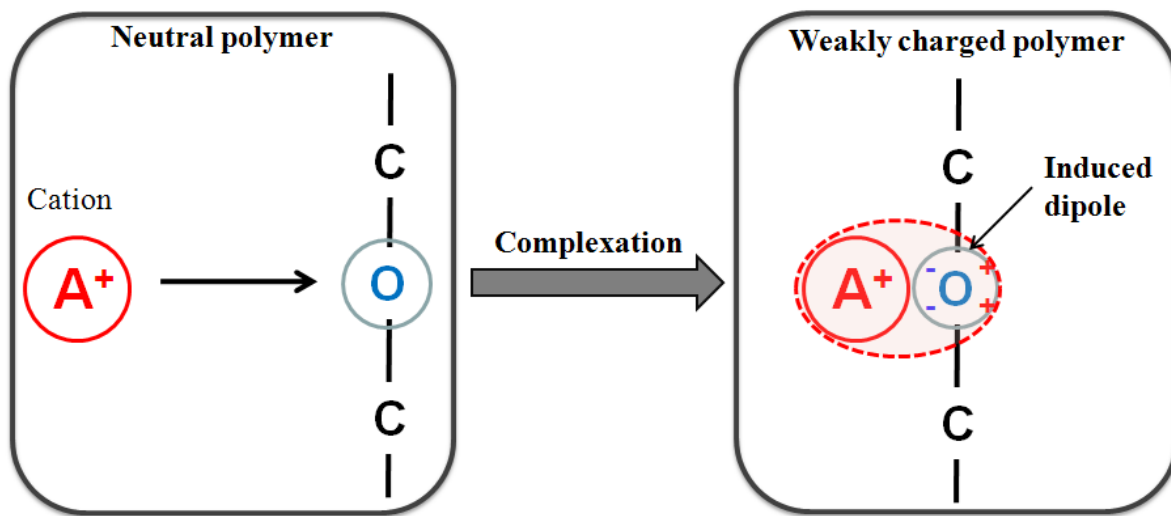


Figure 6.1 Complexation between cations and induced dipoles on the neutral polymer.

(A) PEO solution in ethanol with increasing salt

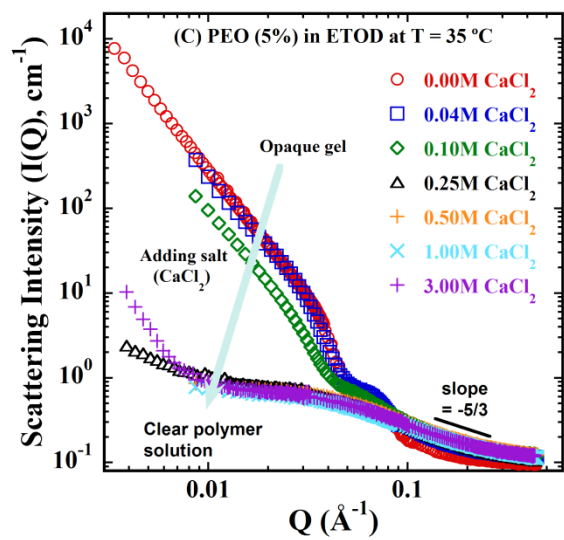
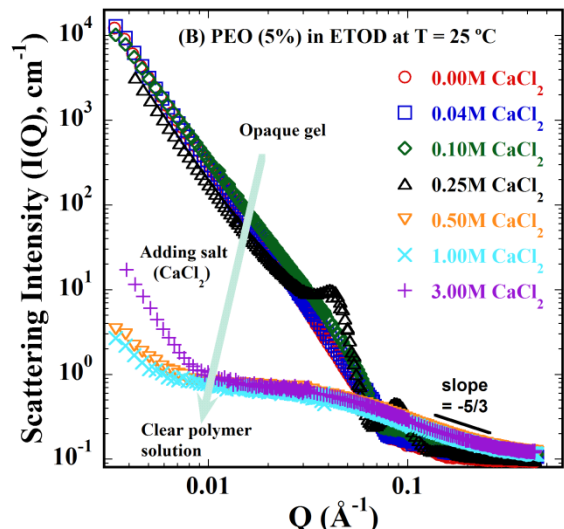
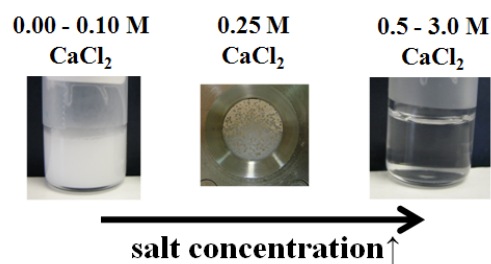


Figure 6.2 (A) Pictures of PEO/ethanol with varying salt concentration. (B) SANS intensity for PEO/ ethanol varying  $\text{CaCl}_2$  concentration at 25 °C and (C) at 35 °C.

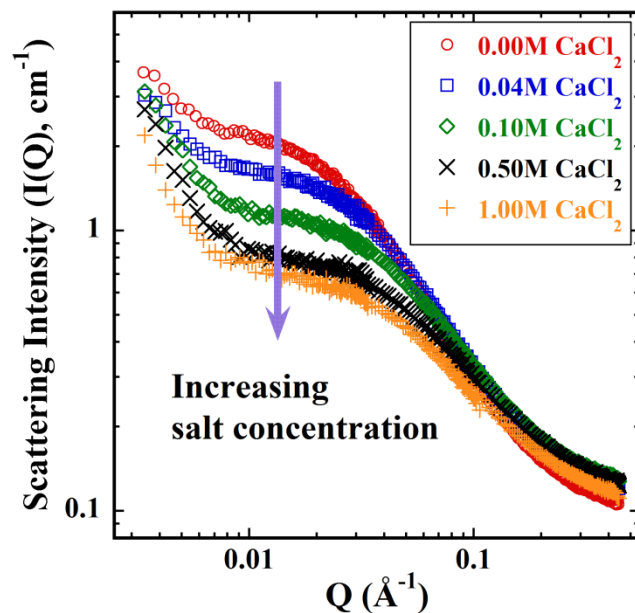


Figure 6.3 SANS intensity for PEO/ethanol/CaCl<sub>2</sub> solutions at 45 °C. The forward scattering intensity decreases as the CaCl<sub>2</sub> concentration increases.

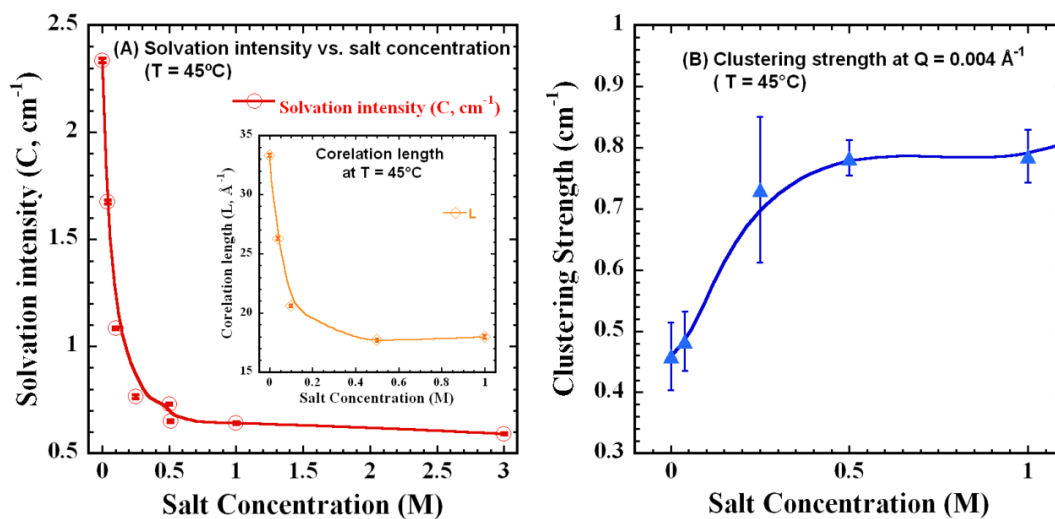


Figure 6.4 (A) Solvation intensity as a function of salt concentration at 45 °C. The inset picture shows variation of the correlation length. (B) Clustering strength as function of salt concentration.

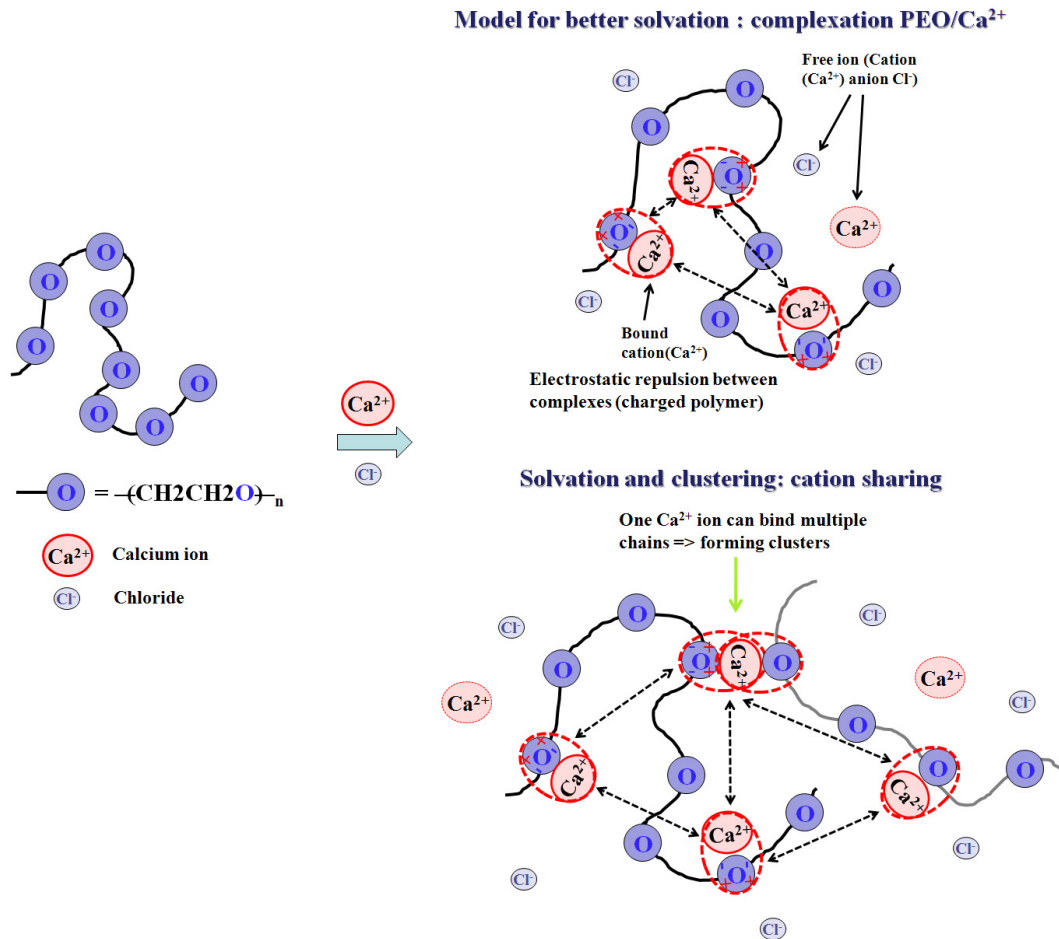


Figure 6.5 Proposed model to describe solvation and clustering in the presence of salt. Cation can exist as two states: bound cation with PEO oxygen and unbound free solvated ion. Complexation between PEO oxygen and calcium ion (bound cation) reduce the solvation intensity (better solvation in the presence of salt). The PEO cluster is formed through cation sharing by multiple chains. Screening effect by counter ion (anion) was not observed in solvation intensity as a function of salt concentration. Chloride exists as free ion in ethanol solvents. Dashed arrows represent columbic repulsion.

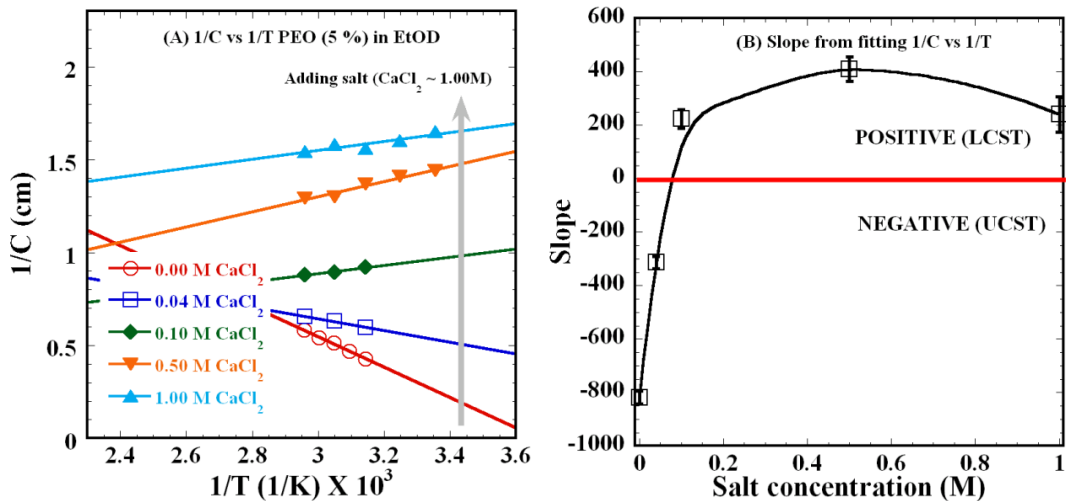


Figure 6.6 (A) Plot of  $1/C$  vs.  $1/T$  with varying salt concentration. (Error bars are smaller than symbols.) (B) slope from the linear fitting of  $1/C$  vs.  $1/T$ . The phase behavior changes from UCST to LCST with the addition of salt. Error bars of (A) are smaller than plot symbols.

## 6.4 Conclusions

The solution behavior of poly(ethylene oxide) in deuterated ethanol was investigated in the presence of salt using small-angle neutron scattering. The divalent cation  $\text{Ca}^{2+}$  from  $\text{CaCl}_2$  was used. In general PEO shows a polyelectrolyte-like behavior in some organic solvents like methanol.<sup>73-76</sup> The origin of the polyelectrolyte-like behavior in PEO is due to the formation of complexes between the oxygens on PEO and the cations. Binding of  $\text{Ca}^{2+}$  ion to the PEO oxygen transforms the neutral polymer into a weakly charged pseudo-polyelectrolyte, resulting in repulsive interactions. The PEO/ethanol solution is better solvated at higher salt concentration due to electrostatic repulsion the PEO/  $\text{Ca}^{2+}$  complexes. The

binding between cation and PEO oxygen can be understood by salt-in mechanism. Salt out mechanism accompanies with salt in with increasing salt concentration. The onset of screening is a signature of salt out condition. The salt out phenomena, however, was not observed even in high salt concentration. There is no evidence for onset screening with high salt concentration. Anion exists as free ion solvated in ethanol. Without salt addition, PEO/ d-ethanol solutions form a gel at room temperature; addition of salt disrupts the gel and is consistent with better solvation as the salt concentration is increased. The change of phase behavior changes from an UCST to LCST is due to the bound cation to PEO chain. Furthermore, we monitored the clustering behavior of PEO/ethanol in the presence of salt in the low- $Q$  region of the SANS data. The clustering behavior is proportional to the salt concentration. We suggested a model to satisfy both characteristics: lower solvation intensity and higher clustering intensity with increasing salt concentrations. A cation shared by multiple monomers induces the repulsive force to reduce solvation intensity and simultaneously enhances clustering.

## Chapter 7

### Conclusions

Poly(ethylene oxide) (PEO) in ethanol forms an opaque gel-like mixture with a partially crystalline structure. Addition of a small amount of water disrupts the gel: 5 wt % PEO in ethanol becomes a transparent solution upon the addition of 4 vol % water. The dramatic change of PEO/ethanol solution with the addition of a small amount of water is believed to originate from the hydrogen bonding between water and the ether oxygen of PEO. The solvation intensity from SANS shows a parabolic variation as a function of d-ethanol/d-water ratio. A cosolvent mixture of ethanol/water is a more effective solvating agent for PEO than pure solvents (water and ethanol). The clustering intensity from SANS is proportional to the inverse of temperature ( $1/T$ ) and to the water fraction in water/ethanol mixtures. The clustering intensity increases and levels off as the water fraction is increased. The water molecules participating in hydrogen bonding with the polymer form a shielding layer around the chain to prevent contact between water and the ethylene group ( $\text{CH}_2\text{CH}_2$ ). The interaction between the ethylene groups and water molecules is due to the hydrophobic effect, which results in aggregation. Hydrogen bonds between water and the ether oxygen and the hydrophobic effect can be induced by adding water to PEO in ethanol solution, resulting in lower solvation intensity (i.e. effective solvation) and higher clustering.

The phase behavior of PEO in mixed solvents has been studied using the zero angle scattering intensity measured by SANS. PEO solutions (5 wt % PEO) which contain 4 vol % – 10 vol % (and higher) water is found to behave as an athermal polymer solution and the phase behavior rapidly changes from UCST to LCST as the fraction of water is increased. The observed phase behavior is consistent with a hydration layer forming upon the addition of water as the system shifts from UCST to LCST behavior. At the molecular level, two or three water molecules can hydrate one PEO monomer which is consistent with the suppression of crystallization and change in the mentioned phase behavior as observed by SANS. The observed phase behavior is consistent with a hydration layer forming upon the addition of water and the system shifting from UCST to LCST behavior. The amount of water necessary to form a hydration layer around PEO chains varies in a self-consistent manner as a function of PEO concentration. This conclusion agrees with previous simulation studies.

The solution behavior of PEO in ethanol was investigated in the presence of divalent salt ( $\text{CaCl}_2$ ) using SANS. Binding of  $\text{Ca}^{2+}$  ions to the PEO oxygen atom transforms the neutral polymer a weakly charged pseudo-polyelectrolyte. The PEO/ethanol solution is better solvated at higher salt concentration due to the electrostatic repulsion of weakly charged monomers. The association of the  $\text{Ca}^{2+}$  ions with the PEO oxygen atoms transforms the neutral polymer to a weakly charged polyelectrolyte and gives rise to repulsive interactions between the PEO/ $\text{Ca}^{2+}$  complexes. Without salt addition, PEO/ethanol solutions form a gel at room temperature; addition of salt disrupts the gel and is consistent with better solvation as the salt concentration is increased. Furthermore, we monitored the clustering behavior

in the low- $Q$  region of the SANS data. The clustering intensity increases with increasing salt concentration and levels off with the salt concentration. We suggested a model to satisfy both characteristics: lower solvation intensity and higher clustering intensity with increasing salt concentrations. A cation shared by multiple monomers results in a coulombic repulsive force which simultaneously reduces solvation intensity and enhances clustering.

## **Chapter 8**

### **Future Work**

Although PEO is one of the most researched synthetic polymers our understanding is still quite limited due to its complex behavior. In this section suggestions are given for extension of current understanding based on the experiments and observation in this dissertation.

The solution behavior of PEO was investigated in detail, but more work needs to be done to fully understand the solvation and aggregation behavior of PEO in water and in ethanol/water mixed solvents. Addition of a small amount of water to the PEO/ethanol solution changes the entire solution behavior in the PEO/ethanol/water system. In order to fully understand the hydration mechanism of PEO diffraction studies would be helpful in order to elucidate the local hydration shell structure of PEO/water and of PEO/ethanol/water. Molecular dynamics (MD) simulation studies could help understand hydrophobic and hydrogen bond interactions in PEO/water and PEO in mixed solvents with water. The clustering behavior of PEO should be explored further. The temperature effect on clustering behavior cannot be explained in terms of simple hydrophobic interaction. The hydrophobic interaction increased with increasing temperature. Hence the clustering intensity should increase as temperature increase. As discussed the clustering intensity of PEO in water is a decreasing function of temperature. The clustering and solvation behavior in mixed

solvents (such as ethanol/water or methanol/water) could further be investigated to understand solution behavior of PEO. Further study of the effect of molecular weight on clustering behavior will be interesting for SANS experiments. A series of scattering experiments with varying molecular weight is informative experiments for further understanding PEO clustering behaviors.

There are many opportunities to advance the study of PEO/solvent/salt and PEO/salt systems. The phase behavior and solution behavior of PEO/solvent/salt systems are a key factor for PEO applications in biology and battery technology. The PEO/solvent/salt system may be a tractable model for biopolymers and in energy technology applications. In a fundamental point the polyelectrolyte behavior should be revisited for PEO/salt system. The polyelectrolyte peak is commonly found in PEO/alcohol/salt when monovalent salt, such as  $K^+$  or  $Na^+$  cation, is used. The polyelectrolyte peak is not observed for PEO/d-ethanol/ $CaCl_2$  as shown in Figure 6.3. This observation may be understood by large clustering intensity at low- $Q$ ; the magnitude of excess low- $Q$  scattering is stronger than that of polyelectrolyte peak intensity. The anionic effect should be studied more to understand the behavior of PEO/solvent/salt system for applications.

## Bibliography

1. Brown, W. (1984) Slow-mode diffusion in semidilute solutions examined by dynamic light scattering, *Macromolecules* 17, 66-72.
2. Devanand, K., and Selser, J. C. (1991) Asymptotic-behavior and long-range interactions in aqueous-solutions of poly(ethylene oxide), *Macromolecules* 24, 5943-5947.
3. Bailey, F. E., Koleske, J. V. (1976) *Poly(ethylene oxide)*, Academic Press, New York.
4. Duval, M. (2000) Monitoring of cluster formation and elimination in PEO solutions, *Macromolecules* 33, 7862-7867.
5. Hammouda, B., Ho, D., and Kline, S. (2002) SANS from poly(ethylene oxide)/water systems, *Macromolecules* 35, 8578-8585.
6. Ho, D. L., Hammouda, B., Kline, S. R., and Chen, W. R. (2006) Unusual phase behavior in mixtures of poly(ethylene oxide) and ethyl alcohol, *J. Polym. Sci. Pt. B-Polym. Phys.* 44, 557-564.
7. Kjellander, R., and Florin, E. (1981) Water-structure and changes in thermal-stability of the system poly(ethylene oxide)-water, *Journal of the Chemical Society-Faraday Transactions I* 77, 2053.
8. Liu, K. J., and Parsons, J. L. (1969) Solvent effects on preferred conformation of poly(ethylene glycols), *Macromolecules* 2, 529.
9. Allcock, H. R. (1992) Rational design and synthesis of new polymeric materials, *Science* 255, 1106-1112.

10. Armand, M., Endres, F., MacFarlane, D. R., Ohno, H., and Scrosati, B. (2009) Ionic-liquid materials for the electrochemical challenges of the future, *Nat. Mater.* 8, 621-629.
11. Matyjaszewski, K. (2005) Macromolecular engineering: From rational design through precise macromolecular synthesis and processing to targeted macroscopic material properties, pp 858-875, Pergamon-Elsevier Science Ltd.
12. Nakashima, K., Maruyama, T., Kamiya, N., and Goto, M. (2006) Homogeneous enzymatic reactions in ionic liquids with poly(ethylene glycol) modified subtilisin, *Org. Biomol. Chem.* 4, 3462-3467.
13. Shimojo, K., Nakashima, K., Kamiya, N., and Goto, M. (2006) Crown ether-mediated extraction and functional conversion of cytochrome c in ionic liquids, *Biomacromolecules* 7, 2-5.
14. Sasaki, T., Miyazaki, A., Sugiura, S., and Okada, K. (2002) Crystallization of poly(ethylene oxide) from solutions of different solvents, *Polym. J.* 34, 794-800.
15. Doi, M. (1996) *Introduction to Polymer Physics*, Oxford University Press.
16. Flory, P. J. (1953) *Principles of Polymer Chemistry* Cornell University Press
17. Hammouda, B. (2007) *SANS tool box*.
18. Hill, T. L. (1987) *An Introduction to Statistical Thermodynamics*, Dover Publications, New York.
19. Gennes, P.-G. d. (1979) *Scaling Concepts in Polymer Physics* Cornell University Press

20. Strobl, G. (1996) *The Physics of Polymers: Concepts for Understanding their Structures and Behavior*, 1 ed., Springer-Verlag, Berlin.
21. Graham, N. B., Zulfiqar, M., Nwachuku, N. E., and Rashid, A. (1989) Interaction of poly(ethylene oxide) with solvents: 2. Water-poly(ethylene glycol), *Polymer* 30, 528-533.
22. Dixit, S., Crain, J., Poon, W. C. K., Finney, J. L., and Soper, A. K. (2002) Molecular segregation observed in a concentrated alcohol-water solution, *Nature* 416, 829-832.
23. Narten, A. H. (1972) Liquid water: atom pair correlation functions from neutron and X-ray diffraction, *The Journal of Chemical Physics* 56, 5681-5687.
24. Soper, A. K. (2000) The radial distribution functions of water and ice from 220 K to 673 K and at pressures up to 400 MPa, *Chem. Phys.* 258, 121-137.
25. Barlow, S. J., Bondarenko, G. V., Gorbaty, Y. E., Yamaguchi, T., and Poliakov, M. (2002) An IR study of hydrogen bonding in liquid and supercritical alcohols, *J. Phys. Chem. A* 106, 10452-10460.
26. Franks, F., and Desnoyers, J. E. (1985) *Water Science Reviews*.
27. Sassi, P., Paolantoni, M., Cataliotti, R. S., Palombo, F., and Morresi, A. (2004) Water/alcohol mixtures: A spectroscopic study of the water-saturated 1-octanol solution, *Journal of Physical Chemistry B* 108, 19557-19565.
28. Smith, J. D., Cappa, C. D., Wilson, K. R., Cohen, R. C., Geissler, P. L., and Saykally, R. J. (2005) Unified description of temperature-dependent

- hydrogen-bond rearrangements in liquid water, *Proceedings of the National Academy of Sciences of the United States of America* 102, 14171-14174.
29. Dormidontova, E. E. (2002) Role of competitive PEO-water and water-water hydrogen bonding in aqueous solution PEO behavior, *Macromolecules* 35, 987-1001.
  30. Matsuyama, A., and Tanaka, F. (1990) Theory of solvation-induced reentrant phase separation in polymer solutions, *Physical Review Letters* 65, 341.
  31. Smith, G. D., Bedrov, D., and Borodin, O. (2000) Molecular dynamics simulation study of hydrogen bonding in aqueous poly(ethylene oxide) solutions, *Physical Review Letters* 85, 5583-5586.
  32. Smith, G. D., Bedrov, D., and Borodin, O. (2000) Conformations and chain dimensions of poly(ethylene oxide) in aqueous solution: a molecular dynamics simulation study, *Journal of the American Chemical Society* 122, 9548-9549.
  33. Smith, G. D., Borodin, O., and Bedrov, D. (2002) A revised quantum chemistry-based potential for poly(ethylene oxide) and its oligomers in aqueous solution, *Journal of Computational Chemistry* 23, 1480-1488.
  34. Trouw, F. R., Borodin, O., Cook, J. C., Copley, J. R. D., and Smith, G. D. (2003) Quasielastic neutron-scattering study of the local dynamics of poly(ethylene glycol) dimethyl ether in aqueous solution, *The Journal of Physical Chemistry B* 107, 10446-10452.
  35. Goldstein, R. E. (1984) On the theory of lower critical solution points in hydrogen-bonded mixtures, *J. Chem. Phys.* 80, 5340-5341.

36. Hirschfelder, J., Stevenson, D., and Eyring, H. (1937) A theory of liquid structure, *J. Chem. Phys.* 5, 896-912.
37. Karlstrom, G. (1985) A new model for upper critical and lower critical solution temperatures in poly(ethylene oxide) solutions, *J. Phys. Chem.* 89, 4962-4964.
38. Wheeler, J. C. (1975) Exactly soluble 2-compenet lattice solution with upper and lower critical solution temperatures, *J. Chem. Phys.* 62, 433-439.
39. Tanaka, F., and Matsuyama, A. (1989) Tricriticality in thermoreversible gels, *Physical Review Letters* 62, 2759.
40. Tanaka, H., and Gubbins, K. (1992) Structure and thermodynamic properties of water-methanol mixtures, *J. Chem. Phys.* 97, 2626-2634.
41. Bae, Y. C., Lambert, S. M., Soane, D. S., and Prausnitz, J. M. (1991) Cloud-point curves of polymer-solutions from thermo-optic measurements, *Macromolecules* 24, 4403-4407.
42. Malcolm, G. N., and Rowlinson, J. S. (1957) The thermodynamic properties of aqueous solutions of polyethylene glycon, polypropylene glycol and dioxane, *Transactions of the Faraday Society* 53, 921-931.
43. Saeki, S., Kuwahara, N., Nakata, M., and Kaneko, M. (1976) Upper and lower critical solution temperatures in poly(ethylene glycol) solutions, *Polymer* 17, 685-689.
44. Aray, Y., Marquez, M., Rodriguez, J., Vega, D., Simon-Manso, Y., Coll, S., Gonzalez, C., and Weitz, D. A. (2004) Electrostatics for exploring the nature

- of the hydrogen bonding in polyethylene oxide hydration, *The Journal of Physical Chemistry B* 108, 2418-2424.
45. Cox, L. R., Dunlop, E. H., and North, A. M. (1974) Role of molecular aggregates in liquid drag reduction by polymers, *Nature* 249, 243-245.
  46. Gadd, G. E. (1968) Effects of drag-reducing additives on vortex stretching, *Nature* 217, 1040.
  47. White, A. (1967) Drag spheres in dilute high polymer solutions, *Nature* 216, 994.
  48. Higgins, J. S., and Benoit, H. C. (1997) *Polymers and Neutron Scattering*, Oxford University Press, New York.
  49. Duval, M., and Sarazin, D. (2000) Identification of the formation of aggregates in PEO solutions, *Polymer* 41, 2711-2716.
  50. Ho, D. L., Hammouda, B., and Kline, S. R. (2003) Clustering of poly(ethylene oxide) in water revisited, *J. Polym. Sci. Pt. B-Polym. Phys.* 41, 135-138.
  51. Devanand, K., and Selser, J. C. (1990) Polyethylene oxide does not necessarily aggregate in water, *Nature* 343, 739-741.
  52. Polverari, M., and van de Ven, T. G. M. (1996) Dilute aqueous poly(ethylene oxide) solutions: clusters and single molecules in thermodynamic equilibrium, *The Journal of Physical Chemistry* 100, 13687-13695.
  53. Hammouda, B., Ho, D. L., and Kline, S. (2004) Insight into clustering in poly(ethylene oxide) solutions, *Macromolecules* 37, 6932-6937.

54. Shetty, A. M., and Solomon, M. J. (2009) Aggregation in dilute solutions of high molar mass poly(ethylene) oxide and its effect on polymer turbulent drag reduction, *Polymer* 50, 261-270.
55. Glinka, C. J., Barker, J. G., B., H., Krueger, S., Moyer, J. J., and Orts, W. J. (1998) The 30 m small-angle neutron scattering instruments at the National Institute of Standards and Technology, *Journal of applied crystallography* 31, 430-445.
56. Squires, G. L. (1978) *Introduction to the theory of thermal neutron scattering*, Cambridge University Press.
57. McQuarrie, D. A. (2000) *Statistical Mechanics*, 2nd ed., University Science Books.
58. Ihmels, E. C., Aufderhaar, C., Rarey, J., and Gmehling, J. (2000) Computer-controlled vibrating tube densimeter for liquid density measurement in a wide temperature and pressure range, *Chemical Engineering & Technology* 23, 409-412.
59. Kratky, O., Leopold, H., and Stabinger, H. H. (1969) *Z. Angew. Phys.* 27, 273.
60. Nabiyeu, N. D., Bashirov, M. M., Safarov, J. T., Shahverdiyev, A. N., and Hassel, E. P. (2009) Thermodynamic properties of the geothermal resources (Khachmaz and Sabir-Oba) of Azerbaijan, *Journal of Chemical & Engineering Data* 54, 1799-1806.
61. Kline, S. R. (2006) Reduction and analysis of SANS and USANS data using IGOR Pro, *Journal of applied crystallography* 39, 895-900.

62. Bassett, D. C. (1981) *Principles of Polymer Morphology* Cambridge University Press, New York.
63. Hemsley, D. A. (1984) *The light microscopy of synthetic polymers*, Vol. 07, Oxford University Press, New York.
64. Pratt, L. R., and Chandler, D. (1977) Theory of hydrophobic effect, *J. Chem. Phys.* 67, 3683-3704.
65. Ruelle, P., and Kesselring, U. W. (1998) The hydrophobic effect. 1. A consequence of the mobile order in H-bonded liquids, *Journal of Pharmaceutical Sciences* 87, 987-997.
66. Ben-Naim, A., and Yaacobi, M. (1974) Effects of solutes on the strength of hydrophobic interaction and its temperature dependence, *The Journal of Physical Chemistry* 78, 170-175.
67. Ben-Naim, A. Y. (1980) *Hydrophobic Interactions* Springer.
68. Wilf, J., and Ben-Naim, A. (1979) Intramolecular hydrophobic interactions in water-ethanol systems, *The Journal of Physical Chemistry* 83, 3209-3213.
69. Horne, R. A., Almeida, J. P., Day, A. F., and Yu, N. T. (1971) Macromolecule hydration and effect of solutes on cloud point of aqueous solutions of polyvinyl methyl ether-a possible model for protein denaturation and temperature control in homeothermic animals, *J. Colloid Interface Sci.* 35, 77.
70. Bedrov, D., Pekny, M., and Smith, G. D. (1998) Quantum-chemistry-based force field for 1,2-dimethoxyethane and poly(ethylene oxide) in aqueous solution, *Journal of Physical Chemistry B* 102, 996-1001.

71. Borodin, O., Douglas, R., Smith, G. D., Trouw, F., and Petrucci, S. (2003) MD simulations and experimental study of structure, dynamics, and thermodynamics of poly(ethylene oxide) and its oligomers, *107*, 6813.
72. Christie, A. M., Lilley, S. J., Staunton, E., Andreev, Y. G., and Bruce, P. G. (2005) Increasing the conductivity of crystalline polymer electrolytes, *Nature* *433*, 50-53.
73. Hakem, I. F., and Lal, J. (2002) Evidence of solvent-dependent complexation in non-ionic polymer-salt systems, *Applied Physics a-Materials Science & Processing* *74*, S531-S533.
74. Hakem, I. F., and Lal, J. (2003) Polyelectrolyte-like behavior of poly(ethylene-oxide) solutions with added monovalent salt, *Europhysics Letters* *64*, 204-210.
75. Hakem, I. F., Lal, J., and Bockstaller, M. R. (2004) Binding of monovalent ions to PEO in solution: Relevant parameters and structural transitions, *Macromolecules* *37*, 8431-8440.
76. Liu, K.-J. (1968) Nuclear magnetic resonance studies of polymer solutions. V. Cooperative effects in the ion-dipole interaction between potassium iodide and poly(ethylene oxide), *Macromolecules* *1*, 308-311.
77. Taubert, A., and Wegner, G. (2002) Formation of uniform and monodisperse zincite crystals in the presence of soluble starch, *Journal of Materials Chemistry* *12*, 805-807.
78. Tarascon, J. M., and Armand, M. (2001) Issues and challenges facing rechargeable lithium batteries, *Nature* *414*, 359-367.

79. Benkovic, S. J., and Hammes-Schiffer, S. (2003) A Perspective on enzyme catalysis, *Science* 301, 1196-1202.
80. Grace, M. J., Lee, S., Bradshaw, S., Chapman, J., Spond, J., Cox, S., DeLorenzo, M., Brassard, D., Wylie, D., Cannon-Carlson, S., Cullen, C., Indelicato, S., Voloch, M., and Bordens, R. (2005) Site of pegylation and polyethylene glycol molecule size attenuate Interferon-antiviral and antiproliferative activities through the JAK/STAT signaling pathway, *Journal of Biological Chemistry* 280, 6327-6336.
81. Grunwald, C., Schulze, K., Reichel, A., Weiss, V. U., Blaas, D., Piehler, J., Wiesmuller, K. H., and Tampe, R. (2010) In situ assembly of macromolecular complexes triggered by light, *Proceedings of the National Academy of Sciences of the United States of America* 107, 6146-6151.
82. Harris, J. M., and Chess, R. B. (2003) Effect of pegylation on pharmaceuticals, *Nat Rev Drug Discov* 2, 214-221.
83. Molineux, G. (2002) Pegylation: engineering improved pharmaceuticals for enhanced therapy, *Cancer Treatment Reviews* 28, 13-16.
84. Satchi-Fainaro, R., Duncan, R., Wagner, E., and Kloeckner, J. (2006) Gene delivery using polymer therapeutics, in *Polymer Therapeutics I*, pp 135-173, Springer Berlin / Heidelberg.
85. Shaunak, S., Godwin, A., Choi, J.-W., Balan, S., Pedone, E., Vijayarangam, D., Heidelberger, S., Teo, I., Zloh, M., and Brocchini, S. (2006) Site-specific PEGylation of native disulfide bonds in therapeutic proteins, *Nat Chem Biol* 2, 312-313.

86. Wittmer, J., Johner, A., and Joanny, J. F. (1995) Precipitation of polyelectrolytes in the presence of multivalent salts, *J. Phys. II* 5, 635-654.
87. Zhivkova, I. V., Zhivkov, A. M., and Stoychev, D. S. (1998) Electrostatic behaviour of polyethylene oxide, *European Polymer Journal* 34, 531-538.
88. Quina, F., Sepulveda, L., Sartori, R., Abuin, E. B., Pino, C. G., and Lissi, E. A. (1986) Binding of electrolytes to poly(ethylene oxide) in methanol, *Macromolecules* 19, 990-994.